Strongly interacting matter in a finite volume

Vom Fachbereich Physik
der Technischen Universität Darmstadt

zur Erlangung des Grades
eines Doktors der Naturwissenschaften (Dr. rer. nat.)

genehmigte Dissertation von
Dipl. Phys. Piotr Piasecki
aus Warschau

Referent: PD. Dr. Lorenz von Smekal
Koreferent: Prof. Dr. Jochen Wambach

Tag der Einreichung: 10.02.2014
Tag der Prüfung: 14.05.2014

Darmstadt 2014
D 17

Was wahr ist, ist wie das, was an sich selbst recht und schön ist, seiner Natur nach ewig, und hat mitten in der Zeit kein Verhältnis zu der Zeit. Sache der Zeit ist die Wissenschaft nur, inwiefern sie durch das Individuum sich ausspricht. Das Wissen an sich ist aber wenig Sache der Individualität als das Handeln an sich. Wie die wahre Handlung diejenige ist, die gleichsam im Namen der ganzen Gattung geschehen könnte, so [ist] das wahre Wissen [nur] dasjenige, worin nicht das Individuum sondern die Vernunft weiß. Die Unabhängigkeit des Wesens der Wissenschaft von der Zeit drückt sich in dem aus, daß sie Sache der Gattung ist, welche selbst ewig ist. Es ist also notwendig, daß, wie das Leben und Dasein, so die Wissenschaft sich von Individuum an Individuum, von Geschlecht zu Geschlecht mitteile. Überlieferung ist der Ausdruck ihres ewigen Lebens. ... Die Wissenschaft richtet gleich unmittelbar den Sinn auf diejenige Anschauung, die, eine dauernde Selbstgestaltung, unmittelbar zu der Identität mit sich und dadurch zu einem wahrhaft seligen Leben führt. Langsam erzieht die Erfahrung und das Leben, nicht ohne vielen Verlust der Zeit und der Kraft. Dem, der sich der Wissenschaft weiht, ist es vergönnt, die Erfahrung sich vorauszunehmen und das, was noch am Ende einzige Resultat des durchgebildetsten und erfahrungsreichsten Lebens sein kann, gleich unmittelbar und an sich selbst zu erkennen.

Friedrich Wilhelm J. Schelling

Vorlesungen über die Methode (Lehrart) des akademischen Studiums

Abstract

In this work we study the Polyakov-Quark-Meson model for $N_f = 2$ and $N_c = 3$ in a finite volume with the Functional Renormalization Group in a local potential approximation. We choose for the spatial momentum modes periodic and antiperiodic boundary conditions. Because of the lack of a zero mode in the case of antiperiodic boundary conditions we realize a clearly different behavior of the results. We solve the gap-equations for the Polyakov-loop-variable Φ and its conjugate Φ^* for different box sizes L as a function of the temperature T and the chemical potential μ. With these we calculate the pion decay constant and obtain the phase diagram and the pressure. We also study whether the results converge with increasing truncation order N and whether the finite volume results converge with increasing volume size to those of the infinite volume case. For the case of an infinite volume we further solve the gap-equations on all scales. Therefore, we include for the solution of the flow equation an indirect scale dependence of the Polyakov-loop-variable. With this we extend recent approaches which solve the gap-equations only at the infrared cutoff. We calculate with this several thermodynamic variables like the pressure and the trace anomaly. Additionally, we include a non-zero magnetic field and study the possibility of an inverse magnetic catalysis under variation of T_0 with the magnetic field.

Zusammenfassung

In dieser Arbeit untersuchen wir das Polyakov-Quark-Meson Modell für $N_f = 2$ und $N_c = 3$ mit Hilfe der Renormierungsgruppe in einem endlichen Volumen in einer Local Potential Approximation. Wir wählen für die Diskretisierung der räumlichen Impulsmoden periodische und antiperiodische Randbedingungen. Auf Grund des Fehlens der Nullmode bei antiperiodischen Randbedingungen stellen wir für diese ein deutlich anderes Verhalten der Ergebnisse fest. Wir lösen die Gap-Gleichungen und errechnen die Polyakov-Loop-Variable Φ und ihr Konjugiertes Φ^* für verschiedene Boxgrößen L als Funktion der Temperatur T und des chemischen Potentials μ. Mit diesen errechnen wir die Pionzerfallskonstante und damit das Phasendiagramm und den Druck. Wir untersuchen weiterhin ob die Ergebnisse mit zunehmender Trunkierungsordnung N konvergieren und ob sie für große Volumina mit den Ergebnisse im unendlichen Volumen übereinstimmen. Für den Fall des unendlichen Volumens lösen wir die Gap-Gleichungen auf allen Skalen und beziehen daher in die Lösung der Flussgleichungen eine indirekte Skalenabhängigkeit der Polyakov-Loop-Variable ein. Wir gehen damit über den bisherigen Zugang hinaus, bei dem die Gap-Gleichungen ausschließlich am Infrarotcutoff ausgewertet wurden. Wir bestimmen damit verschiedene thermodynamische Größen wie den Druck und die Trace-Anomalie. Weiterhin beziehen wir ein nicht verschwindenes magnetisches Feld ein und studieren die Möglichkeiten einer inversen magnetischen Katalysis unter Variation von T_0 mit dem magnetischen Feld.

Contents

1. Introduction and motivation **1**

2. Quantum Chromodynamics **5**
2.1. Experimental evidence for strong interaction 5
2.2. Finite temperature quantum field theory 6
2.3. Quantum chromodynamics as a quantum field theory of strong interaction 8
2.4. QCD and the necessity for non-perturbative methods 10

3. Functional Renormalization Group as a non-perturbative method in quantum field theory **13**
3.1. Physics on different scales 13
3.2. The Functional Renormalization Group 14

4. The Polyakov-Quark-Meson model as an effective model for QCD **19**
4.1. The Polyakov-loop as an order parameter for confinement 19
4.2. The Polyakov-Quark-Meson model 20
4.3. Flow equation for the Polyakov-Quark-Meson model 21
4.4. Polyakov-Quark-Meson model in mean field approximation 24
4.5. Polyakov-Quark-Meson model in infinite volume 28
4.5.1. Gap-Equations and the difference to mean field approximations 28
4.5.2. The influence of the σ-mass and the truncation order N on the chiral condensate and the pressure 30
4.5.3. Influence of different regulator functions on the chiral condensate and the pressure 33
4.5.4. Preliminaries for a scale dependence of Φ 34

5. Polyakov-Quark-Meson model in a finite volume **39**
5.1. Flow equation in a finite volume 39
5.2. Finite volume effects of Polyakov-loop-variable Φ 43
5.3. Pressure in a finite volume 44

6. Phase diagram and fluctuations in a finite volume **51**
6.1. Results for Φ and Φ^* in a finite volume with non-zero μ 51
6.2. Chiral condensate in a finite volume with non-zero μ 61
6.3. Pressure and Quark number density fluctuations in a finite volume with non-zero μ 70

7. Polyakov-Quark-Meson model in a non-zero magnetic field **75**
7.1. Flow equation with a non-vanishing magnetic field 75
7.2. Chiral catalysis and inverse catalysis effect 78

8. Conclusion and outlook **81**

A. Conventions **83**
A.1. Units 83
A.2. Euclidian space-time and Dirac-matrices 83

B. Calculation details of the flow equation **85**
B.1. The bosonic part of the flow equation 85
B.2. The fermionic part of the flow equation 86

Literature **89**

1. Introduction and motivation

According to the contemporary view nature is governed through four elementary forces. Gravitation, the electromagnetic interaction, the weak interaction and the strong interaction. Apart from gravitation, these interactions can be well described by the so called Standard-Model, a quantum field theory that is based on the principle of local gauge invariance. These interactions are explained by the exchange of gauge bosons: in the case of electromagnetism by the massless photon, the weak interaction by the massive electrically charged $W^{\pm}$- and neutral massive Z-bosons and in the case of strong interaction by the color charged, massless and self-interacting gluons. Understanding these interactions is mostly obtained through particle collisions and the scattering processes in particle accelerators. Quantum Electrodynamics (QED) is already well understood and theoretically much easier accessible, but the theory of strong interaction still has open problems.

As in the case of water or other substances like ammonia [1, 2, 3], also hadronic matter could exist in many phases. Figure 1.1 shows a recent conjectured phase diagram of the theory of strong interaction. Despite our provisional knowledge of this diagram, it is remarkable what diversity the different current approaches to Quantum Chromodynamics (QCD) deliver. Apart from the Quark-Gluon-Plasma (QGP) and the transition line to hadronic matter, the figure also shows, e.g. inhomogeneous phases, as well as the diversity of color-superconductivity. But the detailed structure of the whole phase diagram is still not known, thus many efforts in contemporary research are stressed. From first principles one can only calculate the $\mu = 0$ axis, because of the fermion-sign problem and contemporary avoidance of this problem allow only access to small μ or imaginary μ. The region with large chemical potential μ is hitherto only accessible through model calculations or perturbation theory.

From an experimental point of view, the deconfinement phase transition is of particular interest. Asymptotic freedom suggests, that at very high temperatures or very high densities hadronic matter no longer exists in form of mesons and nucleons, but in a phase called Quark-Gluon-Plasma. In this phase the interaction is weak and the quarks and gluons can move almost freely, which however that does not mean that the QGP is a free gas; on the contrary, it rather behaves as a strongly interacting system. Apart from heavy-ion colliders, QGP (and color-superconducting phase(s)) may exist in the core of neutron stars and short after the big bang[1].

Magnetic fields and not only densities of extreme magnitude play an important role in nature: some examples are magnetic neutron stars (magnetars) [5], primordial magnetic fields [6] a few microseconds after the big bang and of course in heavy-ion collisions [7, 8, 9]. Heavy-ion collisions are for performed at the Relativistic Heavy Ion Collider (RHIC) at Brookhaven National Laboratory, the Large Hadron Collider (LHC) at CERN, the Nuclotron based Ion Collider Facility (NICA) in Dubna, and in the future at the Facility for Antiproton and Ion Research (FAIR) in Darmstadt.

Both phases, the hadronic and the QGP are distinguished by the number of degrees of freedom. Due to the fractional charges of the quarks, the phase transition should be measurable by a change in the net charge fluctuation [10], furthermore a dependence on the system-size

[1] For details see, e.g. [4].

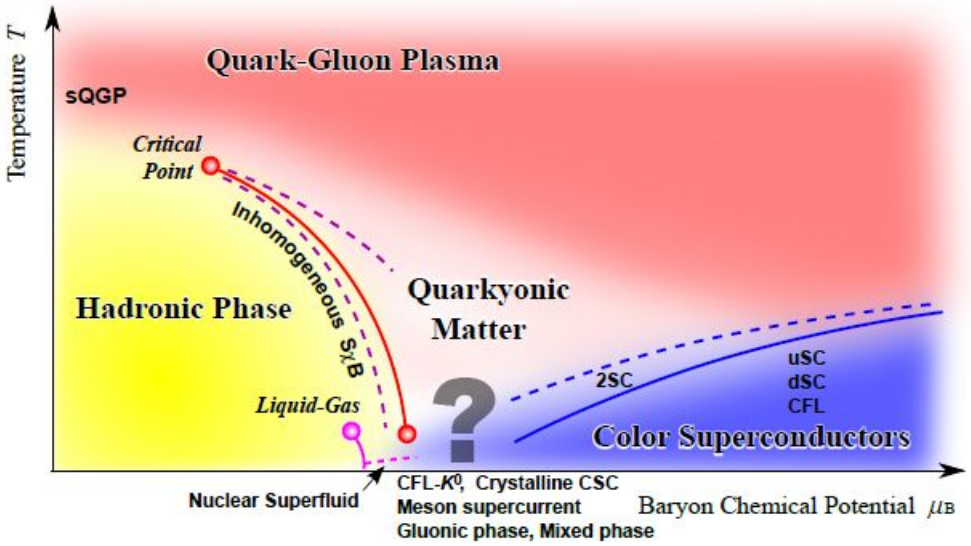

Figure 1.1.: Conjectured phase diagram of Quantum Chromodynamics. Figure taken from Ref. [17].

was observed [11].

In proton-proton collisions the phenomenon of jet-production was observed, which is regarded as an evidence of a substructure of the nucleons (see Section 2.1). In heavy-ion collisions this jet production is suppressed, which is called jet-quenching. This can be interpreted as an energy-loss due to the propagation through a hot and dense medium, i.e. the Quark-Gluon-Plasma [12]. Also, in the case of jet-quenching, a system-size dependence is detectable [13]. Furthermore, in heavy-ion collisions hadronic matter forms an expanding fireball of finite volume, e.g. Ref. [14, 15]. The finiteness of the fireball influences observables, for example the decay-rate of two-particle systems [16]. A theoretical reason for finite volume studies is the fact that Lattice-QCD is by definition performed in a finite volume. Therefore, finite volume model calculations can help to understand lattice results, see Section 2.4. This leads to the reasonable conclusion that in model calculations the finiteness of the system should be taken into account, i.e. the calculation should be performed in a finite volume.

Finite volume calculations have a long history. Numerous studies calculated finite volume effects of, e.g. the chiral condensate and the pion mass using chiral perturbation theory, see e.g. [18, 19, 20, 21, 22, 23]. Recent finite volume studies used functional methods, mainly the Functional Renormalization Group, but also the Dyson-Schwinger equations, e.g. Ref. [24, 25], and solved effective models like the $O(N)$ and the Quark-Meson model.

Within the Quark-Meson model, a low energy effective model of QCD (without any gluonic degrees of freedom) finite size scaling studies can be performed. Also, the universality class can be determined and compared with the corresponding Lattice-QCD results. If the universality class of QCD is known, we could understand more about the nature of the chiral phase transition. Furthermore, with a finite-size scaling analysis we have, in principle, a method to find the presumed critical end point in the QCD phase diagram [26, 27, 28, 29]. The curvature of the transition line in effective models can be compared with the one obtained from full QCD. The curvature of the chiral transition line in a finite volume was calculated in Ref. [30]. The location of the critical point of the phase diagram of the two flavor Quark-Meson model as a

function of the system size can be found in Ref. [31].

Finite volume studies were also performed with the Nambu-Jona-Lasinio model and the Polyakov-Nambu-Jona-Lasinio model (PNJL) in a mean field approximation [32, 33]. The PNJL model contains also gluonic degrees of freedom. The gluonic degrees of freedom, described by the color traced Polyakov-loop, are introduced through an effective potential, whose parameters are fixed such that it can reproduce known Lattice-QCD results, such as the deconfinement transition temperature of pure gauge theory. The same technique is used to implement gluonic degrees of freedom in the Quark-Meson model and thus to obtain the Polyakov-Quark-Meson model.

This thesis is organized as follows: The second chapter gives an introduction to QCD. We recapitulate experimental evidence for it, introduce the temperature in quantum field theory and present QCD a as local gauge theory with its symmetries. It then outlines the need in QCD for non-perturbative methods and what approaches in contemporary physics are used to study the phase diagram of QCD. The third chapter examines the concept of effective field theory and derive the Functional Renormalization Group in detail respectively the Wetterich-Equation. This non-perturbative approach will be used in this work. The fourth chapter presents the Polyakov-Quark-Meson model as an effective model for QCD and reproduces some previously known results in a mean field approximation. Before we perform finite volume calculations of the Polyakov-Quark-Meson model in a local potential approximation, we study selected aspects in infinite volume, which were not performed in previous infinite volume studies of this model (e.g. [34]), like the convergence behavior of the Taylor-expansion[2] of the flow equations and the solution of the gap-equations on all scales. With this we obtain a scale dependence of the Polyakov-loop-variable Φ (strictly speaking this is not the case because we do not have an explicit flow equation for Φ).

In chapter five we calculate the Polyakov-loop-variable Φ due to the gap-equations of the Polyakov-Quark-Meson model and the pressure in a finite volume for periodic and antiperiodic boundary conditions. We show how the results depend on the chosen boundary conditions. In the next chapter we augment our model with a finite chemical potential μ and calculate Φ, Φ^*, the pressure and the chiral condensate for different volume sizes, boundary conditions and for constant T_0 and T_0 as a function of μ. With the transition line of the chiral condensate we obtain the phase diagram of the model.

At last we consider a finite magnetic field B to the infinite volume Polyakov-Quark-Meson model. In a magnetic field electrically charged particles are forced to move in a plane. As in the case of finite volume the particles have to fulfill certain boundary conditions. We will show that for this model under variation of $T_0 = T_0(B)$ a significant inverse magnetic catalysis is not observed.

[2] In the case of other models like the Linear Sigma model convergence studies were performed see, e.g. Ref. [35].

2. Quantum Chromodynamics

2.1. Experimental evidence for strong interaction

The amazing number of discovered elementary particles leads to the assumption that there may exist a deeper substructure of matter which constitutes the whole number of particles. In the sixties the quark-model was invented which explains the diversity of elementary particles which are composed of smaller constituents, called quarks. The idea is that the mesons consist of a quark-antiquark pair $q\bar{q}$ and the baryons of three quarks qqq.

This model was successful, but the hadron Ω^- appears first as anomalous: this particle was supposed to consist of three strange quarks, whose spins are aligned with respect to an angular momentum of $J = 3/2$. Therefore this particle wave function is symmetric and obeys the wrong statistics. To cure this violation of the Pauli-principle one further quantum number, named *color*, was postulated, with color-number $N_c = 3$ for Ω^-.

The effect of the supposed existence of color should be perceivable in theoretical estimates of particular decay rates. For example, consider the theoretical estimation of the neutral pion decay amplitude $\pi^0 \to \gamma\gamma$ which is related to the triangular quark-loop[1]. With $N_c = 3$ we obtain

$$\Gamma(\pi^0 \to \gamma\gamma) = \left(\frac{N_c}{3}\right)^2 \frac{\alpha^2 m_\pi^3}{64\pi^3 f_\pi^2} = 7.73\,\mathrm{eV}, \tag{2.1}$$

with m_π the pion mass, f_π the pion decay constant and α the coupling constant of electromagnetic interaction [37, 38]. The experimental value is $\Gamma = 7.7 \pm 0.6$ eV.

If the quarks are real and not only a mathematical classification scheme, their existence should be indicated via scattering experiments of hadrons like e.g., deep inelastic electromagnetic lepton/hadron scattering, like $e^- p \to e^- p$. For small energies, the proton appears as a point-like particle, but for larger energies, the supposed substructures of the proton should become visible. On the level of experimental framework these substructures are often called *partons* and with QCD they are interpreted as *quarks*. To describe these substructures, so called parton distribution functions are defined. The measurements of these functions suggest, that protons are built from point-like spin 1/2-particles. For large momentum transfers or small distances they behave as if they were free particles. This shows that partons are asymptotically free [37, 39]. Asymptotically free quantum field theories have a negative beta function, and this is indeed the case in Quantum Chromodynamics[2]. Recent measurements confirm that the prediction for the QCD coupling constant is still valid in the TeV regime [40].

If the parton hypotheses is correct, they should also be detected during lepton annihilation processes: $e^+ + e^- \to q\bar{q} \to$ hadrons. Before hadronization[3] the quarks should exists as free particles and propagate in different directions. In 1975 such 2-jet process was observed. Analogous to the case of Quantum Electrodynamics one could assume, that in strong interaction

[1] This is due to the breaking of the classical $U(1)_A$-symmetry. The massless classical QCD-Lagrangian (see Chapter 2.3) is invariant under the following transformation: $\psi_L \to e^{-i\Theta}\psi_L$ and $\psi_R \to e^{i\Theta}\psi_R$. But this symmetry does not longer exist if QCD is quantized see, e.g. Ref. [36].

[2] See Section 2.4.

[3] Hadronization is called the process in that quarks form hadrons.

a similar process to the so called bremsstrahlung exists; a scattering process in which a *bosonic* parton, a gluon is emitted. Such a process was found in a 3-jet event: $e^+ + e^- \to gq\overline{q} \to$ hadrons. This furthermore indicates that the third parton has zero electric charge and spin zero [41]. In contrast to electromagnetism the gluon also has color-charge and is therefore self-interacting. The self-interaction of the gluons has been confirmed [42].

2.2. Finite temperature quantum field theory

In the following the *introduction* of temperature in quantum field theory is considered.[4]

In quantum field theory the generating functional of the n-point correlation functions, the so called partition function Z in Euclidian space-time, is defined as

$$Z[J] = \int \mathfrak{D}\phi \, e^{-S[\phi,J]}. \tag{2.2}$$

The propagator is defined as the time-ordered two-point-correlation function, the second functional derivative of $Z[J]$ with respect to the external source J evaluated at $J = 0$

$$\begin{aligned} \langle 0 \,|T\phi(x_1)\phi(x_2)|\, 0\rangle &= \int \mathfrak{D}\phi \, \phi(x_1)\phi(x_2) e^{-S[\phi,J]} \\ &= \frac{1}{Z[J=0]} \left(\frac{\delta}{\delta J(x_1)}\right) \left(\frac{\delta}{\delta J(x_2)}\right) Z[J]|_{J=0}. \end{aligned} \tag{2.3}$$

From quantum statistics we know the expression for the partition function

$$Z = \mathfrak{Tr}\, e^{-\beta \hat{H}} = \int \mathrm{d}q \, \langle q| \, e^{-\beta \hat{H}} \, |q\rangle \tag{2.4}$$

and the time evolution of two fields is given by

$$\left\langle \phi_b(x)|e^{-it\hat{H}}|\phi_a(x)\right\rangle = \int_{\phi(0)=\phi_a}^{\phi(t)=\phi_b} \mathfrak{D}\phi \, e^{iS[\phi]} = \int_{\phi(0)=\phi_a}^{\phi(t)=\phi_b} \mathfrak{D}\phi \, e^{i\int_0^t \mathrm{d}^4x \mathcal{L}[\phi]}, \tag{2.5}$$

while $\hat{H}$ is the Hamiltonian of the system and t the time. Apparently, the factor $e^{-\beta\hat{H}}$ can be interpreted as a time-evolution operator $T(t) = e^{-it\hat{H}}$ evolving imaginary time on a closed path $[0, \beta]$. Hereby β is the so called inverse temperature $\beta = 1/T$. Thus, the generating functional of the thermal correlation function has the following form

$$Z[\beta, J] = \int \mathfrak{D}\phi \, e^{-\int_0^\beta \mathrm{d}\, x_4 \int \mathrm{d}^3x \{\mathcal{L}(\phi(\vec{x},x_4)) - J(\vec{x},x_4)\phi(\vec{x},x_4)\}}. \tag{2.6}$$

For the thermal propagator we obtain

$$\begin{aligned} \langle |T\phi(x_1)\phi(x_2)| \rangle_\beta &= \int \mathfrak{D}\phi \, \phi(x_1)\phi(x_2) e^{-S[\beta,\phi,J]} \\ &= \frac{1}{Z[\beta, J=0]} \left(\frac{\delta}{\delta J(x_1)}\right) \left(\frac{\delta}{\delta J(x_2)}\right) Z[\beta, J]|_{J=0}. \end{aligned} \tag{2.7}$$

[4] For more details see, e.g. [43, 44, 45].

The thermal expectation value of an operator $\hat{O}$ is defined as

$$\left\langle \hat{O} \right\rangle_\beta = \frac{1}{Z[\beta,0]} \mathfrak{Tr}\left(\hat{O} e^{-\beta \hat{H}} \right), \tag{2.8}$$

with $\hat{O} = T\left\{\phi(\vec{x}_1,0)\phi(\vec{x}_2,-ix_4)\right\}$.

For the time ordered product of two fields we can write

$$\begin{aligned}
\langle T\left\{\phi(\vec{x}_1,0)\phi(\vec{x}_2,-ix_4)\right\}\rangle &= \frac{1}{Z[\beta,0]} \mathfrak{Tr}\left(e^{-\beta\hat{H}} \phi(\vec{x},0)\phi(\vec{x},-ix_4) \right) \\
&\overset{x_4 \geq 0}{=} \frac{1}{Z[\beta,0]} \mathfrak{Tr}\left(e^{-\beta\hat{H}} \phi(\vec{x},-ix_4)\phi(\vec{x},0) \right) \\
&= \frac{1}{Z[\beta,0]} \mathfrak{Tr}\left(\phi(\vec{x},0) e^{-\beta\hat{H}} \phi(\vec{x},-ix_4) \right) \\
&= \frac{1}{Z[\beta,0]} \mathfrak{Tr}\left(e^{-\beta\hat{H}} e^{+\beta\hat{H}} \phi(\vec{x},0) e^{-\beta\hat{H}} \phi(\vec{x},-ix_4) \right) \\
&= \frac{1}{Z[\beta,0]} \mathfrak{Tr}\left(e^{-\beta\hat{H}} \phi(\vec{x},-i\beta)\phi(\vec{x},-ix_4) \right).
\end{aligned} \tag{2.9}$$

In the third step we have used the identity $\mathfrak{Tr}(ABC) = \mathfrak{Tr}(BCA)$.

Here $\phi(\vec{x},-ix_4) = e^{+\beta\hat{H}}\phi(\vec{x},0)e^{-\beta\hat{H}}$ is the imaginary time analogy to the real time evolution $\phi(\vec{x},t) = e^{+it\hat{H}}\phi(\vec{x},0)e^{-it\hat{H}}$.
We get:

$$T\left\{\phi(\vec{x}_1,0)\phi(\vec{x}_2,-ix_4)\right\} = T\left\{\phi(\vec{x}_1,-i\beta)\phi(\vec{x}_2,-ix_4)\right\}. \tag{2.10}$$

With this we can show, that the thermal propagators and thus the fields ϕ have periodic boundary conditions with respect to the direction of imaginary time

$$\phi(\vec{x},\beta) = \phi(\vec{x},0). \tag{2.11}$$

We can expand these fields in the following way

$$\phi(\vec{x},x_4) = \sqrt{\frac{\beta}{V}} \sum_{n=-\infty}^{\infty} \sum_p \left(e^{i(\vec{p}\cdot\vec{x}+\omega_n x_4)} \phi_n(p) \right). \tag{2.12}$$

With the condition of periodicity we obtain for the Matsubara frequencies w_n

$$\omega_n = 2\pi n T. \tag{2.13}$$

The argumentation for the fermionic case is analogous. The difference to the bosonic case has its reason in the anti-commuting character of the fermionic field operators, due to their different statistical behavior,

$$\psi(\vec{x},0) = -\psi(\vec{x},\beta). \tag{2.14}$$

This implies that the Matsubara frequencies for the fermionic fields ν_n are

$$\nu_n = (2n+1)\,\pi T. \tag{2.15}$$

2.3. Quantum chromodynamics as a quantum field theory of strong interaction

The Quantum Chromodynamic is a non-abelian quantum field theory that is defined by the following Lagrangian

$$\mathcal{L} = \overline{\psi}^{\alpha} \left(i \not{D}_{\alpha\beta} - m\delta_{\alpha\beta} \right) \psi^{\beta} - \frac{1}{4} F^{a}_{\mu\nu} F^{\mu\nu}_{a}, \tag{2.16}$$

with $\not{D} = \gamma^{\mu} D_{\mu}$ and the covariant derivative

$$D_{\mu} = \partial_{\mu} + igt^{a} A^{a}_{\mu}. \tag{2.17}$$

g denotes the QCD coupling constant, m the quark mass. If different quark flavors N_f like up (u), down (d), and strange (s) are taken into account, m is a diagonal matrix of size $N_f \times N_f$: $m = \mathrm{diag}\left(\mathrm{m_u}, \mathrm{m_d}, \mathrm{m_s}, ..., \mathrm{m_f}\right)$. $\lambda^a = 2t^a$ are the Gell-Mann matrices, and t^a the generators of the $SU(3)_c$ algebra. These matrices are of size 3×3 and traceless. A^a_μ are the corresponding gauge fields. α, the color index runs form 1 to 3 and a from 1 to 8. ψ^β and its Dirac-conjugate $\overline{\psi}^{\alpha}$ are the fermionic fields. The generator matrices conform to the following relation

$$\left[t^a, t^b \right] = i f_{abc} t^c, \tag{2.18}$$

and furthermore

$$\mathrm{tr}\left(t^a t^b \right) = \frac{1}{2} \delta_{ab}. \tag{2.19}$$

f_{abc} denote the so called structure constants of the algebra.

The full expression of the field-strength tensor $F^{\alpha}_{\mu\nu}$ reads

$$F^{a}_{\mu\nu} = \partial_{\mu} A^{a}_{\nu} - \partial_{\nu} A^{a}_{\mu} - g f_{abc} A^{a}_{\mu} A^{b}_{\nu}. \tag{2.20}$$

We also define for convenience:

$$\begin{aligned} F_{\mu\nu} &= t^a F^a_{\mu\nu}, \\ A_{\mu} &= t^a A^a_{\mu}. \end{aligned} \tag{2.21}$$

The difference to QED lies in the self-interaction of the gluon-fields. From this we can define the generalization of the electric and magnetic fields, the so called chromoelectric and chromomagnetic fields

$$\begin{aligned} E^i &= F^{i0}, \\ B^i &= -\frac{1}{2} \epsilon_{ijk} F^{jk}. \end{aligned} \tag{2.22}$$

In principle we can derive the classical equations of motion from this Lagrangian. In the case of pure $SU(3)$ we would obtain the non-linear generalizations of the Maxwell-equations. Despite their non-linearity, they actually have classical solutions [46].

The QCD-Lagrangian is invariant under $SU(3)_c$ gauge transformation

$$\begin{aligned} \psi(x) &\rightarrow U(x)\psi(x) \\ F_{\mu\nu} &\rightarrow U(x)F_{\mu\nu}U^\dagger(x) \\ D_\mu &\rightarrow U(x)D_\mu U^\dagger(x) \\ gA_\mu(x) &\rightarrow U(x)\left(gA_\mu(x) - i\partial_\mu\right)U^\dagger(x), \end{aligned} \tag{2.23}$$

with the unitary transformation

$$U(x) = e^{-i\Theta_a(x)t^a}. \tag{2.24}$$

This transformation matrix contains the real valued $\Theta_a(x)$, the eight rotation angles, which transform every point of space-time independently (local gauge transformation).

An explicit mass term for the gauge fields $\propto A_\mu A^\mu$ would break this gauge symmetry. For the case of massless quarks, the QCD-Lagrangian has an additional chiral symmetry, which means that the left- and right-handed components of the Dirac-spinors can be transformed independently[5]. An explicit mass term would mix components of different parity. Due to the finite masses of each quark, chiral symmetry is not realized in nature. If that was the case, each fermion of the hadron spectrum would have a partner of the same mass and opposite parity [47].

Nevertheless, at zero temperature this symmetry is spontaneously broken and in fact nucleons acquire most of their mass from breaking of chiral symmetry. The order parameter for the chiral phase transition is the so called chiral condensate $\langle\overline{\psi}\psi\rangle$. According to the Goldstone theorem, a spontaneously broken continuous (global) symmetry leads to the existence of so called massless Goldstone bosons [48]. In QCD these Goldstone-bosons are found to be the pions, which are not massless but have a small mass compared to the nucleon mass; which means that chiral symmetry is also explicitly broken, but because of the small mass of the pions, chiral symmetry is regarded as an approximate symmetry. Nevertheless this approximative symmetry is restored at a given temperature, and the chiral condensate *melts*. The order of this chiral phase transition in QCD is still under discussion; several model calculations suggest that, for the case of massless pions the transition is of second order, while more realistic ones for finite pion masses suggest a crossover, e.g. [49, 50].

Another important (global) symmetry of the $SU(3)$ group is the so called center symmetry. In order to maintain the periodic boundary conditions of the gauge fields

$$A_\mu\left(\vec{x}, x_4 + \beta\right) = A_\mu\left(\vec{x}, x_4\right), \tag{2.25}$$

they also have to be postulated for the gauge transformations

$$U\left(\vec{x}, x_4 + \beta\right) = U\left(\vec{x}, x_4\right). \tag{2.26}$$

Additionally the following transformation is possible

$$U\left(\vec{x}, x_4 + \beta\right) = hU\left(\vec{x}, x_4\right), \tag{2.27}$$

[5]The corresponding transformations can be found in Section 4.2

with a constant matrix $h \in SU(N)$.

If we perform such a transformation on the gluonic fields, we obtain the following

$$\begin{aligned} A_\mu^U(\vec{x}, x_4+\beta) &= U(\vec{x}, x_4+\beta)\left(A_\mu(\vec{x}, x_4+\beta)+\partial_\mu\right)U^\dagger(\vec{x}, x_4+\beta) \\ &= hU(\vec{x}, x_4)\left(A_\mu(\vec{x}, x_4)+\partial_\mu\right)U^\dagger(\vec{x}, x_4)\,h^\dagger \\ &= hA_\mu^U(\vec{x}, x_4)\,h^\dagger. \end{aligned} \tag{2.28}$$

The gauge field obeys the periodic boundary condition only if h commutes with A_μ. An element of a Lie group which commute with all other group elements is called the center $Z(N)$ of the group $SU(N)$. Taking this into account, we obtain a constraint for h

$$h = \mathbb{1}z, \tag{2.29}$$

with

$$z = e^{2\pi i \frac{n}{N}}, \quad n \in \{1, 2, .., N\}. \tag{2.30}$$

In QCD this center symmetry is broken due to the quark fields. They have to fulfill antiperiodic boundary conditions in the temporal direction. The quark fields therefore transform as follows

$$\begin{aligned} \psi^U(\vec{x}, x_4+\beta) &= U(\vec{x}, x_4+\beta)\,\psi(\vec{x}, x_4+\beta) \\ &= -zU(\vec{x}, x_4)\,\psi(\vec{x}, x_4) \\ &= -z\psi^U(\vec{x}, x_4). \end{aligned} \tag{2.31}$$

To fulfill this condition z has to be restricted to the value $z = 1$ and with this the center-symmetry is broken [51].
Considering all possible symmetries in physical QCD, only the local color $SU(3)_c$- and the global $U(1)_B$-symmetry survive. The latter is associated with the conserved baryon number according to the Noether theorem [36].

One further gauge invariant term could be added to the QCD-Lagrangian

$$\mathcal{L}_\Theta = \frac{\Theta}{32\pi^2} F^a_{\mu\nu}\tilde{F}_{a\mu\nu} \propto E^a B^a, \tag{2.32}$$

thereby $\tilde{F}_{a\mu\nu}$ is called the dual field-strength tensor. This term violates CP symmetry. So far there is no experimental evidence that CP-symmetry is violated by strong interaction, furthermore experimental results like the almost zero electromagnetic dipole of the neutron suggest that the parameter Θ is nearly zero. In fact, QCD gives no theoretical explanation for this [46, 52]. A possible solution was provided by R. Peccei and H. Quinn [53].

2.4. QCD and the necessity for non-perturbative methods

As demonstrated above, experiments show that strongly interacting particles seem to interact weakly at small distances or equivalently at large momenta. An adequate quantum field theory

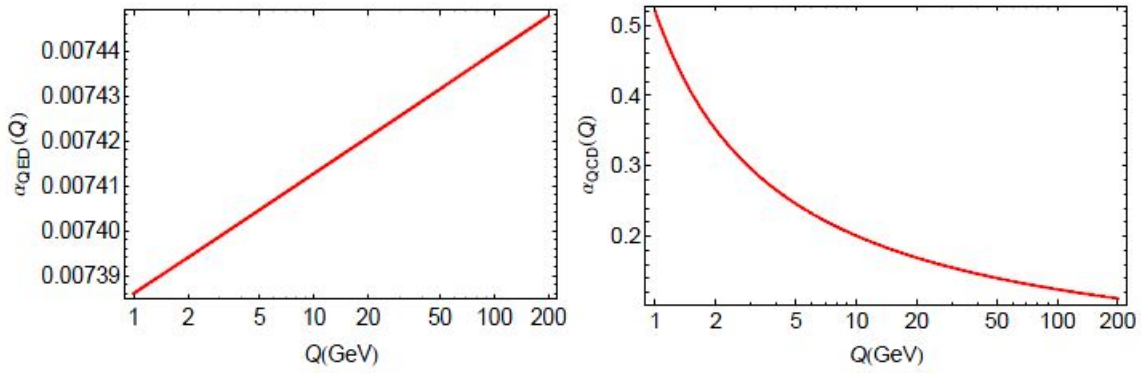

Figure 2.1.: Coupling constant of QED (left) and QCD (right) as a function of the momentum. Figure is taken from Ref. [56].

which contains this feature, should be asymptotically free. Asymptotic freedom means that the coupling constant of the theory should increase with decreasing energy scale, and at least at asymptotically large energy scales it should vanish; the opposite behavior, as in the case of Quantum Electrodynamics [54]. The slope of this is negative and defines the beta function. Various determinations of the coupling constant suggest that this is in Quantum Chromodynamics indeed the case [55]. For the low energy sector, the coupling constant is no longer much less than one, as in the case of QED, which means that perturbation theory is no longer applicable (Figure 2.1). The QCD vacuum is therefore a non-perturbative phenomenon.

To study QCD at low energies, we rely on so called non-perturbative methods. In general there exist two methods, which are complementary to each other: Functional methods and Lattice-QCD. Functional methods like the renormalization group and the Dyson-Schwinger approach [56] are commonly used approaches. In Lattice-QCD, the full QCD Lagrangian is discretized in all four Euclidian dimensions so this method, permits in principle the solution of QCD without any approximations [57]. The disadvantage is that the numerical effort is very large, and the discretization of QCD, with fermions is highly nontrivial. Lattice QCD is by definition restricted to finite volume and for finite chemical potential μ we obtain the so called fermion sign problem of the fermion determinant [58, 59]. This is not the case in other QCD-like theories like in two-color QCD and G_2 gauge theory (which contains $SU(3)$ as subgroup). Studying these may increase our understanding of open problems in QCD at finite density [60, 61, 62, 63, 64].

On the other hand, functional methods like the Functional Renormalization Group and the Dyson-Schwinger approach, are not restricted to finite volume and because of the absence of a fermionic sign problem there is in principle no restriction for any values of the chemical potential. To circumvent the fermion sign problem and study the QCD phase diagram at low density, there exist some methods [17] like, e.g. the expansion of the partition function in μ for $\frac{\mu}{T} \ll 1$. There are therefore no reliable lattice data available for large μ. The structure of the phase diagram of QCD is therefore still under discussion, in particular the possible existence of a critical endpoint was not confirmed or refuted yet [65, 66, 67, 68]. QCD for large chemical potentials and small temperatures, conditions which prevail in the core of neutron stars and may contain color superconducting phase(s), are not accessible to Lattice-QCD. In order to study the QCD phase diagram in this region one typically uses model calculations [69, 70, 71].

The equations which are obtained by the functional methods are generally not solvable with-

out approximations (sometimes also called truncations), because they induce an infinite amount of Feynman-diagrams. Nevertheless, functional methods can help to interpret lattice results and can give us an insight into the mechanisms of, e.g. chiral symmetry breaking and model calculations can give us an impression of possible physics in regions of the QCD phase diagram, in which lattice calculations cannot be performed (yet). Hence both methods complement one another.

For the purpose of studying the QCD phase diagram there are even more reasons for the necessity of non-perturbative methods. Phase transitions in general are a non-perturbative phenomena, since fluctuations are important on all scales near phase transition. Furthermore, finite temperature perturbation theory has its own problems, like infrared divergences, non-analytical structure and poor convergence of the perturbation expansion of the pressure which makes the application of non-perturbative methods seem even more reasonable [72, 73, 74, 75].

3. Functional Renormalization Group as a non-perturbative method in quantum field theory

3.1. Physics on different scales

Despite the fact that the validity of a fundamental theory like QCD is not restricted to a certain energy-scale[1], it is nevertheless reasonable to develop approximations which are adjusted to the regarded problem and its energy scale. For example, to describe low energy photon scattering (Rayleigh scattering) it is not necessary to apply full Quantum Electrodynamics. In nuclear physics it is appropriate to describe nuclei at low energies in terms of hadrons instead of quarks and gluons. At low energies it is not necessary to resolve the interior of the nucleons. The key idea of an effective field theory is the description of a phenomenon in degrees of freedom which are appropriate to the regarded energy scale [77, 78, 79].

For illustration suppose a system with two dimensional parameters which are connected with light (m) and heavy degrees of freedom (M). For the purpose of describing this system at low energy scale $E \propto m \ll M$ it is sufficient to use an effective Hamiltonian $\mathcal{H}^{eff}(\Phi_{light})$ which depends only on the light degrees of freedom. This theory is called an effective theory at low energies or long distances. Furthermore this Hamiltonian can be expressed in an expansion of the small dimensionless number m/M [46]. As an example for Quantum Chromodynamics, a possible low energy effective theory is called chiral effective field theory [80, 81, 82] (whose perturbative expansion is called chiral perturbation theory). However, this distinction is only valid, if we define a certain scale Λ, which separates these two regimes. The region $k > \Lambda$ is called the short-distance region, where the *fundamental* theory can be applied and the other, the long distance region $k < \Lambda$, where the effective theory is applied. In analogy to the scale Λ in the low energy regime, a fundamental scale Λ_{QCD} is also used in the QCD range. Λ_{QCD} is the scale at which the QCD coupling acquires the value one and the non-perturbative region is definitely reached. The validity of chiral perturbation theory has its justification because the light quarks and pions have a mass which is small compared to Λ_{QCD}.

Otherwise an effective model of, e.g. QCD is a model which can reproduce some features of QCD like chiral symmetry for vanishing quark masses, as in the case of the Quark-Meson model or those which include an order parameter for the deconfinement phase transition through an effective potential. Other features may not be included. An effective model is not an effective theory, because an effective model is constructed to imitate some selected features of the fundamental theory and cannot be obtained from a low energy expansion of the fundamental theory, but nevertheless with effective models one may gain insight into the mechanism of the full theory.

Consider the two limiting cases of a full quantum theory and the classical theory. In the first case all quantum fluctuations are taken into account and in the classical case no fluctuations are taken into account. These cases correspond to two limits of momentum scales, the infrared $k \to 0$ and the other the ultraviolet $k \to \Lambda \to \infty$. The physics between both extremes at a certain scale k means that all fluctuations above this scale are integrated out, so that we obtain

[1] According to current knowledge a validity limit was not observed yet see, e.g. Ref. [40]. Also there is no current experimental evidence for a validity limit of QED, see Ref. [76].

an effective theory at the scale k. The procedure to perform this systematically is the so called Renormalization Group.

Originally this idea came from condensed matter physics in connection with the Ising model [83] and block-spin transformation[2]. The idea is to combine the spins of a certain area to an effective *block-spin* and to rewrite the Ising model Lagrangian with these new variables. The number of degrees of freedom has been reduced and we obtain an effective theory corresponding to a certain scale. This can be performed iteratively. With this we obtain a flow of different effective theories at the corresponding scale k. Therefore, through the flow, different effective theories are *connected*. In this picture of Kadanoff the renormalization procedure is discrete, to perform it in a continuous way, one has to switch to momentum space and apply the Wilsonian idea of momentum shell integration [86]. These are the precedent basics of the Wetterich equation [87] (see the next section), with the difference to the latter that the fundamental object is the effective action Γ and that the momentum shell integration is made more controllable through a so called regulator function.

3.2. The Functional Renormalization Group

In the following we will derive the Functional Renormalization Group equation, or also known as Wetterich equation[3]. For this purpose we start with the generating functional of the n-point correlation function in Euclidian space

$$Z[J] = \int \mathfrak{D}\phi \, e^{-S[\phi,J]}. \tag{3.1}$$

This is, as previously explained, the quantum field theoretical generalization of the partition function of statistical physics. The partition function is defined as the integral over all field configurations, weighted by an exponential factor. $S[\phi, J]$ is the action in the presence of an external source J

$$S[\phi, J] = S[\phi] + \int \mathrm{d}^d x \, J(x)\phi(x). \tag{3.2}$$

If we differentiate n-times this functional with respect to the source J, we obtain the n-point time-ordered correlation function[4]

$$\langle 0 \,|T\phi(x_1) \cdots \phi(x_n)|\, 0\rangle = \int \mathfrak{D}\phi \, \phi(x_1) \cdots \phi(x_n) e^{-S[\phi,J]} \tag{3.3}$$

$$= \frac{1}{Z[J=0]} \left(\frac{\delta}{\delta J(x_1)}\right) \cdots \left(\frac{\delta}{\delta J(x_n)}\right) Z[J]\big|_{J=0}. \tag{3.4}$$

This functional generates also disconnected Feynman graphs; to remove them we calculate the logarithm of $Z[J]$ and arrive at the so called Schwinger-functional which generates only connected graphs

[2] For an introduction see, e.g. M.E. Fisher Renormalization group theory: its basis and formulation in statistical physics, in Ref. [84] and more elaborated in Ref.[85].

[3] For more details see, e.g. [88, 89, 90, 91, 92].

[4] For more information and explanation about the time ordered product T, one particle irreducible Feynman graphs (1-PI), the effective action Γ etc. see, e.g. [93, 94, 95].

$$W[J] = \log Z[J] = \log \int \mathfrak{D}\phi \, e^{-S[\phi,J]}. \tag{3.5}$$

If we apply a Legendre transform to this functional, we obtain the so called effective action Γ, a functional which generates only 1-PI-graphs

$$\Gamma[\phi_{cl}] = \sup_J \left(-W[J] + \int \mathrm{d}^d x \, J(y) \, \phi_{cl}(y) \right). \tag{3.6}$$

For a certain ϕ_{cl} the source J is chosen, for that $-W + \int J\phi$ reaches its supremum. Thereby ϕ_{cl} is the classical field, which is defined as the vacuum expectation value of the field operator $\langle 0 \, | \phi(x) | \, 0 \rangle_J$ in the presence of an external source (e.g. the external magnetic field in the case of a ferromagnet)

$$\phi_{cl}(x) = \frac{\int \mathfrak{D}\phi \, \phi(x) \, e^{-S[\phi,J]}}{\int \mathfrak{D}\phi \, e^{-S[\phi,J]}} = \frac{\delta W}{\delta J(x)}. \tag{3.7}$$

The external source can be obtained by derivating the effective action with respect to the classical field

$$\frac{\delta \Gamma[\phi_{cl}]}{\delta \phi_{cl}(x)} = -\int \mathrm{d}^d y \, \frac{\delta W[J]}{\delta J(y)} \frac{\delta J(y)}{\delta \phi_{cl}(x)} + \int \mathrm{d}^d y \, \frac{\delta J}{\delta \phi_{cl}(x)} \phi_{cl}(y) + J(x) = J(x). \tag{3.8}$$

With this result we are able to write down an implicit functional for the effective action $\Gamma[\phi_{cl}]$ in form of a functional integro-differential equation

$$\begin{aligned} \Gamma[\phi_{cl}] \quad &= \quad -\log \int \mathfrak{D}\phi \, e^{-S[\phi] + \int \frac{\delta \Gamma[\phi_{cl}]}{\delta \phi_{cl}} (\phi - \phi_{cl})}, \\ &\overset{\phi \to \phi + \phi_{cl}}{=} -\log \int \mathfrak{D}\phi \, e^{-S[\phi + \phi_{cl}] + \int \frac{\delta \Gamma[\phi_{cl}]}{\delta \phi_{cl}} \phi}. \end{aligned} \tag{3.9}$$

Here ϕ can be regarded as fluctuations around the classical field ϕ_{cl}. Of course such an equation is not easy to solve, especially in the infrared regime, where divergences occur.

This implicit representation of $\Gamma[\phi_{cl}]$ can be expanded around ϕ_{cl} according to

$$\Gamma[\phi_{cl}] = S[\phi_{cl}] - \log \int \mathfrak{D} \, \phi \, e^{-\int (\frac{\delta S[\phi_{cl}]}{\delta \phi} - \frac{\delta \Gamma[\phi_{cl}]}{\delta \phi_{cl}}) \phi - \int\int \phi \frac{\delta^2 S[\phi_{cl}]}{\delta \phi \delta \phi} \phi + \dots}. \tag{3.10}$$

We get with this result the semi-classical one loop approximation of the effective action

$$\Gamma[\phi_{cl}] = S[\phi_{cl}] + \frac{1}{2} \mathfrak{Tr} \log \left(\frac{\delta^2 S[\phi_{cl}]}{\delta \phi \delta \phi} \right). \tag{3.11}$$

Next we want to find an expression for the effective action which interpolates between the infrared, where all quantum fluctuations are taken into account, and the ultraviolet regime where the pure classical theory is valid. We look for an expression which has an ultraviolet and

an infrared cutoff and itself depends on an arbitrary momentum scale k. The scale dependent effective action is then defined as the generating functional of all 1-PI Feynman-graphs with an infrared cutoff k^5. To implement this we add a k-dependent, so called regulator term which regularizes the action in the infrared and has the form of a mass term

$$S_k[\phi] = S[\phi] + \Delta S_k[\phi], \tag{3.12}$$

where $\Delta S_k[\phi]$ is given by

$$\Delta S_k[\phi] = \frac{1}{2}\int \frac{\mathrm{d}^d p}{(2\pi)^d}\phi(-p)R_k(p)\phi(p). \tag{3.13}$$

Consequently, the Schwinger-functional becomes

$$W_k[J] = \log Z_k[J] = \log \int \mathfrak{D}\phi e^{-S_k[\phi,J]}. \tag{3.14}$$

For the purpose of maintaining convexity we apply for $\Gamma_k[\phi]$ a modified Legendre transformation

$$\Gamma_k[\phi] = \sup_J \left(-W_k[J(\phi)] + \int \mathrm{d}^d x J(x)\phi(x)\right) - \Delta S_k[\phi]. \tag{3.15}$$

The choice of $R_k(p)$ is not arbitrary, it has to obey the following properties:

- For the implementation of an infrared regularization, we require at fixed k

$$\lim_{p\to 0} R_k(p) > 0. \tag{3.16}$$

- If all quantum fluctuations are integrated out, we should obtain the full quantum action (at fixed p)

$$\lim_{k\to 0} R_k(p) = 0. \tag{3.17}$$

- In the case $k \to \Lambda$, we have to arrive at the classical action; this is the case if we impose

$$\lim_{k\to \Lambda} R_k(p) = \infty. \tag{3.18}$$

These three conditions are achieved by a regulator of the form

$$R_k(p^2) \propto p^2 r\left(\frac{p^2}{k^2}\right). \tag{3.19}$$

We also have to implement the Wilsonian idea of momentum shell integration [86]: that for the flow of Γ_k only a momentum shell around $p^2 \approx k^2$ contributes. We have already taken this into account with the required form of the regulator, because with $\partial_t R_k$ we obtain a peak-like structure. As an example for $R_k(p)$ a function of the form

$$R_k(p) \propto \frac{p^2}{e^{\frac{p^2}{k^2}} - 1} \tag{3.20}$$

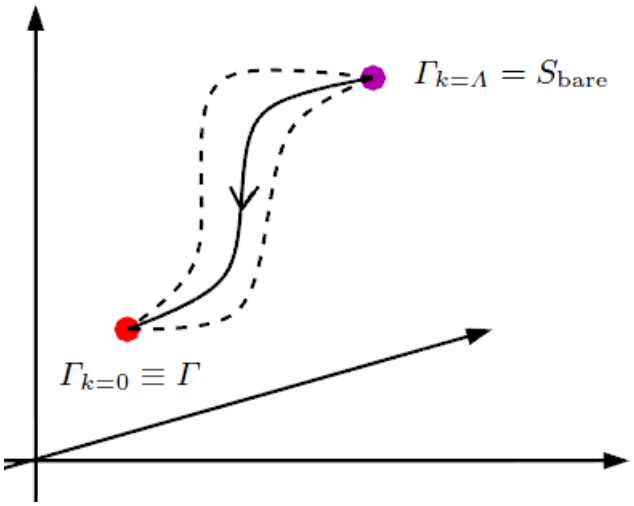

Figure 3.1.: RG-flow for different regulators in theory-space. In the infrared limit $k \to 0$ the different flows should be in agreement. The axes denote possible scale dependent couplings. Figure is taken from Ref. [88].

can be chosen.

Of course the possible choice of a regulator is not unique [92]. If we choose another one, the flow through *theory-space* (i.e. the flow of all scale dependent operators respectively couplings) would be altered because of the different paths of the momentum-shell integrations. Nevertheless, in the infrared limit $k \to 0$ these flows converge, due to the imposed conditions to the regulator, see Figure 3.1 for illustration.

Now we will derive the Functional Renormalization Group equation, or also called Wetterich equation, for the effective action Γ_k. This equation describes the changes of the effective action under variation of the scale k in terms of the full propagator ($\equiv \Gamma_k^{(2)}$). For this purpose we investigate how the scale dependent generating functional of the connected Greens functions change under variation of the scale

$$\begin{aligned} k\frac{\partial}{\partial k}W_k &= e^{-W_k} k\frac{\partial}{\partial k} e^{W_k} \\ &= e^{-W_k} \int \mathfrak{D}\phi \, (-\partial_t \Delta S_k[\phi]) e^{-S_k[\phi,J]} \\ &= -\frac{1}{2} \int \frac{\mathrm{d}^d p}{(2\pi)^d} \left(\partial_t R_k(p)\right) \frac{1}{Z_k} \int \mathfrak{D}\, \phi\phi(-p)\phi(p) e^{-S_k[\phi,J]}. \end{aligned} \tag{3.21}$$

Therein we defined $\partial_t = k\frac{\partial}{\partial k}$ and

$$\begin{aligned} G_k(p) &= \frac{1}{Z_k} \int \mathfrak{D}\phi\phi(-p)\phi(p) e^{-S_k[\phi,J]} \\ &= \langle \phi(-p)\phi(p) \rangle \end{aligned} \tag{3.22}$$

denotes the 2-point correlation function. In Eq. (3.21) we insert an *active zero* of the form

$$0 = -\langle \phi(-p) \rangle \langle \phi(p) \rangle + \langle \phi(-p) \rangle \langle \phi(p) \rangle . \tag{3.23}$$

[5] The scale dependent effective action Γ_k is also called effective average action.

This yields for the expression $\partial_t W_k$

$$\begin{aligned}\partial_t W_k = &- \frac{1}{2}\int \frac{\mathrm{d}^d p}{(2\pi)^d}\left\{\left(\partial_t R_k(p)\right)\left[\langle\phi(-p)\phi(p)\rangle - \langle\phi(-p)\rangle\,\langle\phi(p)\rangle\right]\right. \\ &+ \left.\left(\partial_t R_k(p)\right)\langle\phi(-p)\rangle\,\langle\phi(p)\rangle\right\}. \end{aligned} \tag{3.24}$$

The term in the rectangular bracket is the green function of the connected Feynman graphs: $G_{c,k}(p)$. With $\phi(p) = \langle\phi(p)\rangle$ and with the definition of ΔS_k we obtain

$$\partial_t W_k = -\frac{1}{2}\int \frac{\mathrm{d}^d p}{(2\pi)^d}\left[\left(\partial_t R_k(p)\right) G_{c,k}(p)\right] - \partial_t \Delta S_k[\phi]. \tag{3.25}$$

For the flow of the effective action $\Gamma_k[\phi]$ we get

$$\begin{aligned}\partial_t \Gamma_k[\phi] &= -\left[\partial_t W_k[J(\phi)] + \int \mathrm{d}^d x \frac{\delta W_k[J]}{\delta J(x)}\left(\partial_t J(x)\right)\right] \\ &\quad + \int \mathrm{d}^d x\left(\partial_t J(x)\right)\phi(x) - \partial_t \Delta S_k[\phi] \\ &= \frac{1}{2}\int \frac{\mathrm{d}^d p}{(2\pi)^d}\left[\left(\partial_t R_k(p)\right) G_{c,k}(p)\right], \end{aligned} \tag{3.26}$$

thereby $\frac{\delta W_k[J]}{\delta J(x)} = \phi(x)$. For the last step we rewrite $G_{c,k}(p)$ as a functional derivative of the scale dependent effective action Γ_k

$$G_{c,k}(p) = \frac{\delta^2 W}{\delta J \delta J} = \frac{\delta\phi}{\delta J} = \left(\frac{\delta J}{\delta\phi}\right)^{-1} = \left(\frac{\delta^2\Gamma_k}{\delta\phi\delta\phi} + R_k\right)^{-1}. \tag{3.27}$$

We finally arrive at the Wetterich-Equation [87]

$$\partial_t \Gamma_k = \frac{1}{2}\int \frac{\mathrm{d}^d p}{(2\pi)^d}\partial_t R_k(p)\left(\frac{\delta^2\Gamma_k}{\delta\phi(-p)\delta\phi(p)} + R_k(p)\right)^{-1}. \tag{3.28}$$

The Wetterich-Equation is exact and has a one loop structure, which contains the full propagator. In general, this equation is not solvable without approximations, because this equations induces an infinite number of Feynman-graphs. For the case of fermionic fields we also have to trace over all inner degrees of freedom, like Dirac- and color indices, which is often denoted by $\mathfrak{STr}$ (supertrace).

It should be mentioned that the imaginary time formalism and the exposed derivation of the Wetterich equation is only valid in thermal equilibrium. For considerations out of equilibrium real time formalism is required. This will not be regarded in the following, for an introduction, see Ref. [96].

4. The Polyakov-Quark-Meson model as an effective model for QCD

4.1. The Polyakov-loop as an order parameter for confinement

In the pure gauge theory the order parameter for the breaking of the center-symmetry $Z(3)$ of $SU(3)$, is called Polyakov-loop. The Polyakov-loop is a closed Wilson-loop in time-like direction

$$L(\vec{x}) = \frac{1}{N_c}\mathrm{tr}_c \mathcal{P} e^{i\int_0^\beta \mathrm{d}\, x_4\, A_4(x)}. \tag{4.1}$$

The thermal expectation value of the Polyakov-loop is defined as

$$\Phi(\vec{x}) = \langle L(\vec{x}) \rangle\,. \tag{4.2}$$

The color-traced thermal expectation value of the Polyakov-loop can be associated with the free energy F of a static (anti)quark-pair in the limit of infinite separation

$$\begin{aligned} \Phi^* &\propto e^{-\frac{1}{2}\beta F_\infty^{\bar{q}}(T)} \\ \Phi &\propto e^{-\frac{1}{2}\beta F_\infty^{q}(T)}. \end{aligned} \tag{4.3}$$

In the confined phase, one needs infinite energy to separate them from each other; therefore Φ is zero, and for the case of the deconfined phase, the separation energy is finite and thus the color traced thermal expectation value of the Polyakov-loop Φ has a finite value between zero and one. For the case of infinite quark-mass Φ is an order parameter and the order of the phase transition depends on the color number, e.g. of $N_c = 3$, the phase transition is of first order. For the case of finite quark-masses the confinement/deconfinement phase transition is a crossover and Φ is no longer a real order parameter. In the case of a non vanishing chemical potential μ, the Polyakov-loop and its conjugate are in general no longer identical.

From this we can infer, that the Polyakov-loop should break the $Z(3)$-symmetry.

$$\begin{aligned} L^U(\vec{x}) &= \frac{1}{N_c}\mathrm{tr}_c \mathcal{P} e^{i\int_0^\beta \mathrm{d}\, x_4\, A_0^U(\vec{x},x_4+\beta)} \\ &= \frac{1}{N_c}\mathrm{tr}_c \left[U(\vec{x},x_4+\beta)\mathcal{P} e^{i\int_0^\beta \mathrm{d}\, x_4\, A_0^U(\vec{x},x_4)} U^\dagger(\vec{x},x_4)\right] \\ &= \frac{1}{N_c}\mathrm{tr}_c \left[zU(\vec{x},x_4)\mathcal{P} e^{i\int_0^\beta \mathrm{d}\, x_4\, A_0^U(\vec{x},x_4)} U^\dagger(\vec{x},x_4)\right] \\ &= zL(\vec{x}). \end{aligned} \tag{4.4}$$

To maintain gauge invariance z is restricted to unity. If the expectation value of $L(\vec{x})$ vanishes in the confined phase, the center symmetry is conserved, otherwise, at high temperatures, this symmetry is spontaneously broken[1].

[1] For more on Polyakov-loop and deconfinement transition see, e.g. Ref. [97, 51].

4.2. The Polyakov-Quark-Meson model

The Polyakov-Quark-Meson model (PQM-model) is a low energy effective model for QCD, which contains a confinement/deconfinement phase transition in terms of a Polyakov-loop-variable Φ/Φ^* and a corresponding effective potential $\mathcal{U}$. This potential contains free parameters which are fixed to reproduce known lattice gauge theory results, like the critical temperature of the confinement/deconfinement transition.

In principle the PQM model is the extended Quark-Meson model through gluonic parts [2]. For vanishing quark masses (chiral limit) this model has a chiral symmetry $SU(2)_A \times SU(2)_V$ (which is isomorph to $O(4)$), which leaves the Lagrangian to remain invariant under the following transformations: the vector transformation

$$\begin{aligned} \psi &\rightarrow e^{-i\frac{\vec{\tau}}{2}\vec{\Theta}}\psi, \\ \overline{\psi} &\rightarrow e^{i\frac{\vec{\tau}}{2}\vec{\Theta}}\overline{\psi}, \end{aligned} \tag{4.5}$$

and the axial-vector transformation

$$\begin{aligned} \psi &\rightarrow e^{-i\gamma_5\frac{\vec{\tau}}{2}\vec{\Theta}}\psi, \\ \overline{\psi} &\rightarrow e^{-i\gamma_5\frac{\vec{\tau}}{2}\vec{\Theta}}\overline{\psi}. \end{aligned} \tag{4.6}$$

This symmetry allows to separate the fields due to their helicity. Fields with different helicity would be mixed through an explicit mass term; an explicit mass term therefore breaks chiral symmetry.

This symmetry is spontaneously broken in the vacuum and is reduced to $SU(2)_V$ (isospin-symmetry). According to the Goldstone-theorem the spontaneous breaking of a continuous symmetry leads to the existence of so called Goldstone-bosons [48]. The mesonic part of the PQM model is $O(4)$-symmetric, but spontaneously broken to $O(3)$, which means that we obtain three pions of zero mass in the chiral limit and one massive σ-meson in this model. At high temperatures the chiral symmetry is restored and we have a second order phase transition for massless pions (and $N_f = 2$), otherwise a so called crossover, e.g. [49].

The Polyakov-loop potential $\mathcal{U}$ has a polynomial form in Φ and Φ^*, which is motivated by a Ginzburg-Landau ansatz for the potential [99]. The potential has to be $Z(3)$-symmetric, but it should break this symmetry spontaneously in its ground state. For the case of three colors, in absence of any quarks respective with quarks of infinite mass, it must have a first order phase transition. Therefore quadratic and quartic terms are needed to ensure that the potential has two minima, at $\Phi = 0$ and $\Phi > 0$. However, since these terms conserve $U(1)$-symmetry an additional term is needed to break down this symmetry to $Z(3)$. This can be achieved by including a cubic term

$$\frac{\mathcal{U}(\Phi, \Phi^*, T)}{T^4} = -\frac{b_2(T)}{2}\Phi\Phi^* - \frac{b_3}{6}\left(\Phi^3 + (\Phi^*)^3\right) + \frac{b_4}{4}\left(\Phi\Phi^*\right)^2, \tag{4.7}$$

with the temperature dependent function:

$$b_2(T) = a_0 + a_1\frac{T_0}{T} + a_2\left(\frac{T_0}{T}\right)^2 + a_3\left(\frac{T_0}{T}\right)^3. \tag{4.8}$$

[2] For details on the Quark-Meson model and how the terms of its Lagrangian are motivated see, e.g. [98].

The parameters have the following values: $a_0 = 6.75$, $a_1 = -1.95$, $a_2 = 2.625$, $a_3 = -7.44$, $b_3 = 0.75$ and $b_4 = 7.5$. This potential is also called the polynomial potential (pol).

As already shown in [100] the possible values of Φ of this potential in the high-temperature regime can be larger than one. To cure this misconception, two further Polyakov-loop potentials were derived. The so called logarithmic- (log) and the Fukushima-potential (fuku) [101, 102].

If we compare the logarithmic potential with the Ginzburg-Landau potential we see that the fourth order term is dropped, and it is substituted by a logarithmic term which is related to the path integral of the gauge fields A_μ^3 and A_μ^8. Because this term already breaks $U(1)$-symmetry, the cubic term can also be dropped. Thus the modified potential reads

$$\frac{\mathcal{U}_{\log}(\Phi, \Phi^*, T)}{T^4} = -\frac{a(T)}{2}\Phi\Phi^* + b(T)\log\left(1 - 6\Phi\Phi^* - 3(\Phi\Phi^*)^2 + 4(\Phi^3 + (\Phi^*)^3)\right), \tag{4.9}$$

where

$$\begin{aligned} a(T) &= a_0 + a_1\frac{T_0}{T} + a_2\left(\frac{T_0}{T}\right)^2, \\ b(T) &= b_3\left(\frac{T_0}{T}\right)^3, \end{aligned} \tag{4.10}$$

with $a_0 = 3.51$, $a_1 = -2.47$, $a_2 = 15.2$ and $b_3 = -1.75$. T_0 expresses the back-reaction of the fermionic to the gluonic sector and is a function of flavor and color number (and finite chemical potential μ). In pure gauge theory $N_f = 0$ for three colors it is set to $T_0 = 270$ MeV. For the case of $N_f = 2$ (and $\mu = 0$) the value of T_0 reads $T_0 = 208$ MeV.

Another effective potential, the Fukushima-potential also allows to include the transversal gluons

$$\mathcal{U}_{\text{fuku}}(\Phi, \Phi^*, T) = -bT\left(54e^{-a/T}\Phi\Phi^* + \log\left(1 - 6\Phi\Phi^* - 3(\Phi\Phi^*)^2 + 4(\Phi^3 + (\Phi^*)^3)\right)\right), \tag{4.11}$$

with $a = 0.664$ and $b = 0.1962$[3]. In QCD their contribution to thermodynamic properties becomes more important at very high temperatures [103].

4.3. Flow equation for the Polyakov-Quark-Meson model

The scale dependent Euclidian effective action Γ_k of the Polyakov-Quark-Meson model reads

$$\Gamma_k = \int \mathrm{d}^4\mathrm{x}\left\{Z_{k,\psi,\overline{\psi}}\,\overline{\psi}\left(\not{D} + g(\sigma + i\gamma_5\vec{\pi}\vec{\tau})\right)\psi + \mathcal{U}(\Phi, \Phi^*, T) + U_k\left(\sigma, \vec{\pi}\right) + \frac{Z_{k,\phi}}{2}(\partial_\mu\phi)^2\right\}, \tag{4.12}$$

where U_k is the scale dependent bosonic potential which depends on the four bosonic fields $\phi = (\sigma, \vec{\pi}) = \left(\sigma, \pi^0, \pi^1, \pi^2\right)$, which are abbreviated for convenience by $\rho = \frac{1}{2}\phi^2$, $\mathcal{U}$ the Polyakov-loop potential, $\vec{\tau}$ the Pauli-matrices, g the Yukawa-coupling, which is assumed to be scale independent and after all the covariant derivative $\not{D} = \gamma^\mu D_\mu$ which has the following form

$$D^\mu = \partial^\mu - (iA^\mu - \mu)\,\delta_\mu^4, \tag{4.13}$$

with

$$A^\mu = \frac{\lambda^a}{2} A^\mu_a, \;\; (a = 3, 8). \tag{4.14}$$

λ^a are the diagonal Gell-Mann matrices

$$\lambda_3 = \begin{pmatrix} 1 & 0 & 0 \\ 0 & -1 & 0 \\ 0 & 0 & 0 \end{pmatrix}, \lambda_8 = \frac{1}{\sqrt{3}} \begin{pmatrix} 1 & 0 & 0 \\ 0 & 1 & 0 \\ 0 & 0 & -2 \end{pmatrix}. \tag{4.15}$$

$Z_{k,\psi,\overline{\psi}}$ and $Z_{k,\phi}$ are the wavefunction renormalizations for the fermionic and bosonic fields. The spatial components of the gluon fields are not taken into account. The time component is regarded as a constant background field. Therefore the Polyakov-loops have the following form

$$\begin{aligned} L &= \frac{1}{N_c} \mathrm{tr}_c \mathcal{P} e^{i \int_0^\beta \mathrm{d}\, x_4 A_4(x)} = \frac{1}{N_c} \mathrm{tr}_c\, e^{i\beta A_4}, \\ L^\dagger &= \frac{1}{N_c} \mathrm{tr}_c \mathcal{P} e^{-i \int_0^\beta \mathrm{d}\, x_4 A_4(x)} = \frac{1}{N_c} \mathrm{tr}_c\, e^{-i\beta A_4}. \end{aligned} \tag{4.16}$$

Furthermore, the color-traced Polyakov-loop-variable and its conjugate have the following form

$$\begin{aligned} \Phi &= \frac{1}{N_c} \left(e^{\frac{i\beta}{2}(A_4^3 + \frac{A_4^8}{\sqrt{3}})} + e^{\frac{i\beta}{2}(-A_4^3 + \frac{A_4^8}{\sqrt{3}})} + e^{-i\beta(\frac{A_4^8}{\sqrt{3}})} \right), \\ \Phi^* &= \frac{1}{N_c} \left(e^{-\frac{i\beta}{2}(A_4^3 + \frac{A_4^8}{\sqrt{3}})} + e^{-\frac{i\beta}{2}(-A_4^3 + \frac{A_4^8}{\sqrt{3}})} + e^{i\beta(\frac{A_4^8}{\sqrt{3}})} \right). \end{aligned} \tag{4.17}$$

The PQM model consists of bosonic and fermionic degrees of freedom. The variation of the effective action Γ_k is described by the Wetterich equation as

$$\begin{aligned} \partial_t \Gamma_k &= \frac{1}{2} \mathfrak{Tr} \left\{ \partial_t R_{k,B} \left(\Gamma_k^{(2,0)}[\phi, \psi] + R_{k,B} \right)^{-1} \right\} \\ &- \mathfrak{Tr} \left\{ \partial_t R_{k,F} \left(\Gamma_k^{(0,2)}[\phi, \psi] + R_{k,F} \right)^{-1} \right\}. \end{aligned} \tag{4.18}$$

In order to evaluate this equation one has to rewrite the effective action (Eq. 4.12) in momentum space. The trace is performed over the flavor, color and Dirac indices and it also includes a momentum integration. To perform the momentum integration, the fields are considered as momentum independent and therefore the bosonic part is expanded around a constant background field and furthermore the scale and momentum dependence of the wave function renormalization of the bosonic and fermionic fields are neglected. Both are set to one, and as a consequence the corresponding anomalous dimension $\eta \propto \partial_k \log Z_k$ is zero[3]. This is called local potential approximation. If we neglect the Polyakov-loop potential and the gluonic fields, we reobtain the effective action respectively the Lagrangian of the Quark-Meson model.

The regulator functions $R_{k,B}$ and $R_{k,F}$ depend only on the spatial components of the momentum. The three dimensional regulator functions are given by:

[3]To obtain a flow equation for, e.g. $Z_{k,\phi}$ one has to expand the bosonic fields around a field with a small momentum dependence see, e.g. [104, 105].

$$R_{k,B} = \left(k^2 - \vec{p}^2\right) \Theta\left(k^2 - \vec{p}^2\right), \tag{4.19}$$

$$R_{k,F} = \not{p}\left(\sqrt{\frac{k^2}{\vec{p}^2}} - 1\right) \Theta\left(k^2 - \vec{p}^2\right). \tag{4.20}$$

The zeroth component of the momentum (respectively the fourth in Euclidian notation) is replaced by $p_4 \to \omega_n = 2\pi n T$ for the bosonic and $p_4 \to \nu_n = (2n+1)\pi T$ for the fermionic part. They are called Matsubara modes and arise due to quantum statistic. From the different statistical behavior of bosons and fermions we obtain periodic respectively antiperiodic boundary conditions. The zeroth component of the four dimensional momentum integral is replaced by the sum over the Matsubara modes, see Section 2.2,

$$\int \frac{\mathrm{d}^4 p}{(2\pi)^4} \to T \sum_{n=-\infty}^{\infty} \int \frac{\mathrm{d}^3 p}{(2\pi)^3}. \tag{4.21}$$

The flow equation is given by[4]

$$\partial_t \Gamma_k = \beta V \frac{k^5}{12\pi^2} \left(\frac{3}{E_\pi} \coth\left(\frac{E_\pi}{2T}\right) + \frac{1}{E_\sigma} \coth\left(\frac{E_\sigma}{2T}\right) - \frac{4N_c N_f}{E_q} \left\{1 - N - \overline{N}\right\} \right), \tag{4.22}$$

with

$$N(T, \mu, \Phi, \Phi^*) = \frac{1 + 2\Phi^* e^{\beta(E_q - \mu)} + \Phi e^{2\beta(E_q - \mu)}}{1 + 3\Phi e^{2\beta(E_q - \mu)} + 3\Phi^* e^{\beta(E_q - \mu)} + e^{3\beta(E_q - \mu)}}, \tag{4.23}$$

and

$$\overline{N}(T, \mu, \Phi, \Phi^*) = N(T, -\mu, \Phi^*, \Phi). \tag{4.24}$$

Thereby the energy is given by

$$E_i = \sqrt{k^2 + M_i^2}, \quad i \in \{q, \sigma, \pi\}, \tag{4.25}$$

with the quark mass and the pion and sigma masses

$$\begin{aligned} M_q^2 &= 2g^2\rho, \\ M_\pi^2 &= \partial_\rho U_k, \\ M_\sigma^2 &= \partial_\rho U_k + 2\rho \partial_\rho^2 U_k. \end{aligned} \tag{4.26}$$

Furthermore, we set the flavor and color number to $N_f = 2$ and $N_c = 3$. For $\Phi = \Phi^* = 1$ we reobtain the flow equation for the Quark-Meson model. In the case of a constant field background, the difference between effective action Γ_k and effective potential U_k is only a

[4] Calculation details can be found in Appendix B.

volume factor βV. This cancels out and we obtain a highly coupled non-linear differential equation for the effective potential U_k. To solve it we need to perform so called truncations. In this work we will use a Taylor-expansion, which means that the effective potential (Eq. 4.22) is expanded in a finite Taylor-series around a scale dependent minimum $\rho_{0,k}$. With the left hand side of the flow equation

$$U_k = \sum_{n=0}^{N} \left(\frac{a_{n,k}}{n!}(\rho - \rho_{0,k})^n\right) + c\sigma, \tag{4.27}$$

we can derive flow equations for the chiral order parameter $\rho_{0,k}$ and the couplings $a_{n,k}$. N is the truncation order, c is the explicit symmetry breaking which defines the mass of the pion. In the case of vanishing pion mass, we have a second order phase transition, for the case of a non-zero pion mass we obtain a crossover. The minimum of the bosonic potential

$$\left.\frac{\partial U_k(\rho,\sigma)}{\partial \sigma}\right|_{\rho=\rho_{0,k}} \stackrel{!}{=} 0 \tag{4.28}$$

should be the chiral condensate $\rho_{0,k}$. For this purpose we obtain the following condition for the coupling:

$$a_{1,k} = -\frac{c}{\sqrt{2\rho_{0,k}}}. \tag{4.29}$$

In the Polyakov-Quark-Meson model (and Quark-Meson model) the chiral condensate is due to the Goldberger-Treiman relation [98] connected to the pion decay constant with

$$\left\langle \overline{\psi}\psi \right\rangle = \langle \sigma \rangle = f_\pi = \sqrt{2\rho_{0,k}}. \tag{4.30}$$

Thus, in our approach *chiral condensate*, *scale dependent minimum*, *chiral order parameter* and *pion decay constant* describe the same physical effect.

4.4. Polyakov-Quark-Meson model in mean field approximation

In a mean field approach[5] the bosonic fields are replaced by their expectation values: $\langle \sigma \rangle = \sigma =$ const and $\vec{\pi} = 0$. The mesons are assumed to be space-time independent. For the Lagrangian in a mean field approximation we obtain

$$\mathcal{L} = \overline{\psi} S_0^{-1} \psi + U(\sigma) + \mathcal{U}(\Phi, \Phi^*, T), \tag{4.31}$$

with

$$S_0^{-1} = \not{\partial} + g\sigma. \tag{4.32}$$

In the path integral the fermionic part can be integrated out

$$Z = \int \mathfrak{D}\overline{\psi}\,\mathfrak{D}\psi e^{-\int_0^\beta \mathrm{d}\,x_4 \int \mathrm{d}\,x^3 \left[\overline{\psi} S_0^{-1}\psi + U(\sigma) + \mathcal{U}(\Phi,\Phi^*)\right]} \tag{4.33}$$

[5] Mean field calculations were already performed in [100]. For pedagogical reasons some introductory results are recapitulated here.

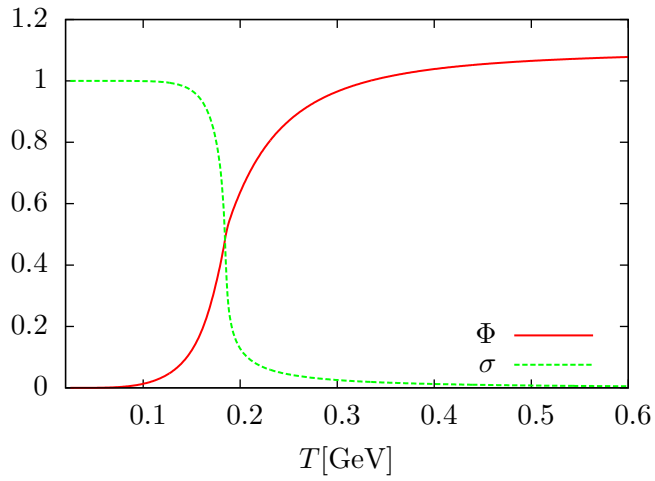

Figure 4.1.: Normalized chiral condensate σ and the Polyakov-loop-variable Φ as a function of temperature for vanishing chemical potential in mean field approximation.

After performing the color-trace[6] we obtain the following grand potential

$$\begin{aligned}\Omega &= -\frac{1}{\beta V_3}\log Z \\ &= -\frac{1}{V\beta}\mathfrak{Tr}\log\left(S_0^{-1}\right) + U(\sigma) + \mathcal{U}(\Phi,\Phi^*) \\ &= \Omega_{\bar{q}q} + U(\sigma) + \mathcal{U}(\Phi,\Phi^*),\end{aligned} \tag{4.34}$$

with

$$U(\sigma) = \frac{\lambda}{4!}(\sigma^2 - v^2) + c\sigma \tag{4.35}$$

and

$$\Omega_{\bar{q}q} = \Omega^{\beta}_{\bar{q}q} + \Omega^{0}_{\bar{q}q}. \tag{4.36}$$

The temperature dependent part of $\Omega_{\bar{q}q}$ has the following form

$$\begin{aligned}\Omega^{\beta}_{\bar{q}q} = -2TN_f\int\frac{d^3p}{(2\pi)^3} \quad & (\log[1 + 3\Phi^* e^{-\beta(E_q+\mu)} + 3\Phi e^{-2\beta(E_q+\mu)} + e^{-3\beta(E_q+\mu)}] \\ + \quad & \log[1 + 3\Phi e^{-\beta(E_q-\mu)} + 3\Phi^* e^{-2\beta(E_q-\mu)} + e^{-3\beta(E_q-\mu)}]).\end{aligned} \tag{4.37}$$

In the so called no-sea approximation the diverging zero point energy $\Omega^0_{\bar{q}q}$ is neglected,

$$\Omega^{0}_{\bar{q}q} = -2N_f N_c\int\frac{\mathrm{d}^3p}{(2\pi)^3}E_q. \tag{4.38}$$

[6] Calculational details are omitted here see, e.g. [106].

$E_q = \sqrt{p^2 + M_q^2}$, with $M_q = g\sigma$. Hereby g denotes the Yukawa-coupling.

For $\Phi = \Phi^* = 1$ we reproduce the grand potential of the Quark-Meson model in a mean field approximation. The values of Φ, Φ^* and σ are obtained by the stationary conditions

$$\frac{\partial\Omega}{\partial\Phi} = \frac{\partial\Omega}{\partial\Phi^*} = \frac{\partial\Omega}{\partial\sigma} \stackrel{!}{=} 0. \tag{4.39}$$

We obtain that the chiral condensate σ vanishes in a high temperature regime, and the Polyakov-loop-variable shows the opposite behavior, see Figure 4.1.

The parameters λ, c, and v of $U(\sigma)$ are fixed such that we obtain at vanishing temperature and chemical potential the physical pion mass $M_\pi = 138$ MeV and the physical pion decay constant $f_\pi = 93$ MeV: $\lambda = 118.44$, $v = 0.0878$ GeV and $c = -1.77108 \cdot 10^{-3}$ GeV^2. With $g = 3.2$ we obtain for the quark mass $M_q \approx 300$ MeV in the vacuum [100].

We obtain the pressure through the grand potential

$$P = -\Omega. \tag{4.40}$$

The pressure has to be normalized so that it vanishes for vanishing temperature and chemical potential. With the pressure we can calculate the remaining thermodynamic variables

$$\begin{aligned} S &= \frac{\partial P}{\partial T}, \\ \epsilon &= -P + TS, \\ C_V &= T\frac{\partial^2 P}{\partial T^2} = T\frac{\partial S}{\partial T} = \frac{\partial \epsilon}{\partial T}, \\ c_s^2 &= \frac{\partial P}{\partial T}\Big/\frac{\partial \epsilon}{\partial T} = \frac{S}{C_V}, \\ \Delta &= \epsilon - 3P = -4P + TS, \end{aligned} \tag{4.41}$$

with entropy S, energy density ϵ, heat capacity C_V, speed of sound c_s^2 and interaction measure. Δ is also called the trace anomaly. The quantity Δ/ϵ is called conformal measure. We will plot in this work only the dimensionless temperature-normalized thermodynamic variables, like P/T^4, S/T^3 and for convenience these still name as pressure, entropy et cetera.

For the Stefan-Boltzmann limit of the pressure we obtain the following expression

$$\frac{P_{SB}}{T^4} = \frac{7\pi^2 N_f N_c}{180} + (N_c^2 - 1)\frac{\pi^2}{45} \approx 4.0575, \tag{4.42}$$

where the second part accounts for the gluonic distribution. Analogously the other variables can be expressed in terms of the Stefan-Boltzmann limit of the pressure

$$\begin{aligned} \frac{s_{SB}}{T^3} &= 4\frac{P_{SB}}{T^4} \approx 16.23, \\ \frac{\epsilon_{SB}}{T^4} &= -\frac{P_{SB}}{T^4} + \frac{s_{SB}}{T^3} \approx 12.1725, \\ \frac{C_{SB}}{T^3} &= 4\frac{\epsilon_{SB}}{T^4} \approx 48.69, \\ c_s^2 &= \frac{s_{SB}}{T^3}\Big/\frac{C_{SB}}{T^3} = \frac{1}{3}. \end{aligned} \tag{4.43}$$

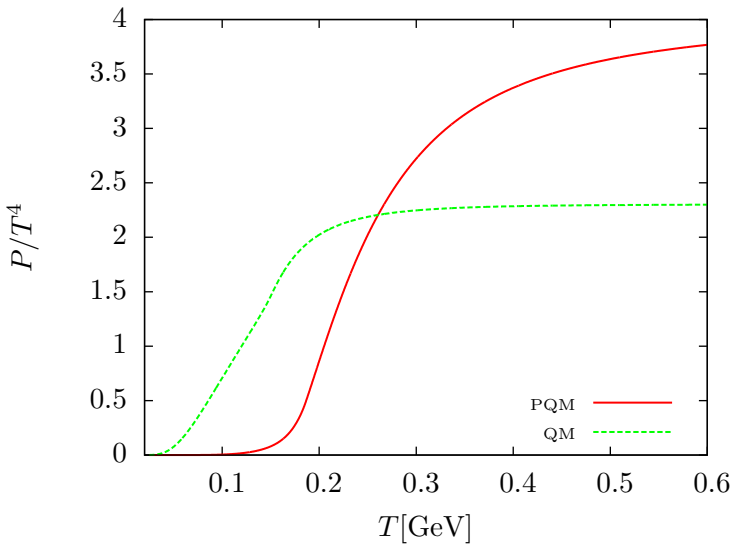

Figure 4.2.: P/T^4 for PQM- and QM-model in mean field approximation with physical pion mass and vanishing chemical potential.

The correct reproduction of the Stefan-Boltzmann limit indicates that at high temperature the Quark-Gluon-Plasma behaves like a non-interacting gas. At $T = 600$ MeV the pressure has reached its Stefan-Boltzmann limit to 93%. The pressure and Stefan-Boltzmann limit of the Quark-Meson model is smaller ≈ 2.3, due to the smaller number of degrees of freedom (without the gluonic ones), see Figure 4.2.

The value of the Polyakov-loop-variable is of course different for the other both regarded Polyakov-loop potentials (see Eq. 4.7, 4.9, 4.11) and for high temperatures the values of Φ remain below one, see Figure 4.3..

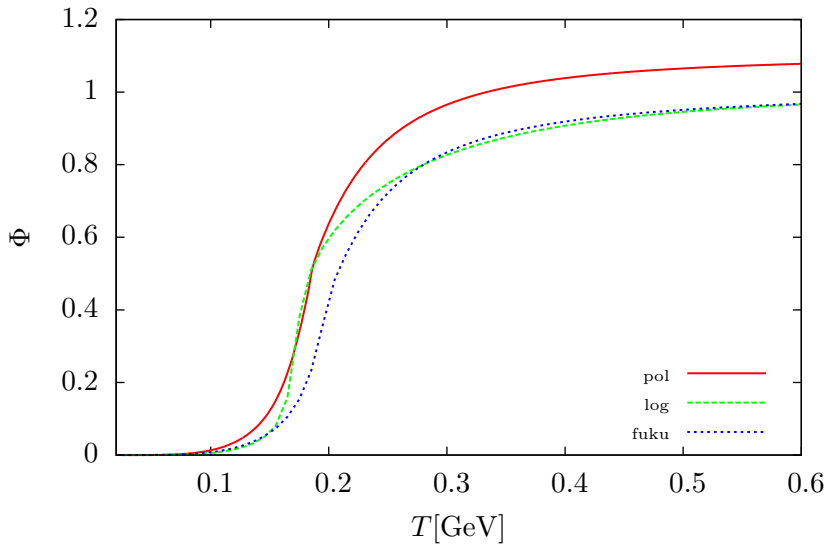

Figure 4.3.: Polyakov-loop-variable Φ as a function of temperature in mean field approximation for the different types of Polyakov-loop potentials.

4.5. Polyakov-Quark-Meson model in infinite volume

4.5.1. Gap-Equations and the difference to mean field approximations

The values for the Polyakov-loop-variables Φ and Φ^* are obtained by minimizing the grand potential:

$$U(T,\mu,\Phi,\Phi^*) = U_{k\to 0}(T,\mu,\Phi,\Phi^*) + \mathcal{U}(T,\Phi,\Phi^*), \tag{4.44}$$

where $\mathcal{U}$ is the Polyakov-loop potential. For the parametrization of the potential the polynomial ansatz is chosen

$$\frac{\mathcal{U}(\Phi,\Phi^*,T)}{T^4} = -\frac{b_2(T)}{2}\Phi\Phi^* - \frac{b_3}{6}\left(\Phi^3 + (\Phi^*)^3\right) + \frac{b_4}{4}\left(\Phi\Phi^*\right)^2. \tag{4.45}$$

From the solution of the flow equations we obtain $U_{k\to 0}(T,\mu,\Phi,\Phi^*)$. This expression is the scale dependent potential

$$U_k = \sum_{n=0}^{N}\left(\frac{a_{n,k}}{n!}(\rho-\rho_{0,k})^n\right) + c\sigma, \tag{4.46}$$

evaluated for the solution of the flow equations at $\rho = \rho_{0,k}$, at least the coefficient $a_{0,k}$ remains. N denotes the truncation order. We obtain the values for the Polyakov-loop-variable by the stationary conditions (gap-equations)

$$\frac{\partial U_{k\to 0}}{\partial \Phi} + \frac{\partial \mathcal{U}}{\partial \Phi} = 0. \tag{4.47}$$

Analogously we obtain such a condition for Φ^*. For the purpose of solving this gap equation, we solve the flow equations and insert the solution in the terms $\partial\mathcal{U}/\partial\Phi$ and in the derivation of the flow equation of $a_{0,k}$ (all terms which does not depend on Φ and Φ^* are omitted)

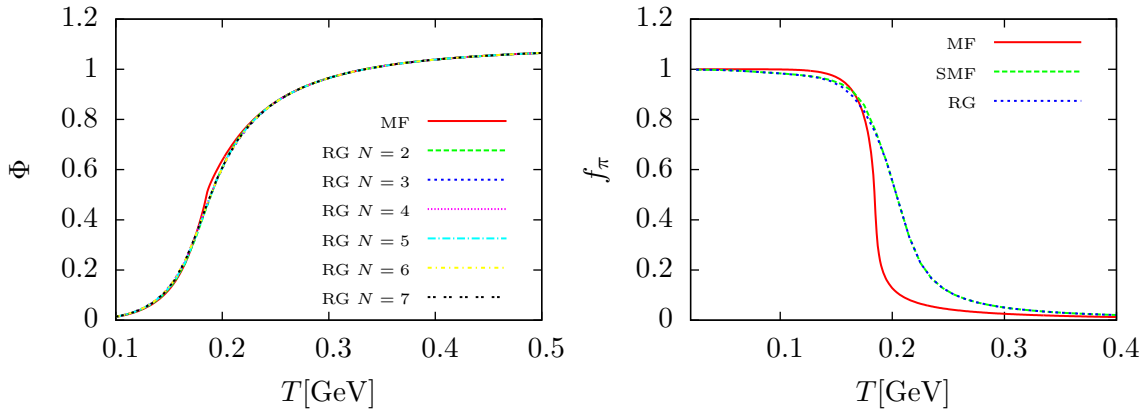

Figure 4.4.: (a): Polyakov-loop-variable in mean field approximation compared to those with different truncation orders in infinite volume and physical pion mass, (b): Normalized pion decay constant $f_\pi = f_\pi(T)/f_\pi(T=0)$ as a function of temperature T. Comparison of the solution of mean field (MF), semi mean field approximation (SMF) and from Functional Renormalization Group flow (RG).

$$k\partial_k \frac{\partial a_{0,k}}{\partial \Phi} = \frac{\partial}{\partial \Phi}\left(\frac{4N_c N_f k^5}{12\pi^2 E_q}(N+\overline{N})\right). \tag{4.48}$$

$k\partial_k\, \partial a_{0,k}/\partial\Phi$ has to be integrated with respect to k from ultraviolet Λ to the infrared $k \to 0$. The same holds for Φ^*. For vanishing chemical potential the values of Φ and Φ^* are identical.

In infinite volume we obtain from the relation Eq. 4.40 and $\Omega = U_k|_{\rho=\rho_{0,k}}$ the following flow equation for the effective action respectively the pressure

$$\partial_t p = -T\,\frac{\partial}{\partial V}\partial_t \Gamma_k\Big|_{\rho=\rho_{0,k}} = -\,\partial_t U_k|_{\rho=\rho_{0,k}}\,. \tag{4.49}$$

From that the pressure is given by

$$p = -a_{0,k\to 0} = -\int_\Lambda^{k\to 0} dt\;\; \partial t U_k\Big|_{\rho=\rho_{0,k}}\,. \tag{4.50}$$

The values of the Polyakov-loop potential in infinite volume are almost the same as in the mean field approximation and they are independent of the truncation order. For Functional Renormalization Group calculations (RG) in infinite volume we can use the values of Φ from the mean field approximation (which we refer to as semi-mean-field, SMF). For, e.g. the case of the normalized chiral condensate, we do not observe significant differences. Compared to mean field it has a larger crossover temperature[7], see Figure 4.4.

In the mean field approximation the explicit temperature independent term $\Omega^0_{\bar{q}q}$ was neglected. In principle it has influence on the solution of the gap equations if it will be included

[7] As already mentioned in Ref. [34].

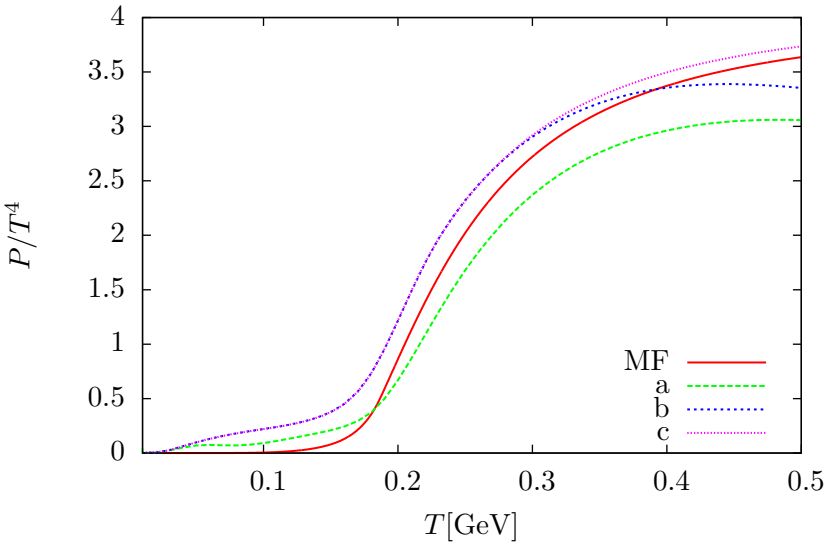

Figure 4.5.: Pressure in mean field compared with RG (a) with zero point term and $\Lambda = 3$ GeV, (b) without zero point term and $\Lambda = 3$ GeV, (c) as (b) but $\Lambda = 10$ GeV.

and thus this term contributes to the observables [107, 108]. The flow equations contain also explicit temperature independent terms, but their negligence is unnecessary, because these terms does not diverge, due to the finite cutoff Λ. Nevertheless, in all cases the pressure has to be normalized, so that it vanishes at zero temperature. If we neglect the explicit temperature independent terms the pressure is automatically normalized. But however these terms contribute implicitly to the pressure; they have the form $\propto 1/\sqrt{k^2 + M_i^2}$ ($i \in \{\pi, \sigma, q\}$, see Eq. 4.26) and of course the masses dependent on the temperature (due to the gap-equations). If they are neglected, their implicit contribution at a certain temperature is ignored. We call this result *pure thermal flow*. With the zero point term the pressure is smaller after normalization, than in mean field approximation. Figure 4.5 shows the results for the pressure compared to mean field and the pure thermal flow calculations. Furthermore, at large temperatures we can observe small finite cutoff effects. The cutoff pushes the pressure slightly down, but this is no longer the case if we increase the cutoff. We expect no cutoff effects if $2\pi T \ll \Lambda$. Of course the Polyakov-Quark-Meson model cannot give reliable physical information at such scale, because it is a low-energy model and it is evaluated in the infrared. The cutoff is used for regularization.

4.5.2. The influence of the σ-mass and the truncation order N on the chiral condensate and the pressure

Usually the σ mass is set to ≈ 600 MeV. Since there exists no such σ-particle in the in the particle spectrum [98], one has to ask, according to which criterion the mass should be adjusted.

We could vary the σ-mass and study how the results change. Unfortunately we cannot adjust at every truncation order N the same variation of values of the σ-mass; under the assumption that the flow should start in the ultraviolet region with manifest chiral symmetry. Otherwise the flow would start with broken chiral symmetry in the ultraviolet and then the chiral symmetry would be restored at some intermediate scale and finally in the infrared be

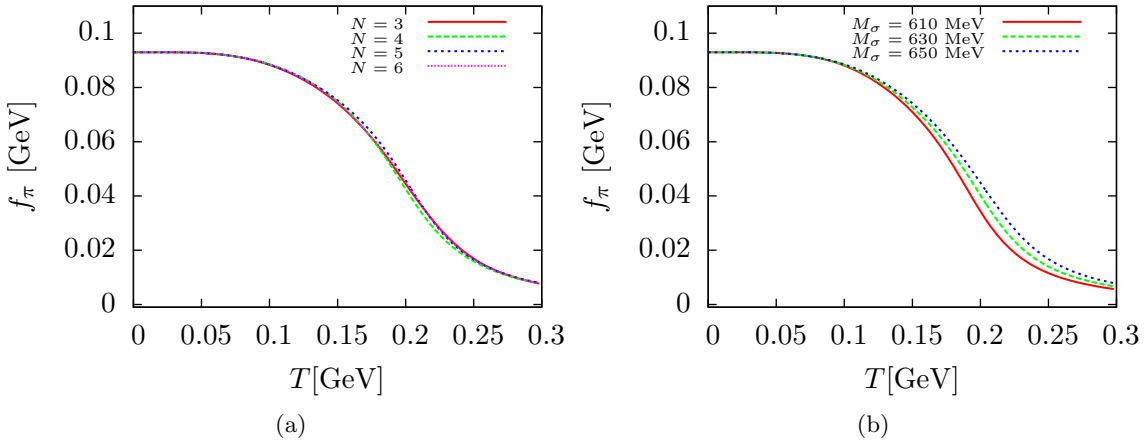

Figure 4.6.: (a) Pion decay constant for different truncation order N with $M_\sigma = 650$ MeV, (b) for $N = 6$ for different σ-masses.

broken again. Physically that does not make any sense[8]. If we take this into account the σ mass can be changed only by tens of MeV.

In infinite volume the Polyakov-loop-variable Φ does not depend on the sigma mass; then it is reasonable to study the σ mass dependence of the pressure and chiral condensate without gluonic contributions. We can study the dependence of the truncation order with fixed σ-mass or the σ mass dependence with fixed truncation order N.

The results show a good convergence for the pion decay constant if the truncation order N is increased. The convergence behavior for the pressure is suboptimal, especially in the region of $\approx$ 100 MeV, see Figure 4.7*a*. This is not the case, if we compute the pure thermal flow of the pressure (Figure 4.7*b*). We can conclude that the suboptimal convergence behavior is caused by the zero point term. If we take the gluonic contribution into account this changes nothing qualitatively in the behavior of the zero point term. The conclusion is that for further computations it is sufficient to expand the flow equation up to $\phi^6 \equiv \rho^3$, i.e. to the truncation order of $N = 3$, Figures 4.6*a*, 4.7$a - b$. If this is also sufficient for finite volume and chemical potential cannot be decided here yet. If we vary the adjusted σ-mass (at $T = 0$) the obtained dependence for the pressure and pion decay constant is weak, as an example for $N = 6$ the corresponding results are shown in Figure 4.6*b* and 4.7*c*.

[8]To study convergence one could in principle ignore this, but nevertheless the physical interpretation is problematic.

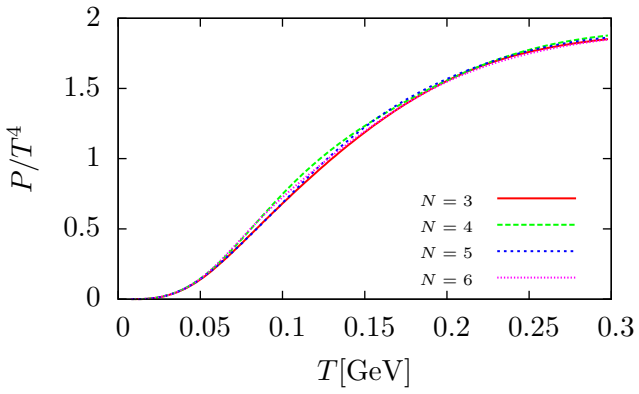

(a)

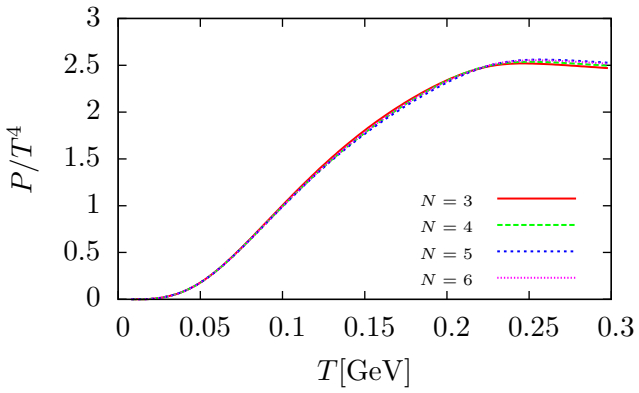

(b)

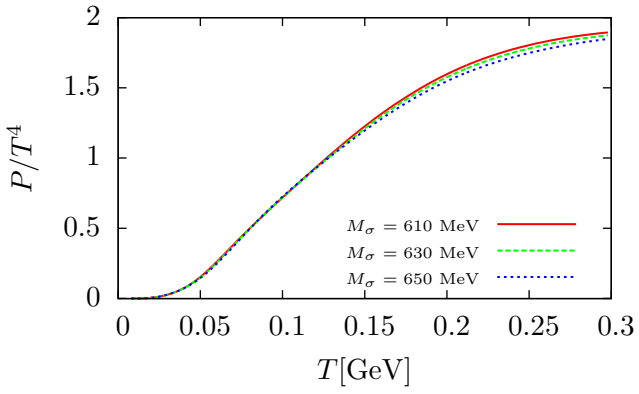

(c)

Figure 4.7.: (a) Pressure for different truncation orders N, (b) pure thermal flow of the pressure for different truncation orders, (c) pressure for $N = 6$ for different σ-masses.

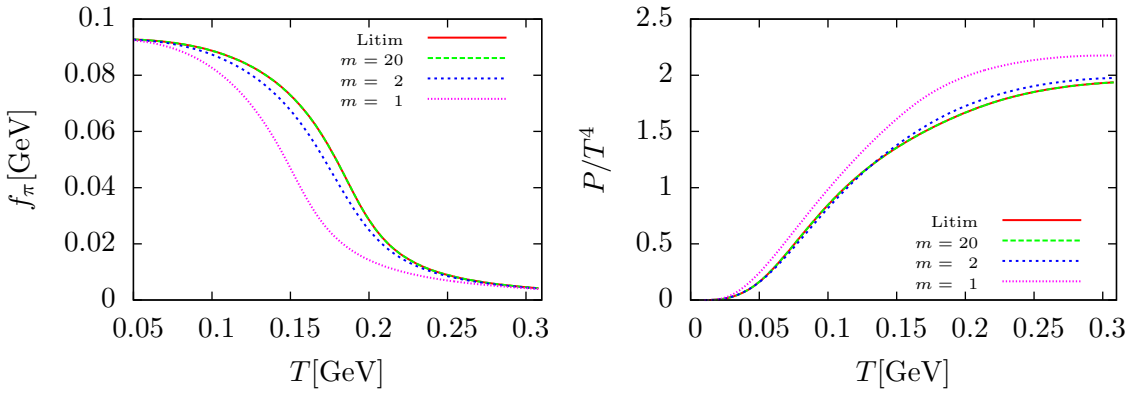

(a) (b)

Figure 4.8.: The pion decay constant f_π (a) and (b) the pressure P/T^4 for the Quark-Meson model for $N = 2$, with the Litim-regulator compared to the Dirac-regulator for different values of m.

4.5.3. Influence of different regulator functions on the chiral condensate and the pressure

As already mentioned above, the Renormalization-Group flow depends on the chosen regulator function[9]. We should obtain a dependence of the results on the chosen regulator function, because we use truncations[10]. Usually the so called optimized *Litim-regulator* is used [92]; thus in the Wetterich equation the momentum integration can be performed analytically, see Appendix B. That is of course no longer the case if we use another regulator.

For better comparison we define the so called *Dirac-regulator*, with a parameter $m > 0$. This function converges to the Litim-regulator when $m \to \infty$.

$$R_{k,B} = \left(k^2 - \vec{p}^2\right) \frac{1}{e^{m\left(\frac{\vec{p}^2}{k^2} - 1\right)} + 1},$$
$$R_{k,F} = \not{p} \left(\sqrt{\frac{k^2}{\vec{p}^2}} - 1\right) \frac{1}{e^{m\left(\frac{\vec{p}^2}{k^2} - 1\right)} + 1}. \tag{4.51}$$

We neglect the gluonic sector first, because it is only indirectly influenced by the flow, so we expect that the solution of the gap-equation should not significantly depends on the chosen regulator, indeed the results for $m = 20$ and $m = 1$, are almost identical. Only in the deconfinement crossover we obtain a small difference. At zero temperature the parameters of the model are adjusted again, such that physical values for pion mass and pion decay constant are reproduced. As we can see in Figure 4.8 the results change if the parameter m is decreased. The (pseudo)-critical temperature decreases and the pressure is closer to the Stefan-Boltzmann limit. There are more possible regulator functions which can be used, as shown, e.g. in [92].

[9] The motivation was originally the assumption that the low temperature peak of the pressure in a finite volume with periodic boundary conditions (see Chapter 5.3) is caused by the Litim-regulator itself, but this was not the case, so in finite volume were not further performed calculations with different regulator functions.

[10] In general one would not expect a dependence of the full flow equation on the regulator, see Chapter 3.2, but since we truncate one would expect that this is no longer the case.

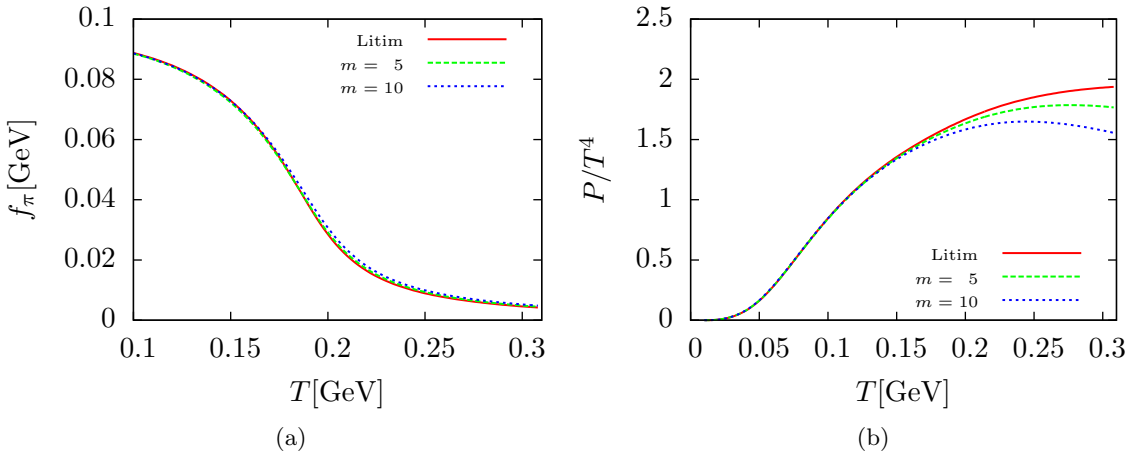

Figure 4.9.: The order parameter (a) and (b) the pressure for the Quark-Meson model for $N = 2$, with the Litim-regulator compared to the power-regulator for different values of m.

Nevertheless, the influence of other regulator functions to the results show a smaller difference to those of the Litim-regulator, e.g. like the *power-regulator* which is inspired from Ref. [92] (with $m > 0$):

$$R_{k,B} = \left(k^2 - \vec{p}^2\right) \frac{1}{(\vec{p}^2/k^2 + 1)^m},$$
$$R_{k,F} = \not{p} \left(\sqrt{\frac{k^2}{\vec{p}^2}} - 1\right) \frac{1}{(\vec{p}^2/k^2 + 1)^m}. \tag{4.52}$$

For the chiral condensate the results do not depend on the parameter m but in case of the pressure m behaves like an additional ultraviolet cutoff: for large temperature the pressure tends down.

With the different regulator functions the momentum integration is performed in different ways, for instance it defines the width of the momentum shell. This should influence the scale dependence of, e.g. the chiral condensate, especially the chiral symmetry breaking scale, see Figure 4.10.

One could ask how the gap equations and thus the chiral condensate (and other observables) are influenced if the gap equations are solved on all scales. This is performed in the next section, where we use the traditional Litim-regulator.

4.5.4. Preliminaries for a scale dependence of Φ

Because of the lack of an explicit flow equation for Φ and Φ^*, we obtain both due gap equations, see Section 4.5.1.. For different values of Φ and Φ^* the flow equations are integrated from the ultraviolet to the infrared and these due gap equations obtained values are inserted as a scale independent constant variable in the flow equations (Method I). Naively we can try a first step to include the back reaction of the fermionic and mesonic (pion and sigma degrees of freedom) to the gluonic sector. Assume we would solve the flow equation on all scales, so that we could

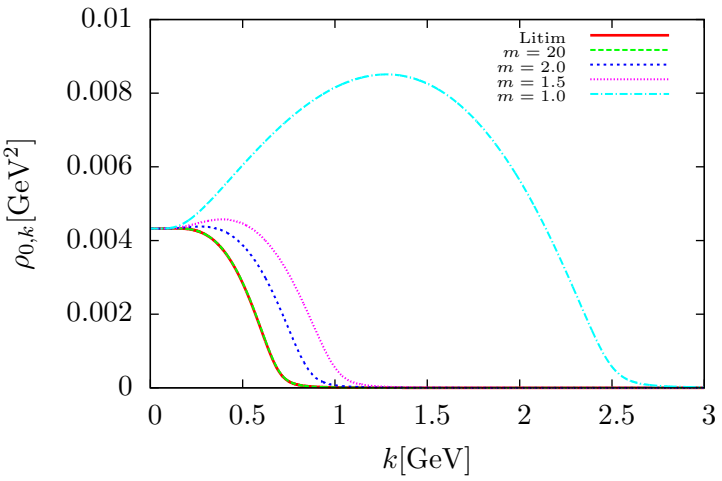

Figure 4.10.: The order parameter as a function of the scale k of the Quark-Meson model for $N = 2$ and $T = 0$ with the Litim-regulator compared to the Dirac-regulator for different values of m.

include the effect of the flow of the chiral condensate itself[11]. How would that influence the solution of the gap equation, and this furthermore the solution of the flow equations if we put in Φ and Φ^* as a function of k? At this point note that this is not a real scale dependence of the Polyakov-loop-variable, because of the lack of an explicit flow equation for Φ, so we can denote it more accurately as a *pseudo scale dependence*.

We can implement a pseudo scale dependence of Φ by the use of the stationary conditions at all scales

$$\frac{\partial U_{k\to k_i}}{\partial \Phi} + \frac{\partial \mathcal{U}}{\partial \Phi} = 0, \tag{4.53}$$

where

$$\frac{\partial U_{k\to k_i}}{\partial \Phi} = \int_\Lambda^{k_i} \frac{1}{k} \frac{\partial}{\partial \Phi} \left(\frac{4N_c N_f k^5}{12\pi^2 E_q} (N + \overline{N}) \right) \Big|_{\rho_{0,k}=\rho_{0,k_i}} . \tag{4.54}$$

We obtain Φ and Φ^* as a function of T and k. With the function $\Phi = \Phi(k)$ the flow equations are solved and thus we include the influence of the flow dependence of $\Phi(k)$ for the flow of the chiral order parameter $\rho_{0,k}$ and the scale-dependent couplings (Method II).

The other possibility to implement pseudo scale dependence of the Polyakov-loop-variable is the following: We solve the flow equations, starting form the ultraviolet $k = \Lambda$ for a step δk for a table with at first arbitrary Φ_i and solve the gap equation for this and obtain Φ at the scale $\Lambda - \delta k$. So we continue solving the flow equations for the next step δk for a table of new Φ_i which are around $\Phi(k = \Lambda - \delta k)$. This procedure continues until we reach the infrared cutoff (Method III).

Figure 4.11*a* shows the result for Φ for some selected temperatures (for $T = 100$ MeV, $T = 200$ MeV, $T = 210$ MeV and $T = 300$ MeV) as a function of the scale. At the ultraviolet,

[11] The chiral condensate respective the pion decay constant is a function of the scale k and obtain a finite value at some chiral-symmetry breaking scale, see Figure 4.10 and for finite volume, Figure 5.3*c*.

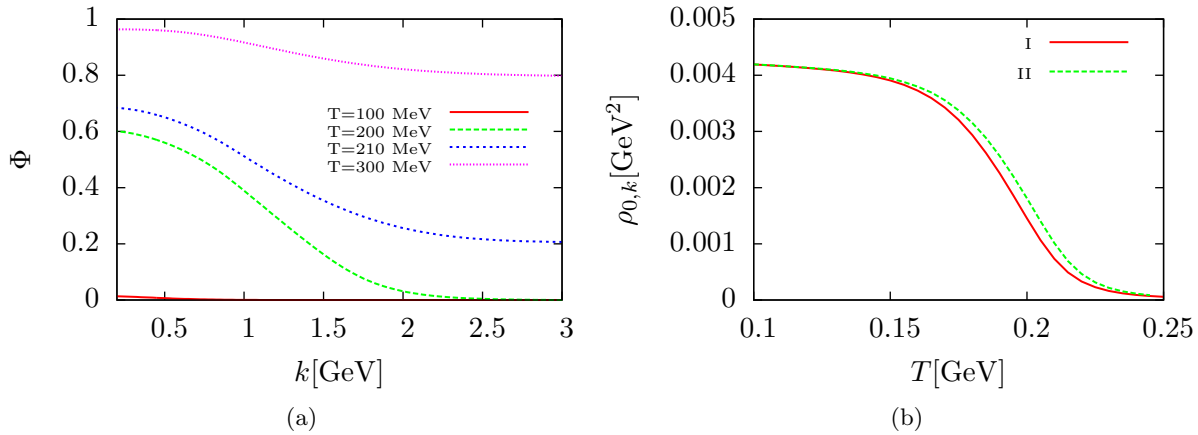

Figure 4.11.: (a): Φ as a function of the scale for some selected temperatures. (b): Chiral order parameter in the infrared for $N = 2$ as a function of the temperature for a constant Φ (I) and a Φ which *pseudodepends* on the scale (II). The pseudocritical temperature differs by about 3 MeV.

where the chiral condensate is almost zero, the values of Φ are given by the solution of the gap equation of the effective potential $\partial\mathcal{U}/\partial\Phi = 0$, where at $T = 208$ MeV we have a first-order phase transition. By decreasing the scale, the chiral condensate grows and the value of Φ increases. This effect is dominated in the region of the chiral phase transition (respectively crossover) around $T = 200$ MeV. Thus, Figure 4.11*b* shows that for the chiral condensate we obtain only small difference between both methods.

Figure 4.12 shows the results for some selected thermodynamic observables for $N = 5$. For these we obtain, that Method II and III are equivalent within numerical precision and show both significant difference to Method I. Before the phase transition, the pressure remains almost constant. As a consequence the derivatives of the pressure like the energy density and the heat capacity decrease in this region. For the trace anomaly we obtain even a (almost) vanishing value in this region (for $N < 5$ even slightly negative). This unphysical result is caused by the zero-point term of the pressure[12]. If we neglect it and calculate the *pure thermal* flow of the trace anomaly we do not observe this phenomenon. Even if we change T_0 to its pure gauge value of 270 MeV (to avoid possible *double counting* of the back reaction of the fermionic sector to the gluonic one) this changes nothing qualitatively.

The decreasing of the heat capacity at high temperatures is due to the finite ultraviolet cutoff of $\Lambda = 3$ GeV. For higher derivatives of the pressure with respect to the temperature (see Eq. 4.41) this is more sensitive, as in the case of the pressure itself or a first derivative like the energy density.

Our approach, which tried to improve recent approaches to solve the gap-equations of the Polyakov-loop-variable, produce unphysical results for the trace anomaly. It could be possible that this is cause through the chosen regulator function or has its origin in the neglected wavefunction renormalizations. In future studies these extensions could be taken into account.

[12]Lattice results and results from the hadron resonance gas model show no decreasing of the trace anomaly before phase transition, see, e.g. [109].

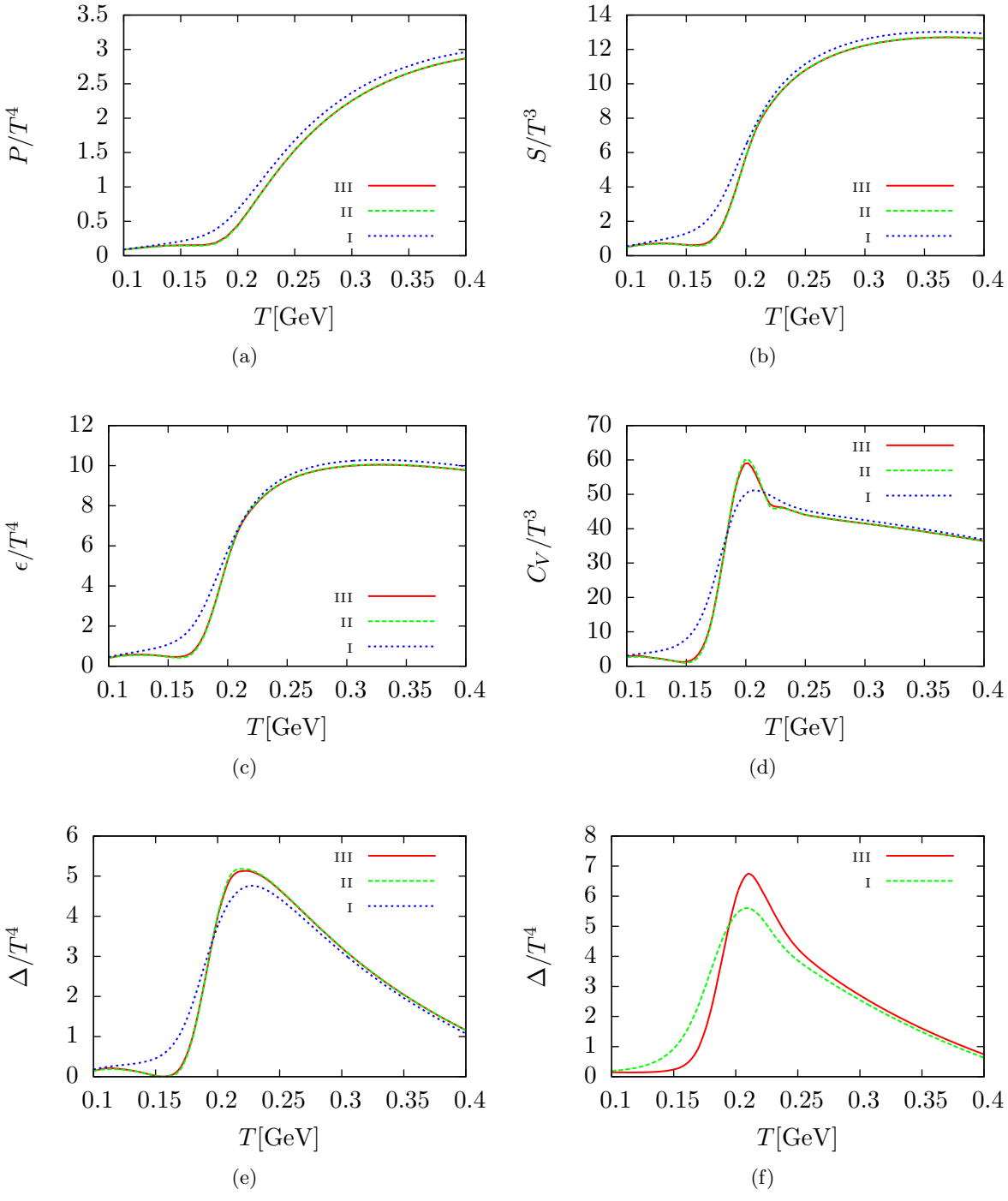

Figure 4.12.: (a) Pressure P/T^4,(b) entropy S/T^3,(c) energy density ϵ/T^4 (d) heat capacity C_V/T^3, (e) trace anomaly Δ/T^4, (f) pure thermal flow of trace anomaly Δ/T^4.

5. Polyakov-Quark-Meson model in a finite volume

5.1. Flow equation in a finite volume

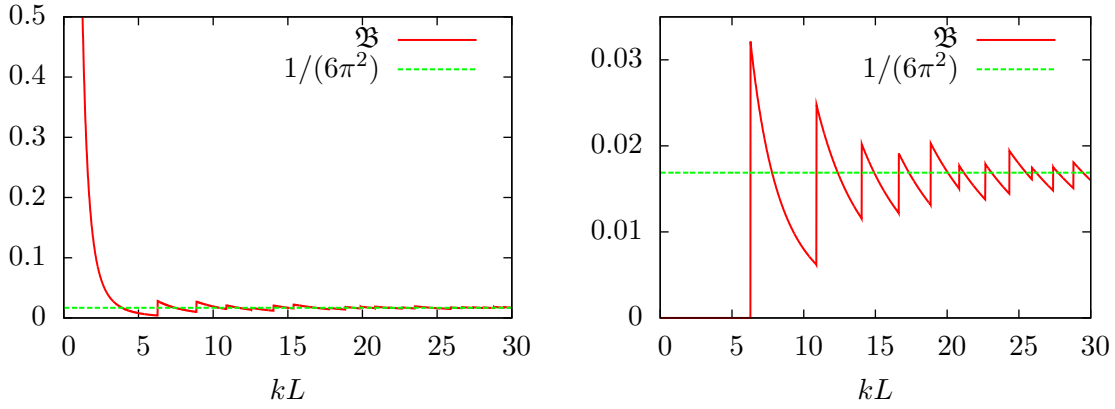

(a) (b)

Figure 5.1.: Mode function $\mathfrak{B}$ compared with its infinite volume limit for (a) periodic (b) antiperiodic boundary conditions as a function of (dimensionless) kL.

The derivation of the flow equation in a finite volume is performed analogously to the infinite volume case, see Section 4.3. The only difference is the momentum integration, which is performed in the last step of evaluating the supertrace, see Appendix B. In finite volume the spatial momentum needs to be discretized and therefore the momentum integration is substituted by a three dimensional sum

$$\int \frac{\mathrm{d}^3 p}{(2\pi)^3} \to \frac{1}{L^3} \sum_{n_1=-\infty}^{\infty} \sum_{n_2=-\infty}^{\infty} \sum_{n_3=-\infty}^{\infty} , \tag{5.1}$$

where L denotes the box size of a rectangular box with volume L^3. With this the flow equation for the effective action reads

$$\partial_t \Gamma_k = \beta V \frac{k^5}{2} \left\{ (N-1) \frac{\coth \frac{\sqrt{k^2+M_\pi^2}}{2T}}{\sqrt{k^2+M_\pi^2}} + \frac{\coth \frac{\sqrt{k^2+M_\sigma^2}}{2T}}{\sqrt{k^2+M_\sigma^2}} - \frac{4N_f N_c}{\sqrt{k^2+M_q^2}} \left(1 - N - \overline{N}\right) \right\} \mathfrak{B}. \tag{5.2}$$

The mode function $\mathfrak{B}$ has the following form

$$\mathfrak{B} = \frac{1}{(kL)^3} \sum_{n_1=-\infty}^{\infty} \sum_{n_2=-\infty}^{\infty} \sum_{n_3=-\infty}^{\infty} \Theta\left((kL)^2 - 4\pi^2 n^2\right), \tag{5.3}$$

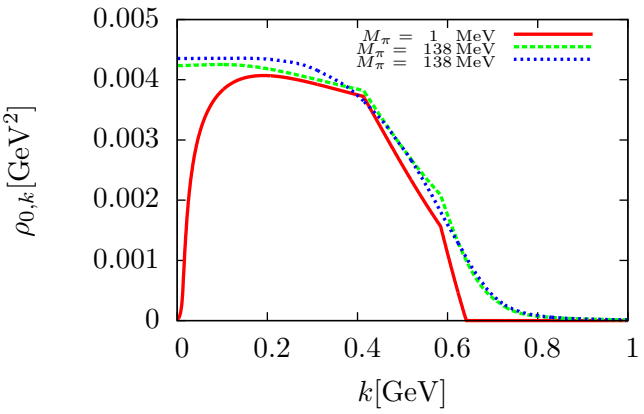

Figure 5.2.: Chiral order parameter $\rho_{0,k}$ of the Polyakov-Quark-Meson model for $N = 2$, $L = 3$ fm and $T = 0$ as a function of the scale k.

where $n^2 = n_1^2 + n_2^2 + n_3^2$. The mode function counts the number of modes that fit in the rectangular box. The number of modes depends on the scale kL and slightly on the chosen boundary conditions.

For the discrete momentum we can choose periodic boundary conditions (pBC):

$$\vec{p}^2 = \frac{4\pi^2}{L^2}\left(n_1^2 + n_2^2 + n_3^2\right) = \frac{4\pi^2}{L^2} n^2 \tag{5.4}$$

and for antiperiodic boundary conditions (apBC) $n_i \to n_i + \frac{1}{2}$, $i \in \{1, 2, 3\}$.

For $kL \to \infty$ we get $\mathfrak{B} \to 1/6\pi^2$ and reproduce the flow equations for the infinite volume case. For antiperiodic boundary conditions the mode function has no zero mode and $B \to 0$ with $kL \to 0$, while diverges for periodic boundary conditions with $\mathfrak{B} \propto \frac{1}{(kL)^3}$, see Figure 5.1.

For both cases the chiral limit cannot be considered because in finite volumes we would remain in the symmetric phase, in the infrared, if the correlation length of the pion is much larger than the length of the box, $L \ll 1/M_\pi$. Nevertheless, in that case there exists scale regions where the chiral symmetry is broken, see Figure 5.2.

We compute the pion decay constant at vanishing temperature and chemical potential for different box sizes L as a function of $1/L$. In the case of antiperiodic boundary conditions we observe that the pion decay constant as a function of $1/L$ behaves like the pion decay constant as a function of the temperature: for smaller volume sizes the pion decay constant decreases [110][1]. On the other hand, the case of periodic boundary conditions shows rather the opposite behavior: for decreasing box size, the pion decay constant is enhanced (after a slight decreasing), Figure 5.3$a - b$. This enhancement is similar to the chiral catalysis in finite magnetic field calculations (see Chapter 7). Figure 5.3c shows the pion decay constant for both boundary conditions and the infinite volume case as a function of the scale k. Because of the lack of the zero mode in the case of antiperiodic boundary conditions the flow stops at a certain scale $kL = 2\pi$ and with decreasing volume size this happens at a higher scale, so we obtain a smaller value for f_π in the infrared. In the case of periodic boundary conditions the mode function $\mathfrak{B}$ diverges $\propto 1/(kL)^3$ for $kL \to 0$. This should explain the difference between both. If we mix the boundary conditions, periodic for the bosons and antiperiodic for the fermions

[1]For $T \to 0$ the Quark-Meson and the Polyakov-Quark-Meson model are identical, so both expressions are exchangeable. This has the simple reason, that the corresponding flow equations are identical.

and vice versa, we observe for the first case that the pion decay constant shrinks as $1/L$ is increased; for the latter we obtain that f_π is increasing monotonously with increasing $1/L$. To restore chiral symmetry in a finite volume at vanishing temperature one should choose for the fermions antiperiodic boundary conditions in spatial as well as in temporal directions.

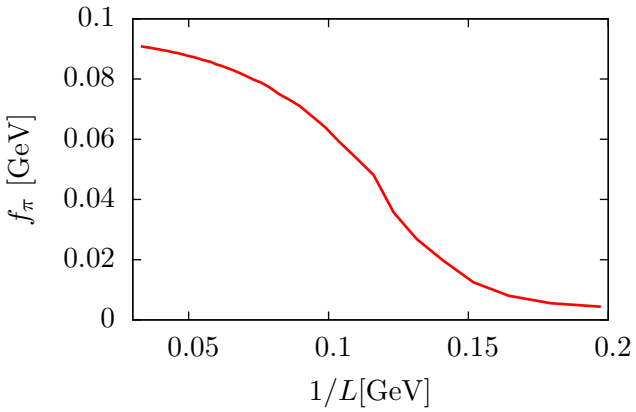

(a)

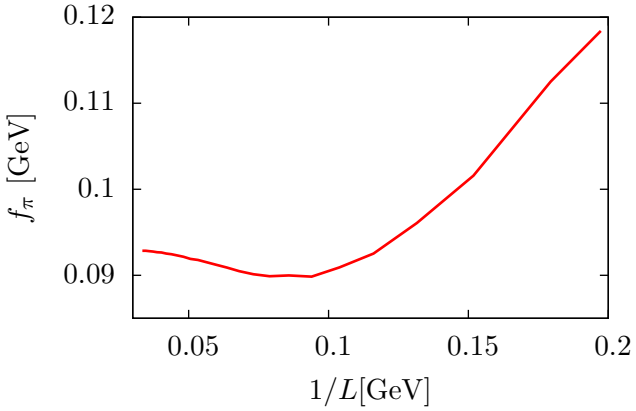

(b)

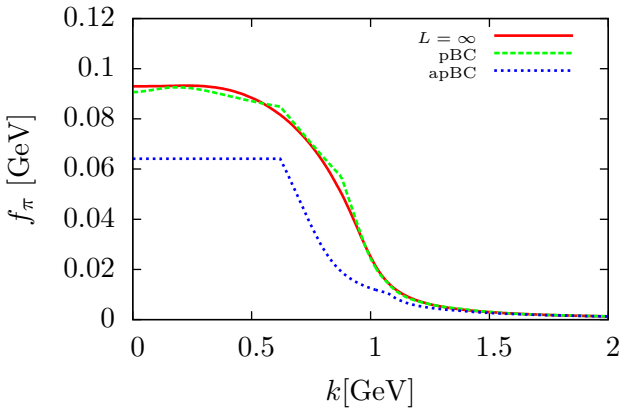

(c)

Figure 5.3.: Pion decay constant f_π of the PQM model for $N = 3$, $T = 0$, $\mu = 0$, physical pion mass as a function of the inverse box size $1/L$, with L between $L = 1$ fm and $L = 6$ fm: (a) apBC and (b) pBC. Same for (c) $N = 3$, $L = 2$ fm, $T = 0$ as a function of the scale k for periodic and antiperiodic boundary conditions compared with the infinite volume limit.

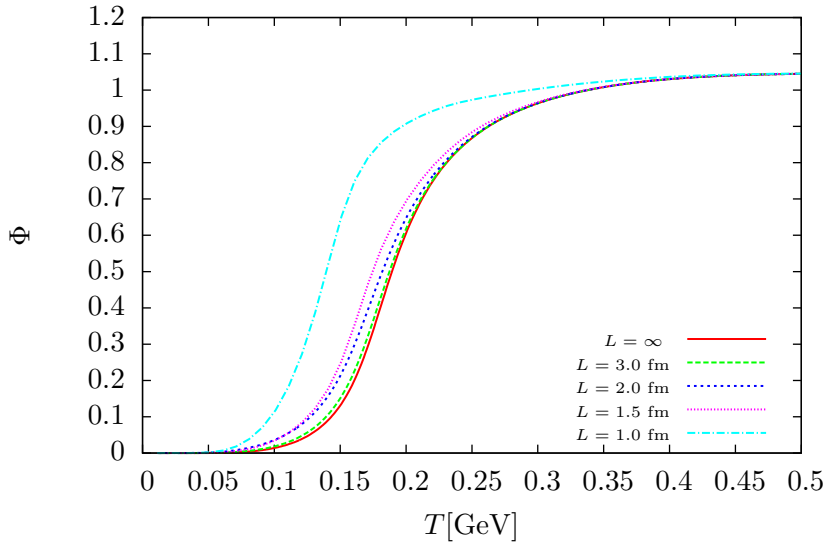

Figure 5.4.: Polyakov-loop-variable Φ for different volume sizes with $N = 3$, $\Lambda = 3$ GeV and periodic boundary conditions.

5.2. Finite volume effects of Polyakov-loop-variable Φ

In this section we will present calculations for the Polyakov-Quark-Meson model in a finite volume. We choose periodic and antiperiodic boundary conditions, as described above. We neglect a possible volume-dependence of the parameters of the Polyakov-loop potentials. The truncation order is set to $N = 3$, the pion mass and the pion decay constant are fixed for vanishing temperature and $L \to \infty$ to their physical values, $M_\pi = 138$ MeV, $f_\pi = 93.0$ MeV and fix the mass of the σ-meson to $M_\sigma = 650$ MeV.

Figure 5.4 shows the Polyakov-loop-variable Φ as a function of temperature for different volume sizes in the case of periodic boundary conditions. At a box size of $L = 3$ fm the values of Φ do not differ from the infinite volume results significantly. If we decrease the volume size, the confinement/deconfinement phase transition takes place at lower temperatures. For volume sizes below ≈ 1 fm Φ grows even more. For small volumina the Polyakov-loop Φ overshoots the value one at small temperatures[2]. For the case of the other Polyakov-Potentials that is no longer the case. Its logarithmic structure diverges at $\Phi = 1$ and this prevents the gap equations from obtaining Φ larger than one, see Figure 5.6*a*.

The situation in the case of antiperiodic boundary conditions is different. Because of the non-existence of a zero mode, the flow stops at a certain scale: $kL = 2\pi$. This has the effect that for smaller volume sizes the finite volume effects seem as if the flow does not reach the infrared, the smaller the box size L the large the scale k where this happens. Thus for finite volume all results should be smaller than those for the infinite volume case, see Figure 5.5, analogous to the behavior of f_π as a function of $1/L$ (see Section 5.1). For box sizes L below one Fermi, the non-gluonic contribution is almost negligible, and we converge to the pure gluonic case; where we obtain at the temperature of $T = 208$ MeV a first order phase transition.

If we compute the case of periodic boundary conditions, but under disregard of the zero mode, we obtain that we do not see any significant differences to the results of antiperiodic

[2]Presupposed this region is numerical accessible at a given truncation order. For the case of periodic boundary conditions this may not be the case.

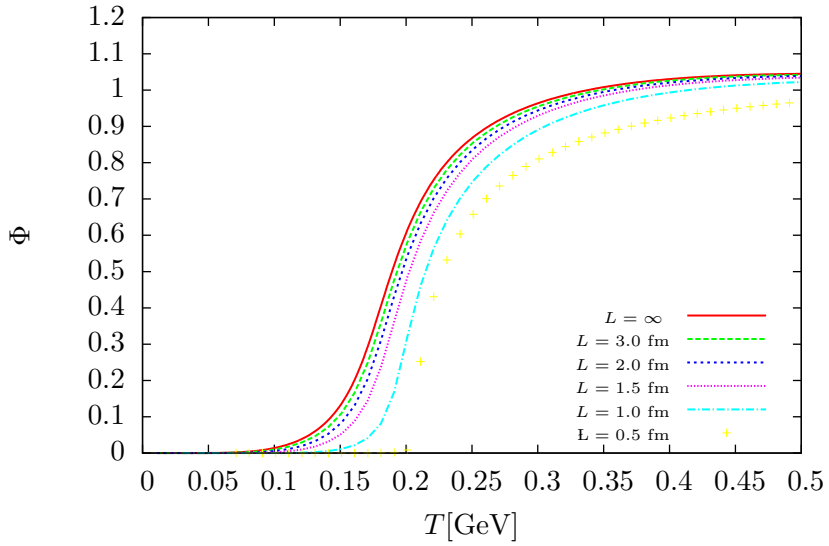

Figure 5.5.: Polyakov-loop-variable Φ for different volume sizes with $N = 3$, $\Lambda = 3$ GeV and antiperiodic boundary conditions.

boundary conditions, even for small volumina (Figure 5.6*b*). The small different mode number for scales $kL > 2\pi$ has no visible effect for the results.

5.3. Pressure in a finite volume

As described above (Section 4.5.1.) we obtain for the flow equation of the pressure the expression

$$\partial_t p = -T \left.\frac{\partial}{\partial V}\partial_t \Gamma_k\right|_{\rho=\rho_{0,k}} = -\left.\partial_t U_k\right|_{\rho=\rho_{0,k}} . \tag{5.5}$$

To obtain the pressure this term has to be integrated

$$p = -a_{0,k\to 0} = -\int_{\Lambda}^{k\to 0} dt \left.\partial t U_k\right|_{\rho=\rho_{0,k}} . \tag{5.6}$$

As before the pressure is normalized such, that it vanishes at zero temperature.

For the case of finite volumes the flow equation of the pressure gets an additional term, due to the explicit volume dependence of the effective potential

$$\begin{aligned}
\partial_t p &= -T\left.\frac{\partial}{\partial V}\partial_t \Gamma_k\right|_{\rho=\rho_{0,k}} \\
&= -\left.\partial_t U_k\right|_{\rho=\rho_{0,k}} - V\left.\frac{\partial}{\partial V}\partial_t U_k\right|_{\rho=\rho_{0,k}} \\
&= -\left.\partial_t U_k\right|_{\rho=\rho_{0,k}} - \frac{L}{3}\left.\frac{\partial}{\partial L}\partial_t U_k\right|_{\rho=\rho_{0,k}} .
\end{aligned} \tag{5.7}$$

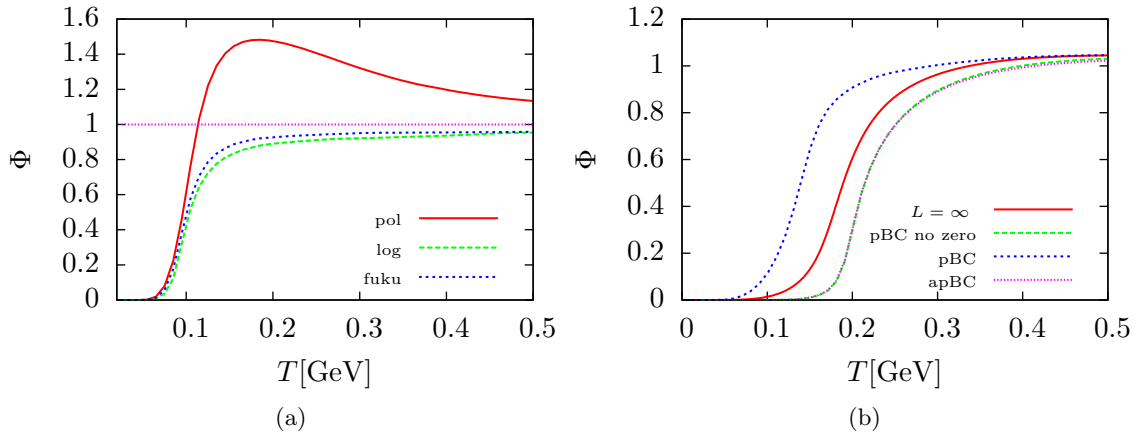

Figure 5.6.: (a) Comparison of Φ for the different Polyakov-loop potentials. The truncation order is $N = 2$ and the volume size $L = 0.5$ fm. (b) Polyakov-loop for different boundary conditions (pBC zero: periodic but without zero mode) with $L = 1$ fm, $N = 3$, $\Lambda = 3$ GeV.

The total pressure contains also the part of the gluonic sector

$$P = \int_{\Lambda}^{k\to 0} \partial_t p - \mathcal{U}(\Phi, \Phi^*, T) - \frac{L}{3}\frac{\partial}{\partial L}\mathcal{U}(\Phi, \Phi^*, T), \tag{5.8}$$

with $\mathcal{U}(\Phi, \Phi^*, T)$ the Polyakov-loop potential, see Section 4.2.

The derivative is expressed by the difference quotient

$$\frac{\partial}{\partial L} f(L) = \frac{f(L + \Delta L) - f(L - \Delta L)}{2\Delta L}. \tag{5.9}$$

For antiperiodic boundary conditions, we observe the analogous phenomenon as in the case of Φ: for decreasing volume size the value of the pressure at a given temperature is slightly smaller compared to the infinite volume case (Figure 5.7). Significant finite volume effects we observe only for the case of very small volumina.

For periodic boundary conditions this is no longer the case. Especially in the low temperature regime we observe peaks (Figure 5.8$a-b$). The same peaks we observe also in the case of the Quark-Meson model (Figure 5.9$a-b$): In the low temperature regime, the contribution of the gluonic sector[3] can be neglected; below $T = 50$ MeV the pressure is identical with the one of the Quark-Meson model.

These peaks are not a derivative effect and they do not vanish if the ultraviolet cutoff is changed; they have their origin in the zero mode of the mode function $\mathfrak{B}$ for periodic boundary conditions. If this mode is neglected, these peaks vanish, and the results are identical with those of antiperiodic boundary conditions (Figure 5.10a). Apart from the low-temperature regime, the thermodynamic results of both boundary conditions are slightly different to each other in intermediate box sizes. For smaller box size with antiperiodic boundary conditions the other thermodynamic observables like the entropy and heat capacity behave analogous to the

[3] $P_{\text{gluon}} = -\mathcal{U}(\Phi, \Phi^*, T) - \frac{L}{3}\frac{\partial}{\partial L}U(\Phi, \Phi^*, T)$.

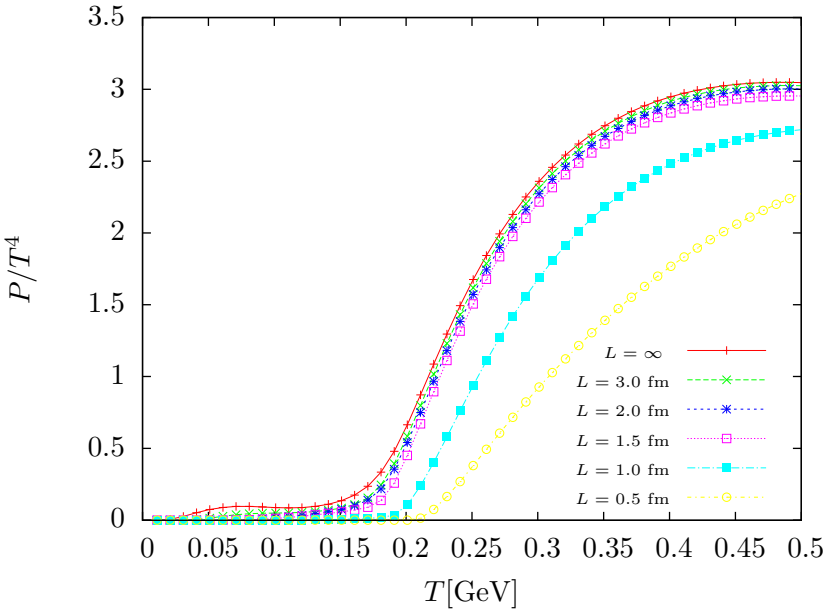

Figure 5.7.: Pressure for the PQM-model for $N = 3$ and $\Lambda = 3$ GeV where the pressure is normalized to $P(T = 0) = 0$ for antiperiodic boundary conditions (pBC zero: periodic but without zero mode).

pressure (Figure 5.10$b - c$). If for periodic boundary conditions the volume size gets further reduced, the pressure can become negative (and therefore the entropy et cetera). From this unphysical result we can assume that for periodic boundary conditions the parameters of the Polyakov-loop potential might be a function of the box size L. If T_0 (see Section 4.2) would be a function of the box size, we would shift the deconfinement temperature. With this the low temperature behavior may not be cured. Nevertheless, these obtained results do not change if we alter the effective potential for the gluonic degrees of freedom, i.e. if we calculate the gap-equations instead of the chosen Ginzburg-Landau potential with the logarithmic or the Fukushima-potential.

If we mix the boundary conditions: periodic for the bosons and antiperiodic for the fermions and vice versa, we obtain for the first case for box sizes $L > 2$ fm still peaks (for larger volumes the difference between antiperiodic and periodic is negligible), but not for the second. For both cases we observe no negative values for the pressure in the low temperature regime for small box sizes, even for $L = 1$ fm. From this we conclude, that the interplay of the bosonic and fermionic part of the flow equations, both with periodic boundary conditions, is responsible for the unphysical results of the pressure.

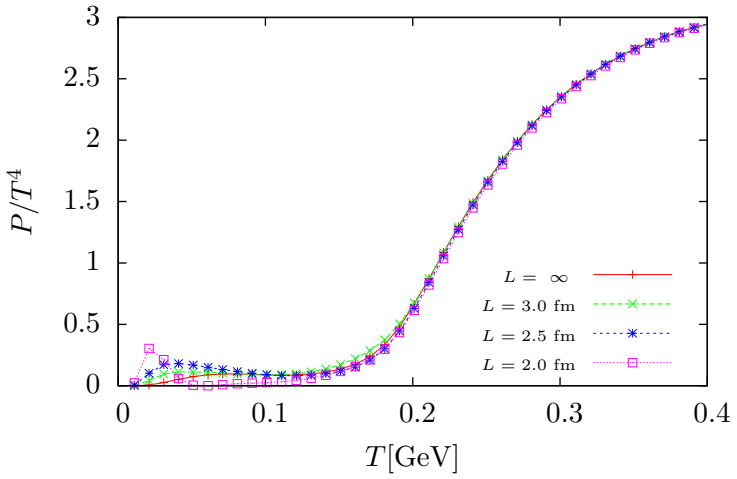

(a)

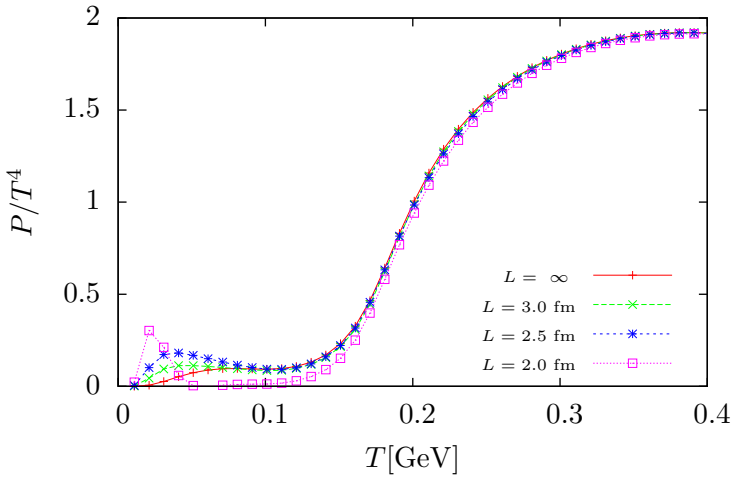

(b)

Figure 5.8.: (a) Pressure for the PQM-model with $N = 3$, $\Lambda = 3$ GeV. The pressure is normalized to $P(T = 0) = 0$; (b) same as (a) but without the contribution of the gluonic sector.

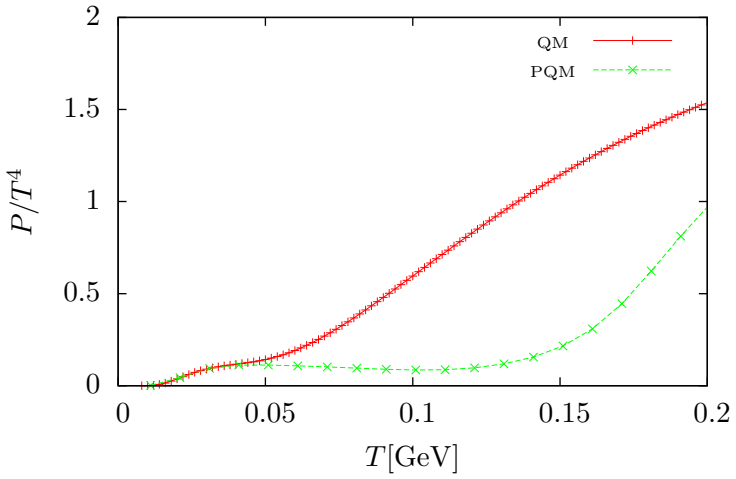

(a)

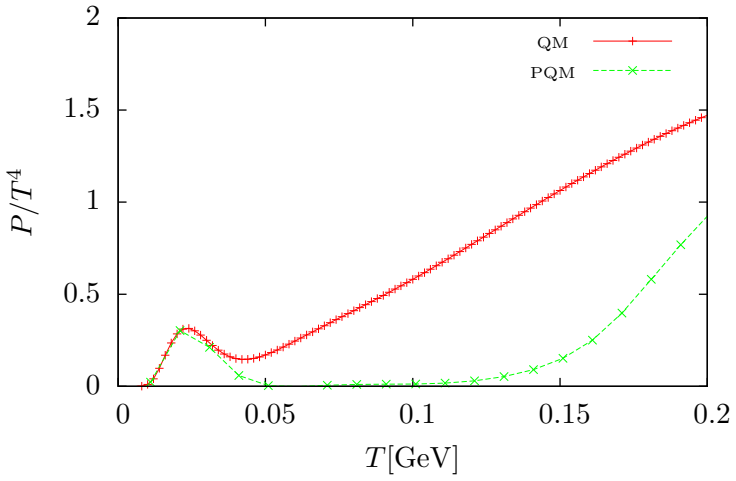

(b)

Figure 5.9.: Comparison of the pressure of Polyakov-Quark-Meson model (without gluonic contributions) with Quark-Meson model for $N = 3$, $\Lambda = 3$ GeV with (a) $L = 3$ fm, (b) $L = 2$ fm.

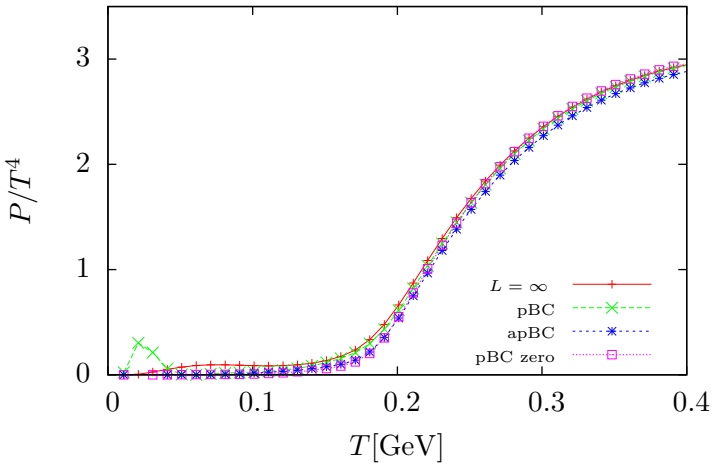

(a)

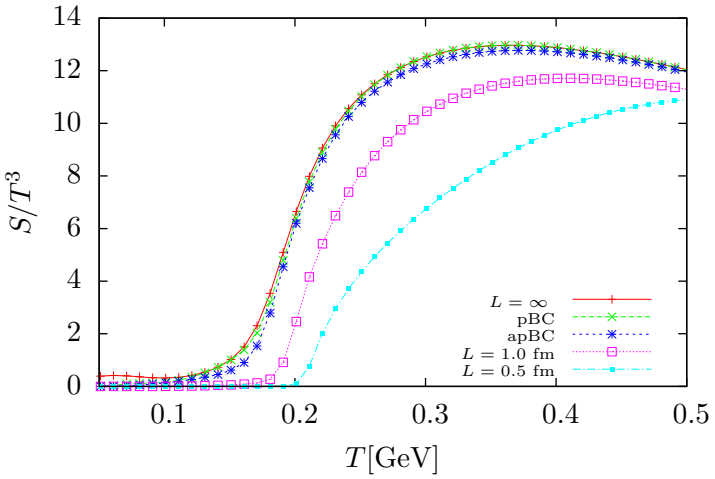

(b)

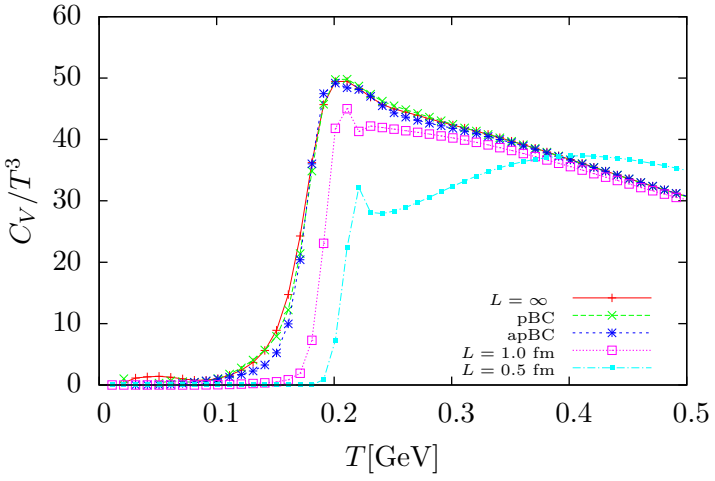

(c)

Figure 5.10.: (a) Pressure for $L = 2$ fm, $N = 3$, $\Lambda = 3$ GeV and different boundary conditions, (b) entropy and (c) heat capacity also for box-sizes $L = 1$ fm and $L = 0.5$ fm for antiperiodic boundary conditions.

6. Phase diagram and fluctuations in a finite volume

6.1. Results for Φ and Φ^* in a finite volume with non-zero μ

In this section the results for Φ and Φ^* for different values of box size L for periodic and antiperiodic boundary conditions in spatial momentum direction are presented. As previously mentioned the solution of the gap equations yield different values for Φ and Φ^* if we perform calculations with non-zero μ. This yields two different temperatures for the deconfinement transition. Thus in a strict sense the Polyakov-loop-variable Φ and its conjugate cannot be used as an order parameter for the deconfinement/confinement crossover.

Notably the obtained values of Φ are always lager than those of Φ^* for antiperiodic boundary conditions. The opposite behavior is founds in the low temperature regime for small box sizes and large chemical potentials in the case of periodic boundary conditions.

In Figure 6.1 the results for Φ and Φ^* for different box sizes L with antiperiodic boundary conditions and a chemical potential μ in a range between $\mu = 0$ and $\mu = 300$ MeV are shown. At a box size of $L = 3$ fm the crossover temperature for Φ lowens if the chemical potential is increased; for a finite μ the curves are above the $\mu = 0$ line. If the box size is decreased every line is shifted to larger temperatures and the μ-dependence of Φ is smaller.

For Φ^* the situation is sightly different. At a box size of $L = 1$ fm, the curves with $\mu > 0$ lie below the $\mu = 0$ case. The μ-dependence is weaker than in the case of Φ. If the volume size is enlarged the behavior of the lines with $\mu \geq 200$ MeV changes in the low and intermediate temperature regime. The μ-dependence behavior is inverted and for large μ and small temperatures the results tend to lie above the case with vanishing chemical potential; for $L = 3$ fm and $\mu = 300$ MeV that is clearly the case.

The constant T_0 in the Polyakov-loop potential (see Section 4.2) is a function of color number N_c and flavor number N_f

$$T_0(N_f, N_c) = T_\tau e^{-1/(\alpha_0 b(N_f, N_c))}, \tag{6.1}$$

with $T_\tau = 1.77$ GeV, $\alpha_0 = 0.304$ and the first coefficient of the QCD beta function

$$b(N_f, N_c) = \frac{1}{6\pi}\left(11N_c - 2N_f\right). \tag{6.2}$$

This function can be extended by an explicit μ dependence as

$$b(N_f, N_c) = \frac{1}{6\pi}\left(11N_c - 2N_f\right) - \frac{16}{\pi}N_f\frac{\mu^2}{T_\tau^2}. \tag{6.3}$$

With this correction T_0 is a decreasing function with increasing μ[1] and the back-reaction of the fermionic to the gluonic sector is taken into account. Therefore, the deconfinement temperature should show a more sensitive dependence with increasing μ than in the case of constant T_0.

[1] For more details on this issue see Ref. [100]. Another approach to construct T_0 as a function of μ can be found in Ref. [111].

We repeat the above calculations with a μ-dependent T_0-constant. In Figure 6.2 the corresponding results are depicted. For the case of Φ the finite μ-effects are similar, but much more pronounced. For the case of Φ^* with box-sizes $L = 3$ fm and $L = 2$ fm all lines lies above the $\mu = 0$ case, except for $\mu \leq 150$ MeV in the region around $T \approx 150$ MeV. For $L = 1$ fm this low temperature behavior is negligible. If we increase the chemical potential further the deconfinement temperature tends to reach $T \to 0$.

The convergence behavior of Φ and Φ^* in finite volume to those of the infinite volume limit gets worse for larger chemical potentials, particularly when we allow T_0 to be μ-dependent. The corresponding values of Φ are depicted in Figure 6.3 (left) for, e.g. a chemical potential of $\mu = 100$ MeV, $\mu = 200$ MeV and $\mu = 300$ MeV for constant T_0 and similar for $T_0 = T_0(\mu)$ in Figure 6.3 (right).

For the case of periodic boundary conditions we observe a non-monotonous behavior for $L \leq 2$ fm and $\mu \geq 150$ MeV for constant T_0 (Figure 6.4). In the case of μ-dependent T_0 these effects are increased (Figure 6.5). These effects are also increased if we further decrease the volume size to, e.g. $L = 1$ fm. With periodic boundary conditions the convergence behavior of Φ and Φ^* in the infinite volume limit seem to be better in the large μ-regime in contrast to antiperiodic boundary conditions, see Figure 6.6. These effects still remain if we solve the gap-equations with the logarithmic or the Fukushima-potential (as an example for $L = 1.5$ fm and $\mu = 300$ MeV in Figure 6.7), which is not surprising, since the main contribution of finite volume effects comes from the RG-part $\partial U_{k\to 0}/\partial\Phi$ of the gap-equations (see Section 4.5.1.). Those vanish however, if we increase the chemical potential up to $\mu = 500$ MeV, see Figure 6.8. If we enlarge the truncation order to $N = 4$ or $N = 5$ these peaks respective non-monotonous behavior do not vanish. With the exception of this peak-region we can observe good convergence behavior. Figure 6.9 shows, as an example, the results for $L = 1.5$ fm and $\mu = 0$ and $\mu = 200$ MeV. In the case of antiperiodic boundary conditions the convergence behavior is good at all temperatures and chemical potentials.

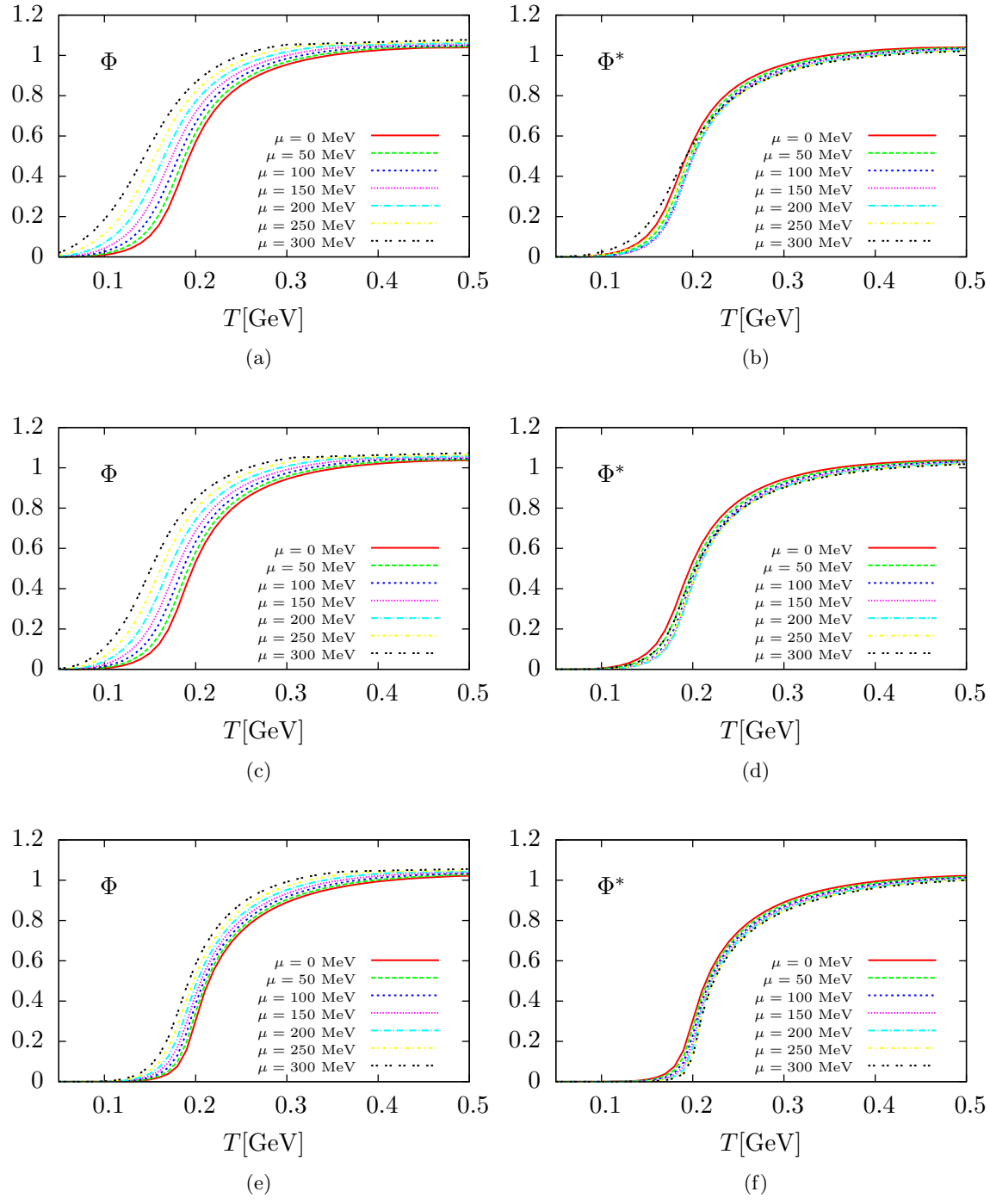

Figure 6.1.: Φ and Φ* box size (a-b) $L = 3$ fm, (c-d) $L = 2$ fm, (e-f) $L = 1$ fm with antiperiodic boundary conditions and constant T_0.

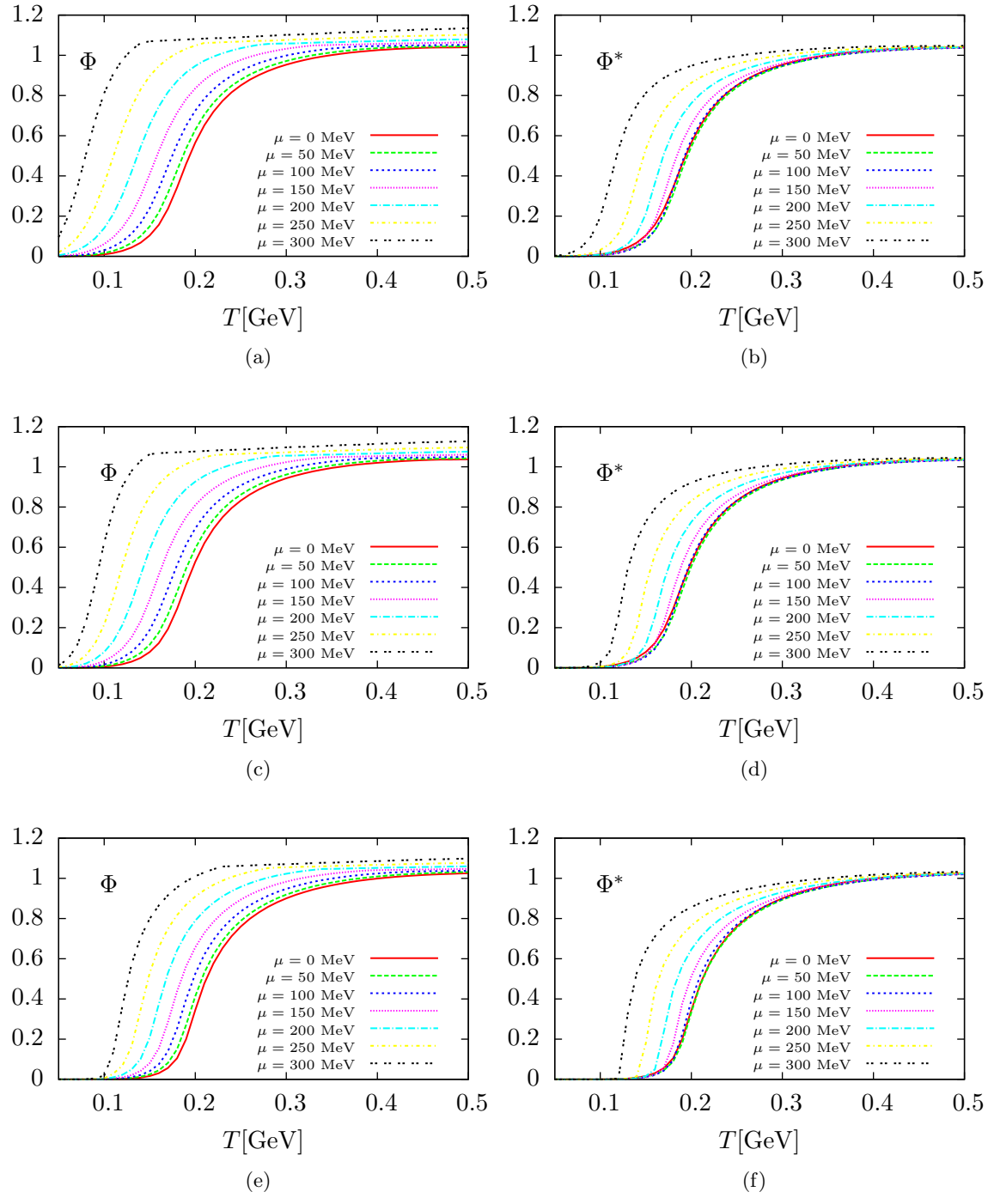

Figure 6.2.: Φ and Φ^* in a finite volume with box size (a-b) $L = 3$ fm, (c-d) $L = 2$ fm, e-f) $L = 1$ fm with antiperiodic boundary conditions and $T_0 = T_0(\mu)$.

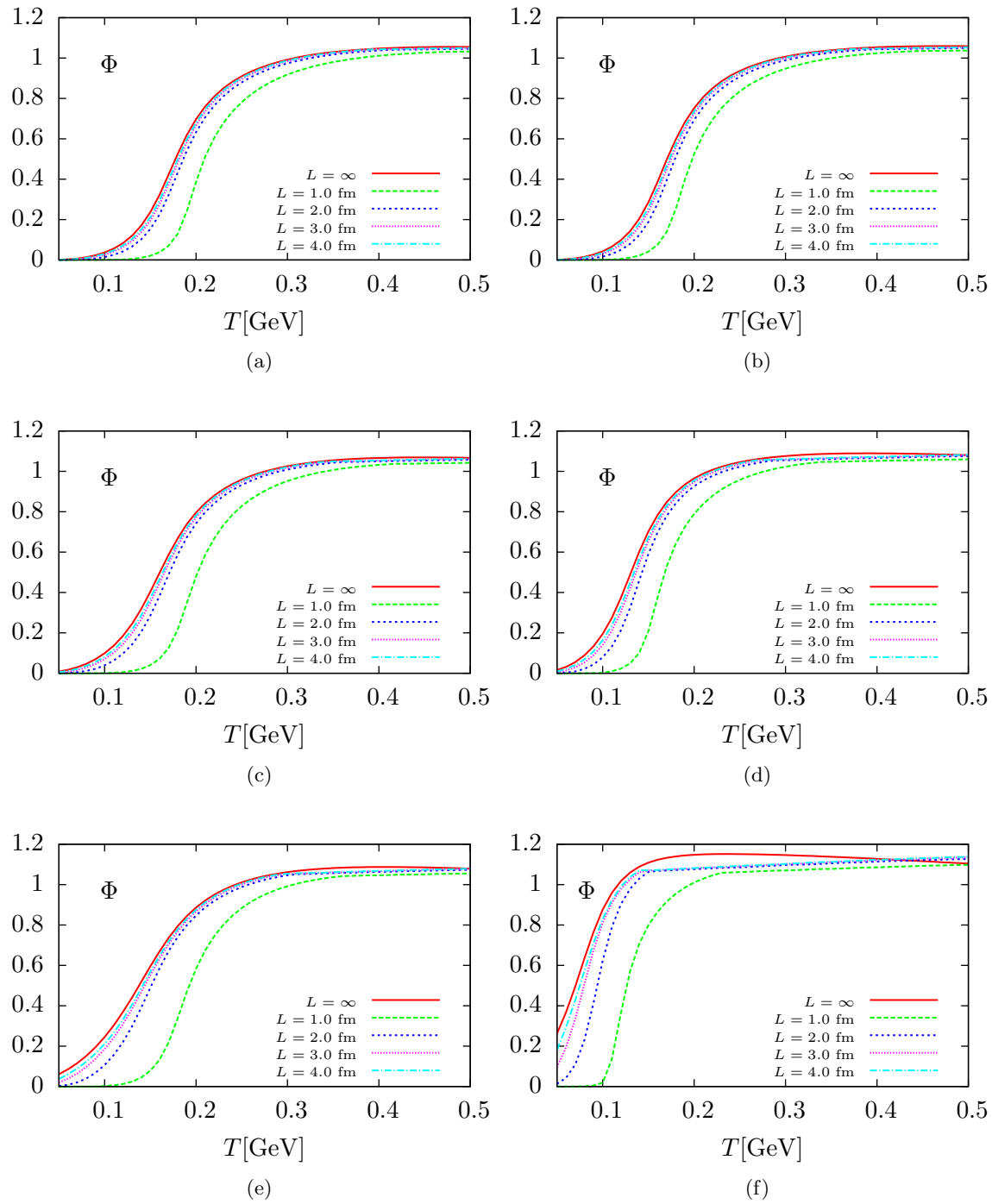

Figure 6.3.: Convergence behavior of Φ with constant T_0 (left) and $T_0 = T_0(\mu)$ (right) with chemical potential (a-b) $\mu = 100$ MeV, (c-d) $\mu = 200$ MeV, (e-f) $\mu = 300$ MeV and antiperiodic boundary conditions.

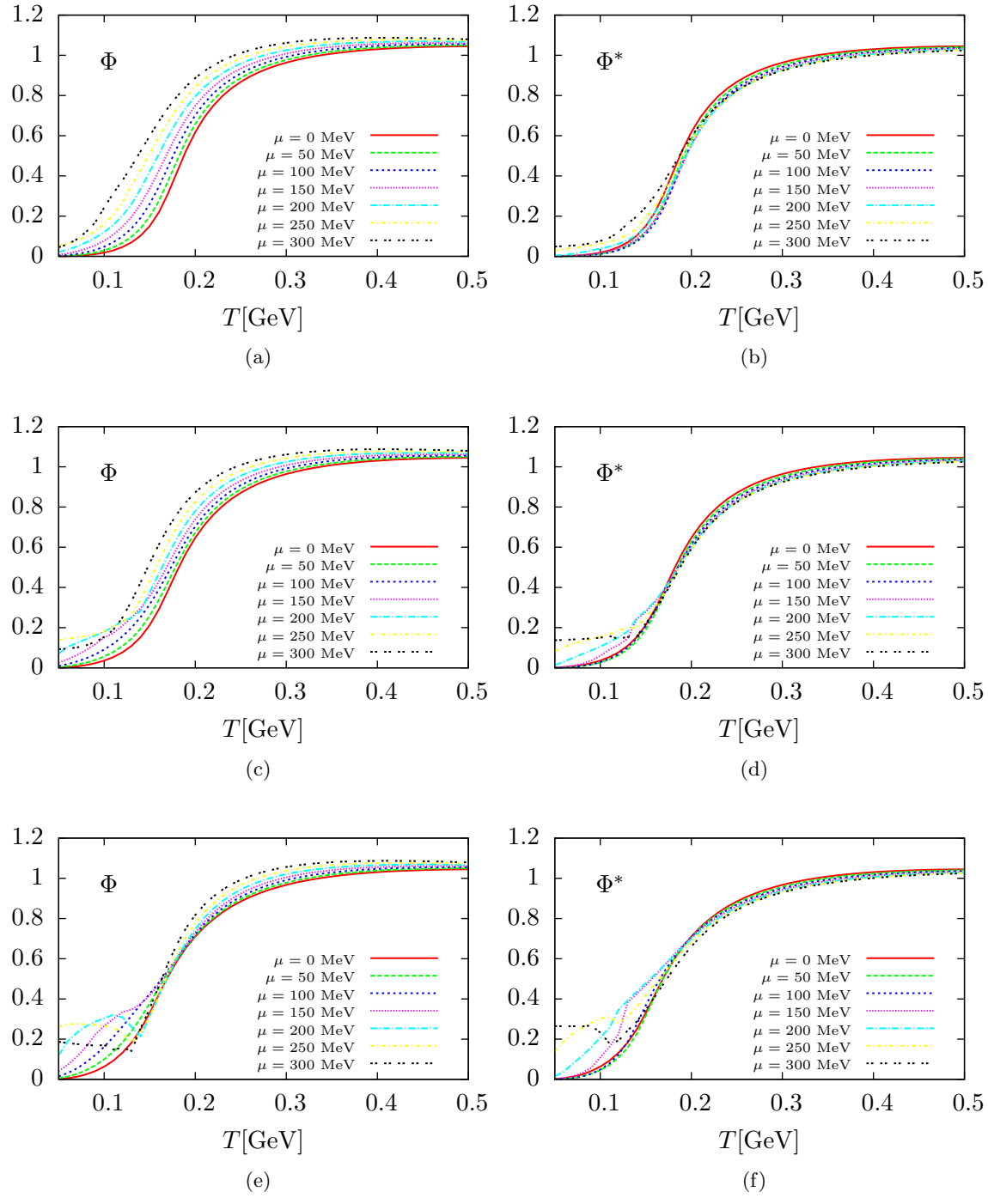

Figure 6.4.: Φ and Φ^* in a finite volume with box size (a-b) $L = 3$ fm, (c-d) $L = 2$ fm, (e-f) $L = 1.5$ fm with periodic boundary conditions and constant T_0.

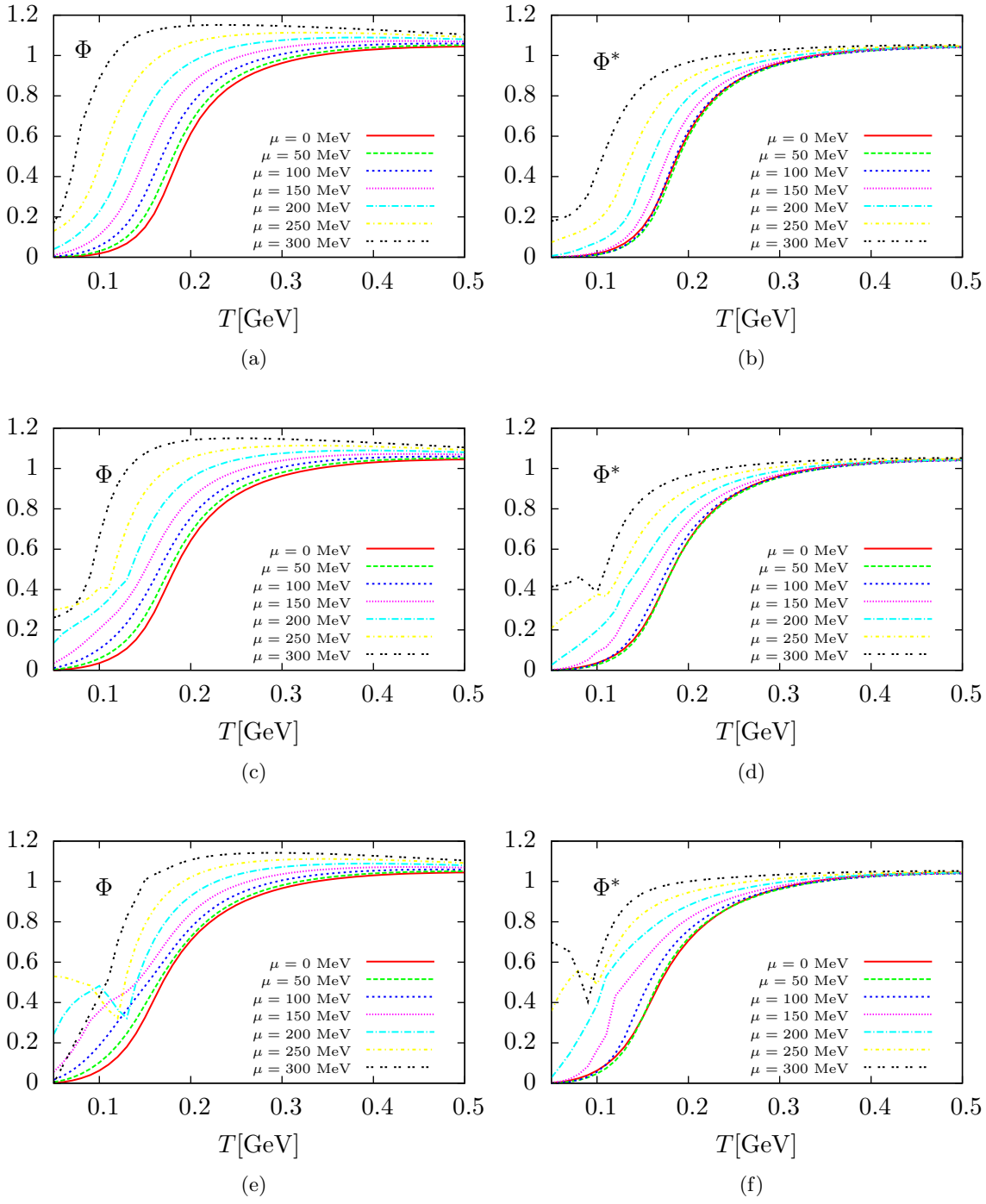

Figure 6.5.: Φ and Φ* in a finite volume with box size (a-b) $L = 3$ fm, (c-d) $L = 2$ fm, (e-f) $L = 1.5$ fm with periodic boundary conditions and $T_0 = T_0(\mu)$.

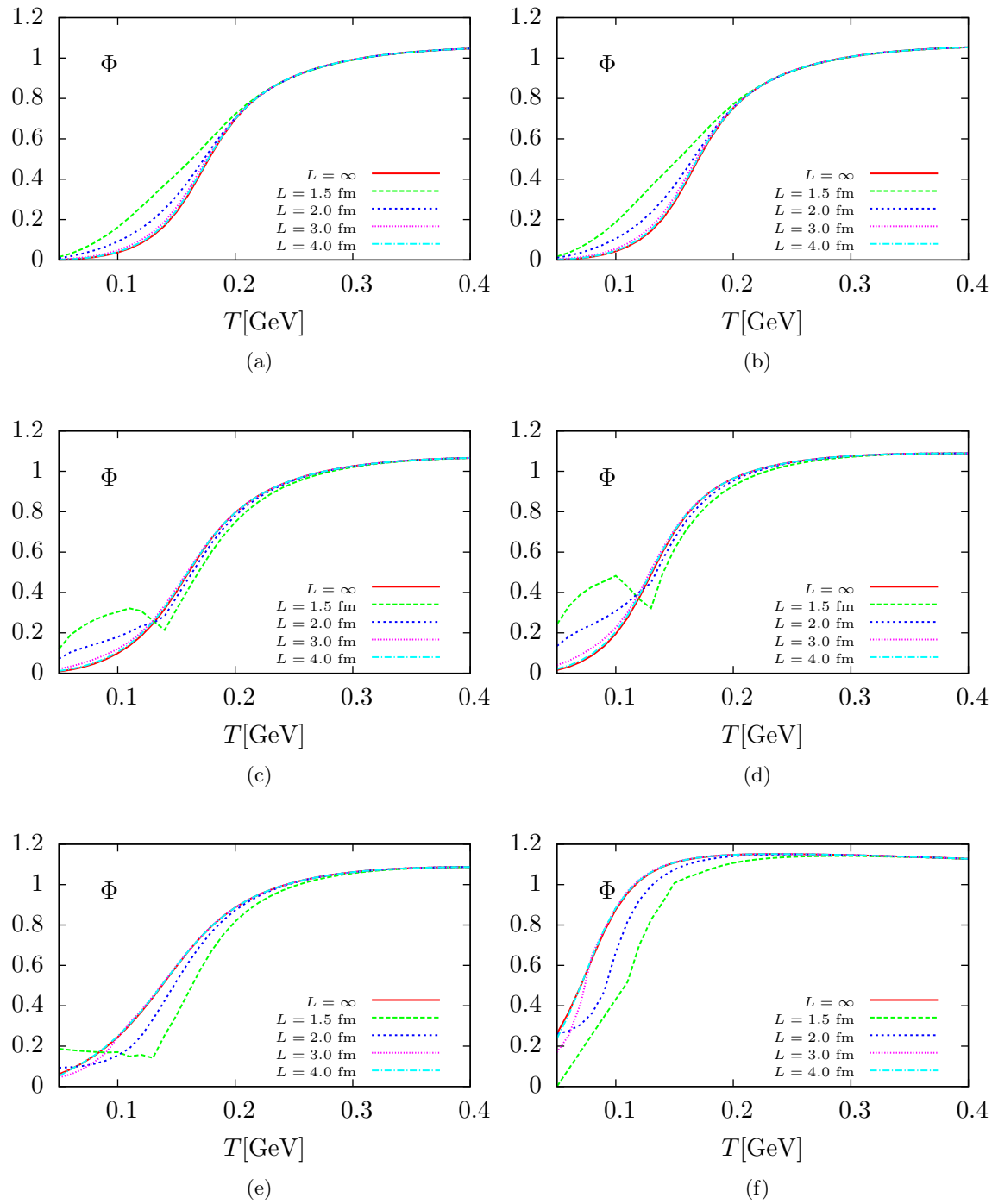

Figure 6.6.: Convergence behavior Φ with constant T_0 (left) and $T_0 = T_0(\mu)$ (right) with chemical potential (a-b) $\mu = 100$ MeV, (c-d) $\mu = 200$ MeV, (e-f) $\mu = 300$ MeV and periodic boundary conditions.

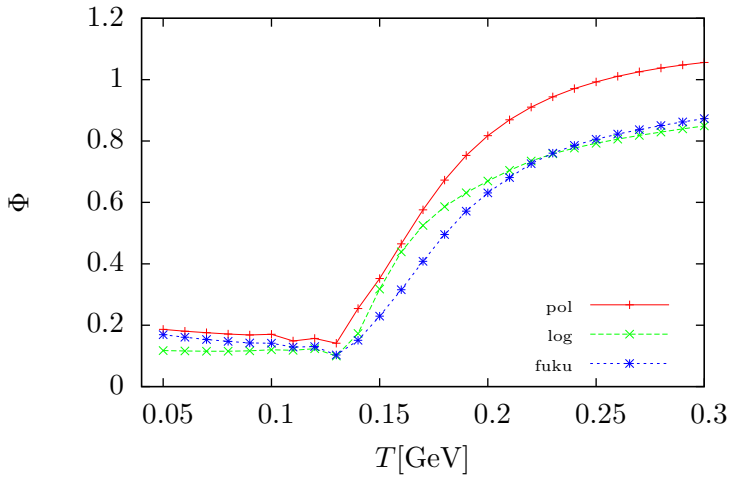

(a)

Figure 6.7.: (a) Comparison of Φ for $L = 1.5$ fm, $\mu = 300$ MeV constant T_0 and periodic boundary conditions for different gluonic potentials.

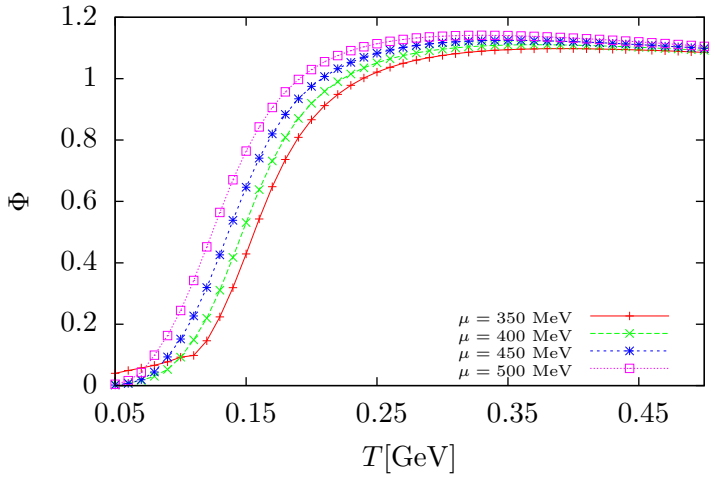

(a)

Figure 6.8.: (a) Φ for $L = 1.5$ fm with periodic boundary conditions and large chemical potentials.

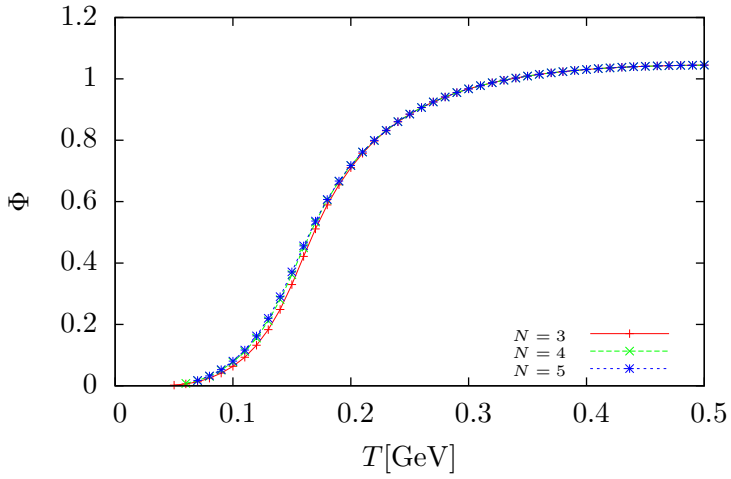

(a)

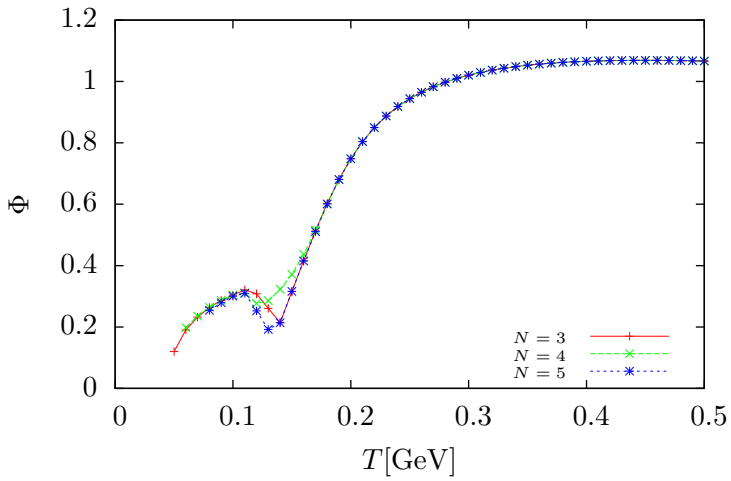

(b)

Figure 6.9.: Φ for $L = 1.5$ fm, constant T_0 for different truncation orders N and periodic boundary conditions, (a) $\mu = 0$ MeV and (b) $\mu = 200$ MeV.

6.2. Chiral condensate in a finite volume with non-zero μ

The crossover temperature of the chiral condensate and equally the pion decay constant,[2] tends to lower values as the chemical potential is increased. In the case of antiperiodic boundary conditions, because of the lack of the zero mode, the chiral condensate is decreased as the box size is decreased. In the case of $L = 1$ fm the chiral condensate is almost zero, see Figure 6.10. For this the chiral condensate is already very small at low temperatures, because $1/L$ acts, in the case of antiperiodic boundary conditions, as a temperature (see Figure 5.3 in Section 5.1). Thus, for small volume sizes, the chiral symmetry is already approximately restored at small temperatures, therefore it is no longer a real crossover as the temperature is increased. A full restoration of chiral symmetry is not possible, because of the chosen finite value of the pion mass, we have an explicit broken chiral symmetry.

In the case of antiperiodic boundary conditions we observe a crossover throughout nearly the whole range of the chemical potential. We observe a first-order transition for only very large chemical potentials, like e.g. for $L = 3$ fm at $\mu \geq 450$ MeV, see Figure 6.11*a*. If we enlarge the considered volume, this can occur at smaller chemical potentials, like in the case of $L = 4$ fm at $\mu \geq 350$ MeV; but then the difference to the infinite volume limit is almost negligible. The driving moment for a first order phase transition is therefore a sufficient large chiral condensate; this is too small in the case of antiperiodic boundary conditions if the volume size is too small, because of the lack of the zero mode and thus the flow stops at $kL = 2\pi$. If we enlarge the truncation order N we observe convergence as well for vanishing chemical potential as for finite chemical potential. Figure 6.12 shows an example for $L = 3$ fm and $\mu = 0$ and $\mu = 200$ MeV.

If we choose periodic boundary conditions the crossover temperature also decreases if we increase the value of the chemical potential at a given volume size. If we further increase the chemical potential we can already observe at moderate values of the chemical potential a first order phase transition, in contrast to the case of antiperiodic boundary conditions.

At a given volume size, the first order phase transition takes place at a smaller temperature the larger the chemical potential is. After the first-order phase transition we obtain for the pion decay constant a local maximum, see Figure 6.13. These peaks almost vanish if the chemical potential is further increased, see Figure 6.14. We believe these are truncation effects. If we perform calculations with T_0 as a function of μ the difference to the latter is small, especially for antiperiodic boundary conditions and especially for $L \leq 3$ fm and $\mu \leq 300$ MeV the difference is negligible. For calculations with a μ-dependence of T_0 the pseudocritical temperature is slightly shifted to smaller temperatures.

If we enlarge the truncation order N we observe convergence behavior only for small or zero chemical potential, see Figure 6.15. We observe no convergence in the region around the first order phase transition[3].

To obtain the crossover region of the phase diagram for the chiral phase transition, we calculate the pseudocritical temperature T_p from the chiral condensate, since a precise definition of a critical temperature does not exist for a crossover. We obtain this temperature by determining the maximum of the derivative

[2] Please note that the chiral condensate and the pion decay constant describe the same physical effect, see Eq. 4.30

[3] Please note: If we increase the truncation order the numerical calculation in the low temperature regime $T < 100$ MeV becomes more and more difficult.

$$-\left.\frac{\partial f_\pi}{\partial T}\right|_{T=T_p} \stackrel{!}{=} \text{Max.} \tag{6.4}$$

In the case of the first order phase transition a precise definition of the phase transition temperature exists and can be determined from the discontinuity in the chiral condensate. In our numerical calculations we obtain the chiral condensate only at discrete values. Thus, after an interpolation, we can use Eq. 6.4 also for the first order region of the phase diagram to obtain the critical temperature within our precision.

Figure 6.16 shows the phase diagram for periodic and antiperiodic boundary conditions. We conclude from the non-convergence due to our truncation scheme of the pion decay constant for periodic boundary conditions that for this case the result for the phase diagram is most likely incorrect. A critical endpoint was not located. A possible reason might be the chosen truncation scheme. Instead of the Taylor-expansion the full flow equations are often solved through discretization, like in a finite volume study [112]. Furthermore, the numerical tractability of our approach hinders the possible detection of signatures of the critical endpoint, which should be improved further for future studies.

The first order region starts in the phase diagram at the kink, due to our μ-interval. Nevertheless, we find that for a chemical potential of $\mu \leq 200$ MeV in the case of antiperiodic boundary conditions for $L > 1$ fm almost no volume dependence is visible, in contrast to the case with periodic boundary conditions. For $L = 1$ in the case of antiperiodic boundary conditions the chiral symmetry is due to the $1/L$-scale at small temperatures already approximately restored (see above), insofar we cannot refer to a crossover at small volumes. Thus, the tendency of $T_p(\mu)$ depends on the chosen boundary conditions. To connect finite volume studies with heavy-ion experiments, one should choose boundary conditions which are (approximately) realized in experiments, since our idealized boundary conditions are probably not realized in an expanding fireball.

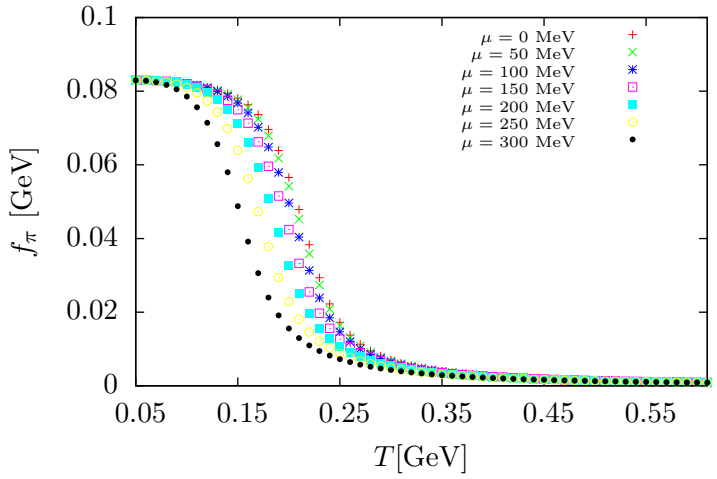

(a)

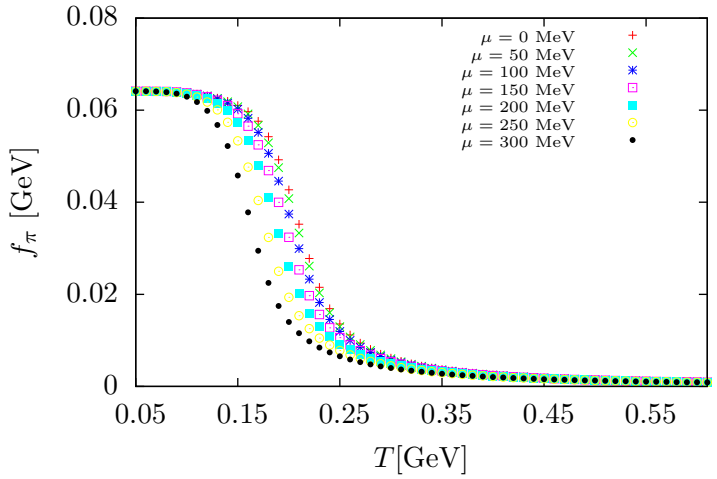

(b)

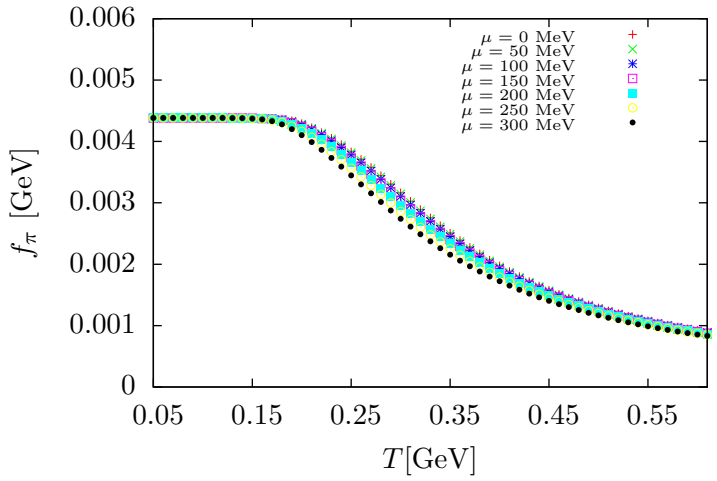

(c)

Figure 6.10.: Chiral condensate for antiperiodic boundary conditions for constant T_0 and box sizes (a) $L = 3$ fm, (b) $L = 2$ fm, (c) $L = 1$ fm.

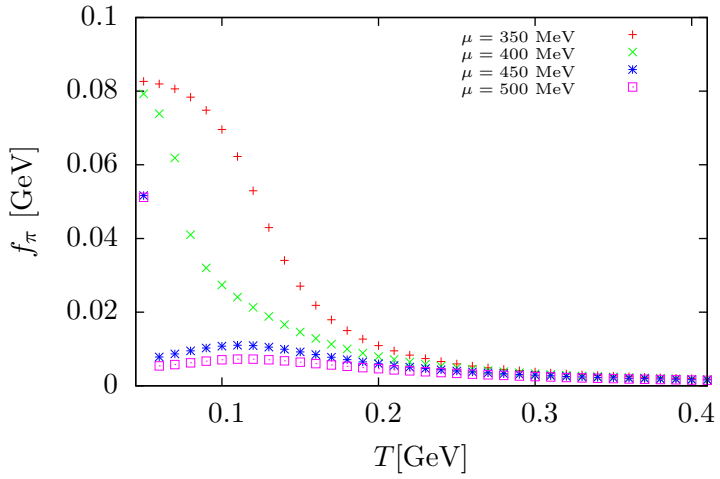

(a)

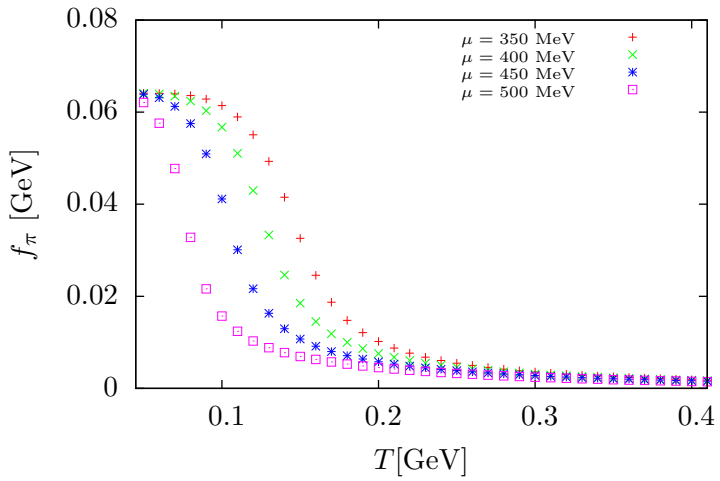

(b)

Figure 6.11.: Chiral condensate for constant T_0 and box sizes (a) $L = 3$ fm and (b) $L = 2$ fm for antiperiodic boundary conditions for large μ.

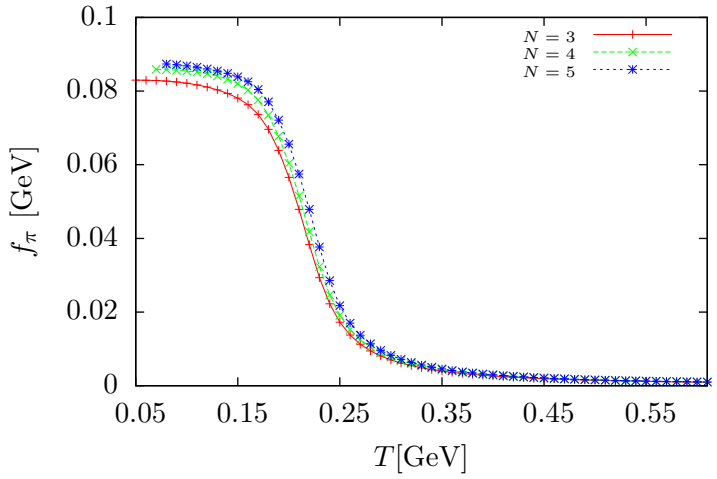

(a)

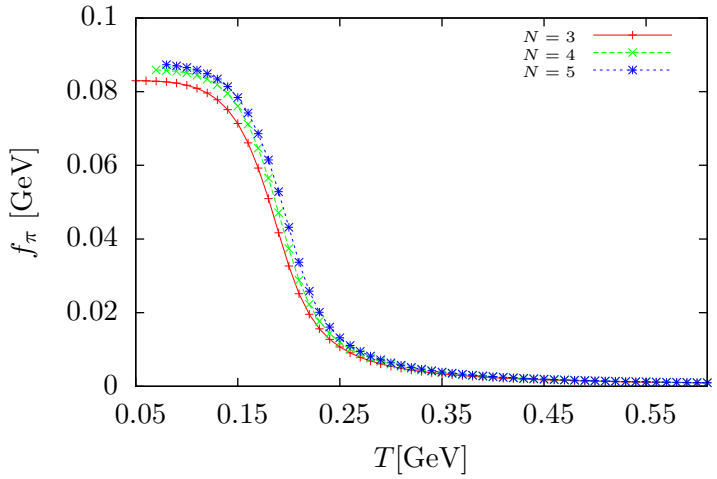

(b)

Figure 6.12.: Convergence behavior of chiral condensate for antiperiodic boundary conditions, constant T_0 and $L = 3$ fm, (a) $\mu = 0$ MeV and (b) $\mu = 200$ MeV for different truncation orders.

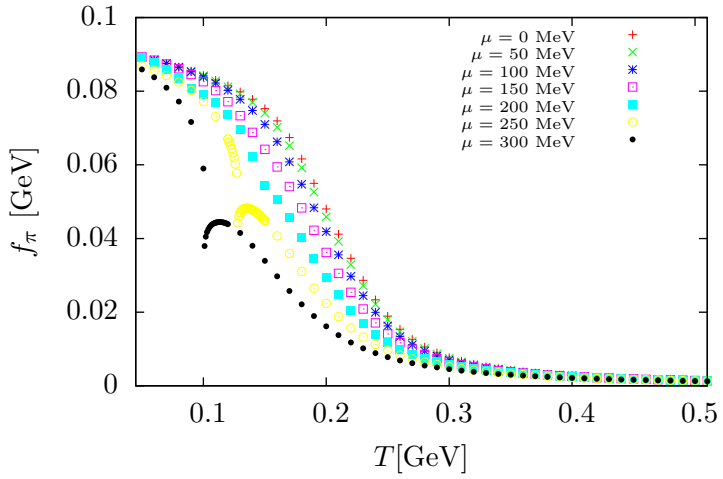

(a)

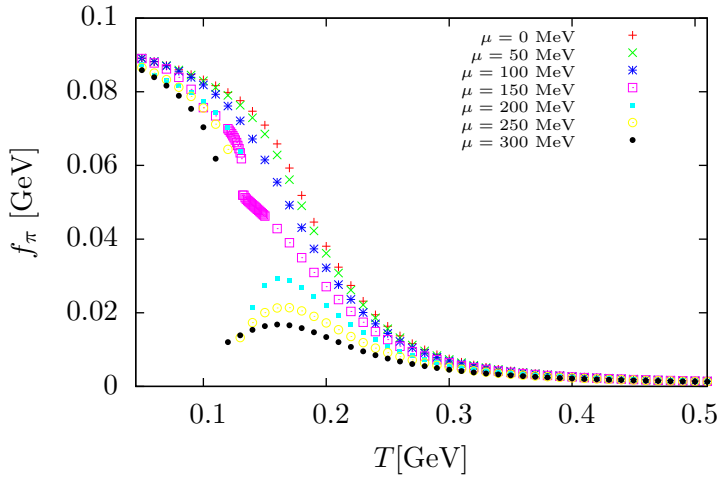

(b)

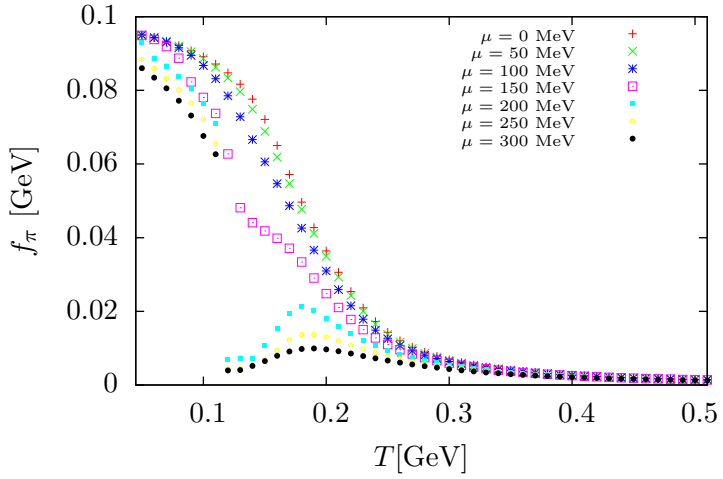

(c)

Figure 6.13.: Chiral condensate for periodic boundary conditions for constant T_0 and box sizes (a) $L = 3$ fm, (b) $L = 2$ fm, (c) $L = 1.5$ fm.

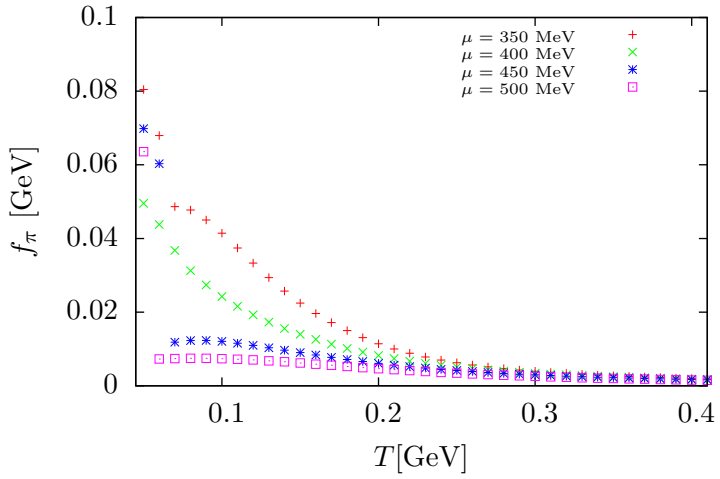

(a)

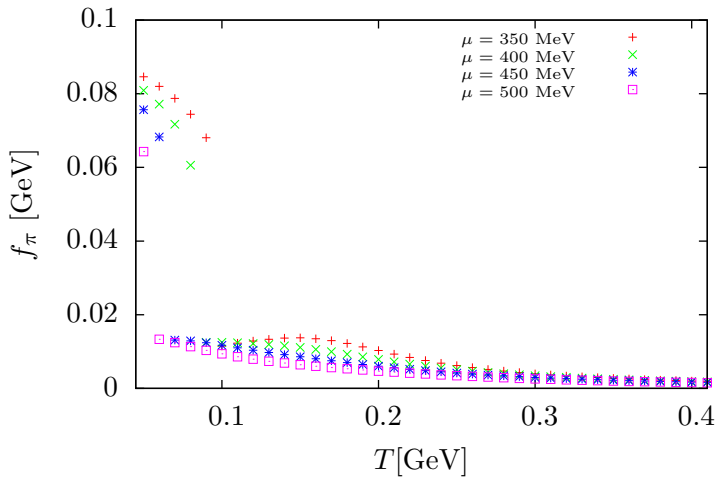

(b)

Figure 6.14.: Chiral condensate for for constant T_0 and box sizes (a) $L = 3$ fm and (b) $L = 2$ fm for periodic boundary conditions and large μ.

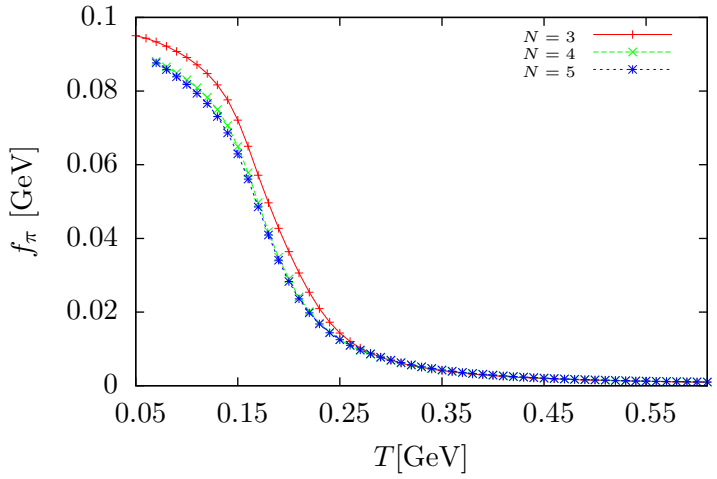

(a)

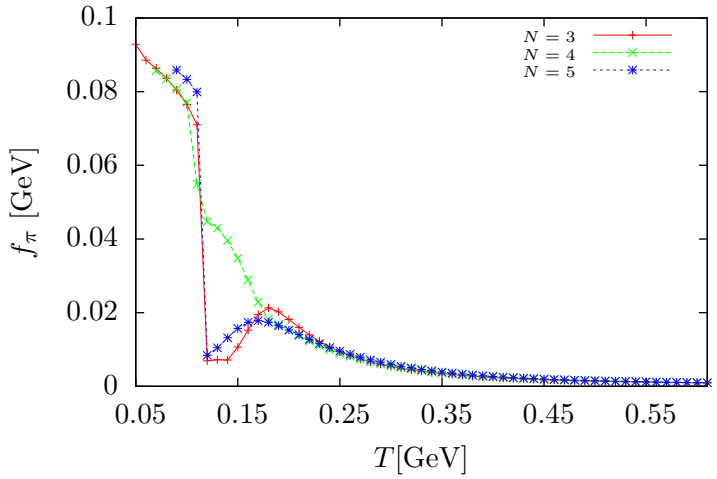

(b)

Figure 6.15.: Convergence behavior of chiral condensate for periodic boundary conditions, constant T_0 and $L = 1.5$, (a) $\mu = 0$ MeV and (b) $\mu = 200$ MeV for different truncation orders.

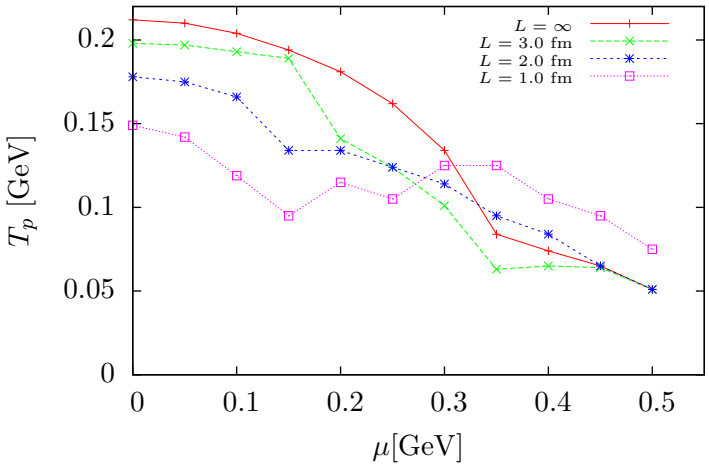

(a)

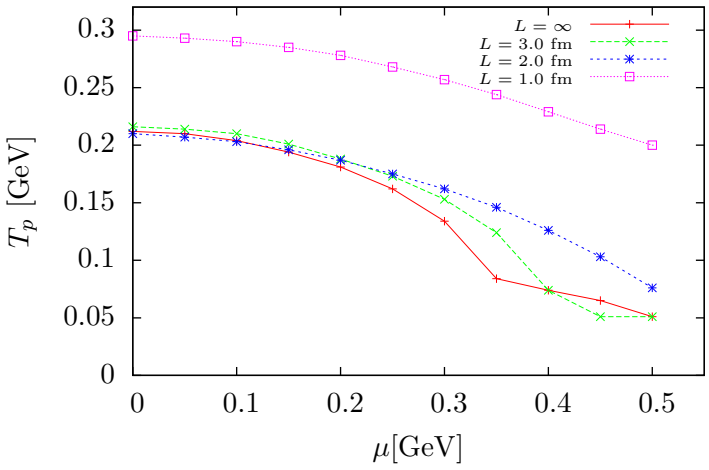

(b)

Figure 6.16.: Phase diagram for $N = 3$ constant T_0 and (a) periodic boundary conditions and (b) antiperiodic boundary conditions.

6.3. Pressure and Quark number density fluctuations in a finite volume with non-zero μ

In this section we compute the pressure P and the quark number fluctuations $\chi^{(2)}$ in a finite volume with a non-zero chemical potential. For the first calculation we choose antiperiodic boundary conditions and omit calculations with periodic boundary conditions, because of the unphysical behavior for small volume sizes. The pressure is obtained as explained in Section 5.3. At a given box size, the pressure is increasing if the chemical potential is increased for both cases of the T_0-function. For constant T_0 in intermediate box sizes and $\mu \gtrsim 150$ MeV a peak is visible. A similar phenomenon we observe in the case of a variable $T_0(\mu)$, but with a μ-dependence of T_0 the enhancement of the pressure is even stronger if μ is enlarged, see Figure 6.17. Nevertheless, the convergence behavior of the pressure to the infinite volume case is bad for the case of large chemical potentials. We would expect a good convergence for a box size $L \approx 4$ fm. Especially in the low temperature regime for, e.g. $\mu = 300$ MeV this is obviously not the case, see Figure 6.18. The Convergence behavior for calculations with $T_0 = T_0(\mu)$ is qualitatively identical to the case of constant T_0.

From the pressure respectively the partition function we can define generalized susceptibilities, the so called n-th order cumulant

$$\chi^{(n)}(T) = \frac{1}{VT^3} \frac{\partial^n \log \mathrm{Z}}{\partial(\mu_B/T)^n}\bigg|_{\mu=0}. \tag{6.5}$$

These functions are the expansion coefficients of the pressure

$$\frac{P(T,\mu_B)}{T^4} = \sum_{n=0}^{n=\infty} \frac{1}{n!} \chi^{(n)}(T) \left(\frac{\mu_B}{T}\right)^n. \tag{6.6}$$

From these cumulants we can derive the following functions which can in principle be related to measurements: the variance σ^2, skewness S and kurtosis κ

$$\begin{aligned} \sigma^2 &= \chi^{(2)}, \\ S &= \frac{\chi^{(3)}}{(\chi^{(2)})^{3/2}}, \\ \kappa &= \frac{\chi^{(4)}}{(\chi^{(2)})^2}. \end{aligned} \tag{6.7}$$

At this point, note also that in a finite volume, the pressure has two terms, the second because of the explicit volume dependence of the effective action, see Eq. 5.7 and 5.8. For the case of $\chi^{(2)}$ we obtain therefore three numerical derivatives. The derivatives are obtained through the difference quotient (Eq. 5.9), especially for the second derivative of the pressure with respect to μ we used

$$\frac{\partial^2 P}{\partial \mu^2} = \frac{P(\mu + 2\Delta\mu) - 2P(\mu) + P(\mu - 2\Delta\mu)}{(2\Delta\mu)^2}. \tag{6.8}$$

In order to study the phase diagram of QCD or effective models like the Polyakov-Quark-Meson model, one has to calculate the cumulant functions. The higher the order, the higher the sensitivity to critical behavior. In particular the skewness should change the sign, when the calculated values pass the phase boundary.

In heavy-ion experiments the net baryon number is not directly accessible, but what can be measured is the fluctuation of the proton number [113]. The net proton number is defined as $N = N_{p-\overline{p}} = N_p - N_{\overline{p}}$. In experiments, low p_T protons are lost due to detector efficiency. Therefore, we can define the mean $\langle N \rangle$ ensemble average of an event-by-event distribution. With the deviation δN of N from its mean $\delta N = N - \langle N \rangle$, we can define various order cumulants of event-by-event distributions:

$$C_{1,N} = \langle N \rangle \, , C_{2,N} = \left\langle (\delta N)^2 \right\rangle , C_{3,N} = \left\langle (\delta N)^3 \right\rangle , C_{4,N} = \left\langle (\delta N)^4 \right\rangle - 3 \left\langle (\delta N)^2 \right\rangle^2 . \tag{6.9}$$

These can be related to the variance σ^2, skewness S and kurtosis κ by

$$\begin{aligned} \kappa\sigma^2 &= \frac{C_{4,N}}{C_{2,N}}, \\ S\sigma &= \frac{C_{3,N}}{C_{2,N}}. \end{aligned} \tag{6.10}$$

With this we have in principle a connection between heavy-ion collisions and numerical calculations see, e.g. [114, 115, 116, 117, 118] for completeness.

The first two coefficients have the following explicit form

$$\begin{aligned} \chi^{(1)} &= \frac{1}{T^3} \left. \frac{\partial P}{\partial \mu} \right|_{\mu=0}, \\ \chi^{(2)} &= \frac{1}{T^2} \left. \frac{\partial^2 P}{\partial \mu^2} \right|_{\mu=0}. \end{aligned} \tag{6.11}$$

Figure 6.19 depicts the $\chi^{(2)}$ coefficient for periodic and antiperiodic boundary conditions at $\mu = 0$ for different box sizes as a function of the temperature. In the case of periodic boundary conditions the volume dependence is small, unless we consider small volumes $L < 2$ fm. Then we obtain, as in the case of the pressure unphysical results, due to the same reasons, i.e. the divergence of the mode function $\mathfrak{B}$ because of the zero-mode, see Section 5.3. For the case of antiperiodic boundary conditions the volume dependence is more strongly pronounced and comparable to that of the pressure (see Figure 5.7). But in contrast to the values of the pressure, those of $\chi^{(2)}$ do not decrease monotonously. The reason may be the fact that $P(\mu) \neq P(-\mu)$, which also means that $\chi^{(1)}$ does not vanish. If we replace $\mu \to -\mu$, e.g., the gap-equation for Φ would change and we obtain a small difference for $\Phi(-\mu)$, unless we substitute in the gap equation $\Phi \to \Phi^*$ and vice versa. This is a contradiction to the statement [119] that the odd terms in the expansion Eq. 6.5 should vanish because of the symmetry of the partition function $Z(\mu) = Z(-\mu)$ (because of CP-symmetry of QCD), but otherwise for the calculation of the skewness S $\chi^{(3)}$ is used [113] and furthermore $\chi^{(1)}$ refers to the quark number density see, e.g. [120]. To calculate furthermore, e.g. the kurtosis, one has to calculate $\chi^{(4)}$. But the numerical accurateness is not sufficient in our approach; to calculate further cumulants one has to use a resummation formula, which is based on Padé approximation see, e.g.[119].

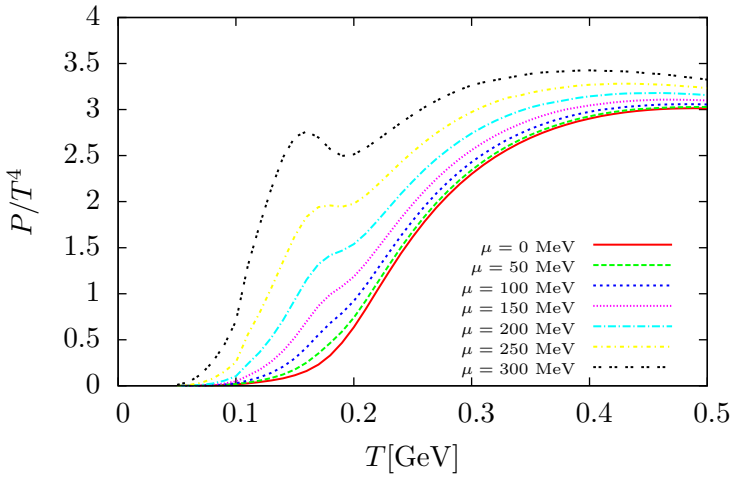

(a)

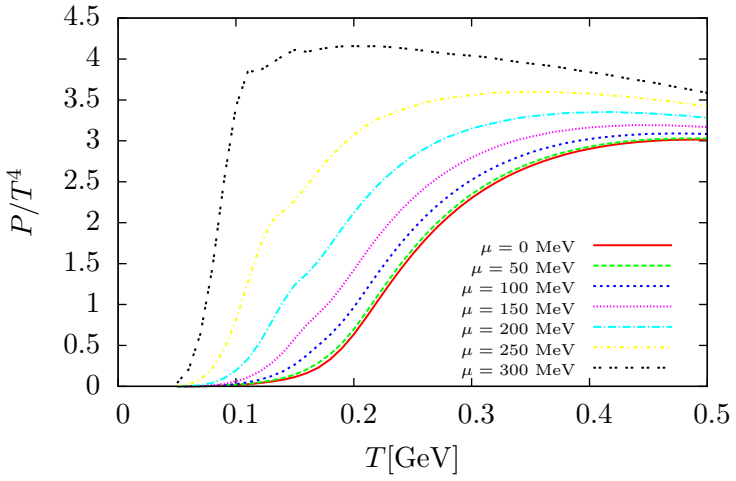

(b)

Figure 6.17.: Pressure for antiperiodic boundary conditions and box size $L = 2$ fm for (a) constant T_0 and (b) $T_0 = T_0(\mu)$.

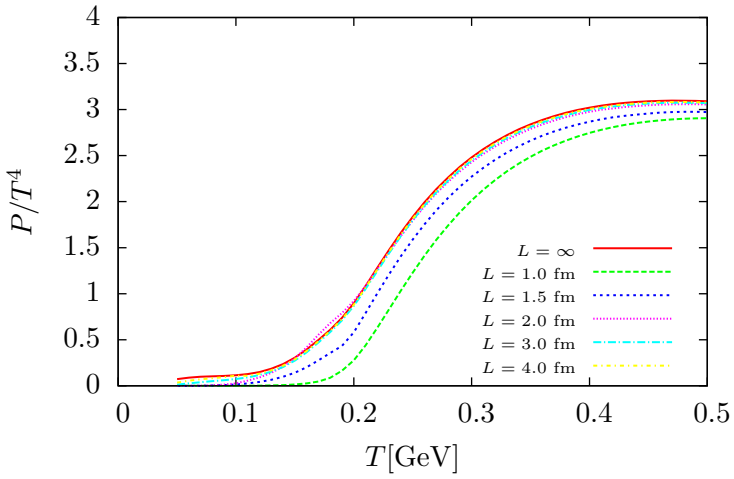

(a)

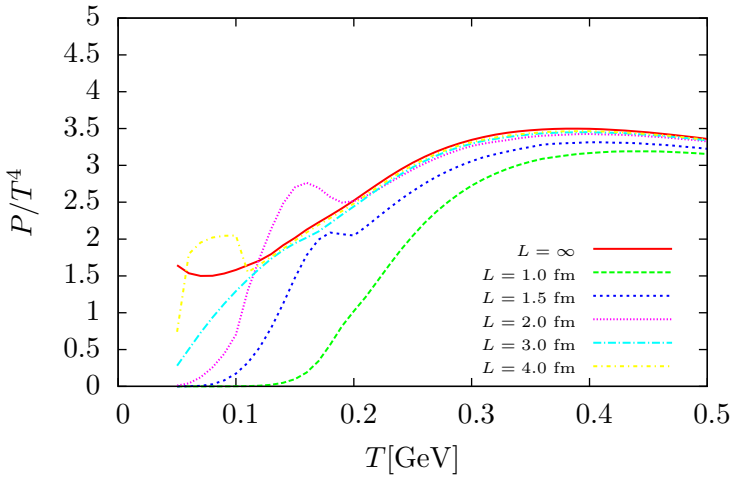

(b)

Figure 6.18.: Convergence behavior of the pressure with constant T_0 and a) $\mu = 100$ MeV, b) $\mu = 300$ MeV and antiperiodic boundary conditions.

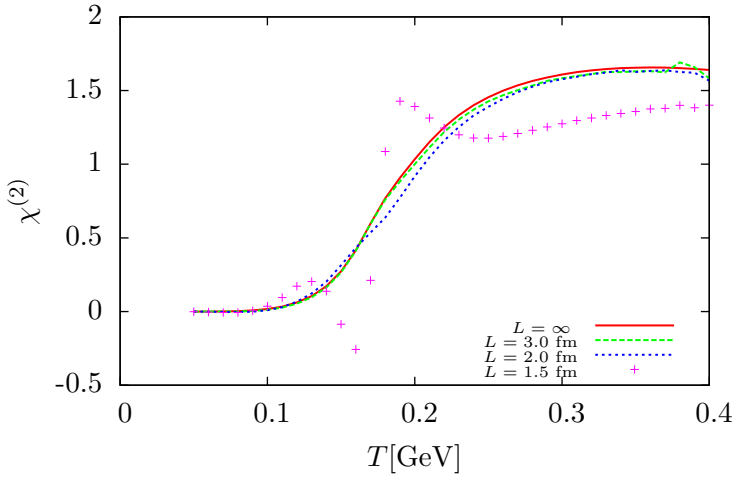

(a)

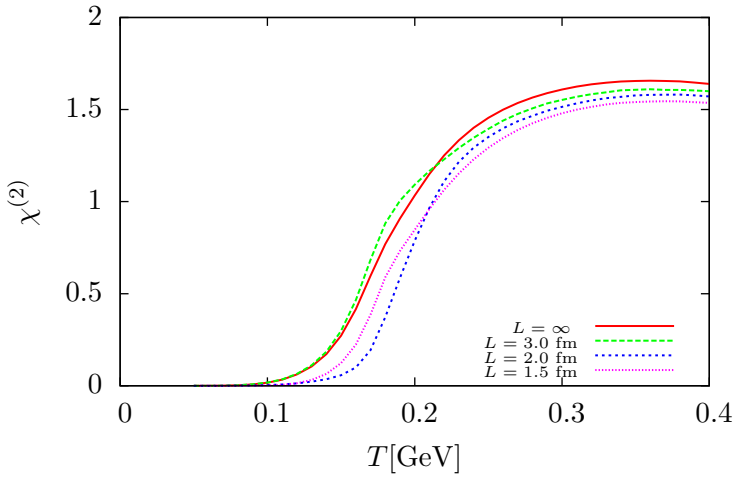

(b)

Figure 6.19.: Coefficient $\chi^{(2)}$ at $\mu = 0$ for (a) periodic and (b) antiperiodic boundary conditions, $N = 3$ and $\Lambda = 3$ GeV.

7. Polyakov-Quark-Meson model in a non-zero magnetic field

7.1. Flow equation with a non-vanishing magnetic field

As previously described lattice calculations with a non-zero chemical potential are affected by the fermion sign problem. That makes it difficult to compare model calculations with Lattice-QCD, since there are no reliable known results for an arbitrary large μ. QCD with a non-vanishing magnetic field has no sign problem in the fermion determinant, which makes model calculations with a non-vanishing magnetic field attractive, hence they can be directly compared with the corresponding lattice results.

Thus, we augment our model (see Section 4.3) in infinite volume with a constant magnetic field in z-direction see, e.g.,[121]. The covariant derivative of the fermionic part is modified with an additional term, with the electromagnetic gauge field

$$D^\mu = \partial^\mu - iA^\mu \delta^4_\mu - iQA^\mu_{EM}, \tag{7.1}$$

where $A^\mu_{EM} = (0, Bx, 0, 0)$ and $Q = \text{diag}\left(\frac{2}{3}\text{e}, -\frac{1}{3}\text{e}\right)$ denotes the fractional electric charge of the up and down quark flavor.

The kinetic term of the charged pions is modified in the following way

$$\begin{aligned}&\frac{1}{2}\left(\partial_\mu \pi_1\right)^2 + \frac{1}{2}\left(\partial_\mu \pi_2\right)^2 \to \mathcal{D}_\mu \pi^+ \mathcal{D}^\mu \pi^- \\ &= \frac{1}{2}\left(\partial_\mu \pi_1\right)^2 + \frac{1}{2}\left(\partial_\mu \pi_2\right)^2 + \frac{1}{2}e^2 B^2 x^2 (\pi_1^2 + \pi_2^2) + eBx(\pi_1 \partial_\mu \pi_2 - \pi_2 \partial_\mu \pi_1),\end{aligned} \tag{7.2}$$

with $\mathcal{D}_\mu = \partial_\mu + ieA^{EM}_\mu$ and $\pi^\pm = \frac{1}{\sqrt{2}}\left(\pi_1 \pm i\pi_2\right)$.

For the case of the charged particles the three dimensional momentum integral is replaced by the sum over Landau-levels and momentum integration in z-direction

$$\int \frac{\mathrm{d}^3 p}{(2\pi)^3} \to \frac{|qB|}{2\pi} \sum_{m=0}^{\infty} \int \frac{\mathrm{d}p_z}{2\pi}, \tag{7.3}$$

thereby q denotes the corresponding charge of the regarded particle. In the regulator and propagator we need to substitute the momentum according to

$$\vec{p}^{\,2} \to p_z^2 + (2m+1)\left|eB\right|, \tag{7.4}$$

and for the bosons and for the fermions according to

$$\vec{p}^{\,2} \to p_z^2 + (2m+1-s)\left|Q_{ff}B\right|, \tag{7.5}$$

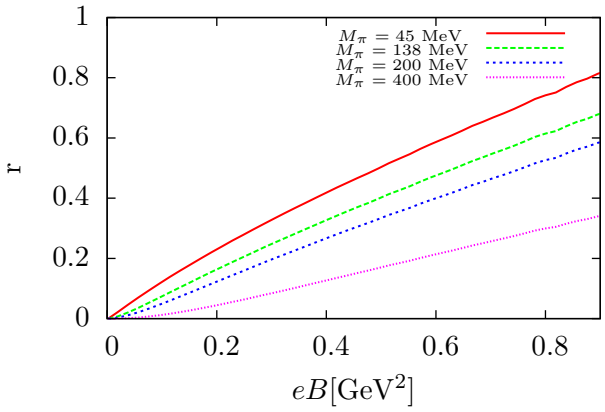

Figure 7.1.: Relative increment r as a function of eB for different pion masses.

where $s = \pm 1$ denotes the spin directions, e the elementary charge of the bosons and $Q_{ff} \in \left\{\frac{2}{3}e, -\frac{1}{3}e\right\}$ the fractional charge of the quarks.

With these modifications (under disregard of the $\propto B^2$- and $\propto B$-dependent terms of Eq. 7.2.) we arrive at the following flow equation for the effective potential

$$\begin{aligned}\partial_t U_k &= \frac{k^5}{12\pi^2}\left(\frac{1}{E_\pi}\coth\left(\frac{E_\pi}{2T}\right)+\frac{1}{E_\sigma}\coth\left(\frac{E_\sigma}{2T}\right)\right)\\ &+ \mathcal{B}_b\frac{|eB|}{2\pi^2}\frac{k^2}{E_\pi}\coth\left(\frac{E_\pi}{2T}\right)\\ &- \mathcal{B}_f N_c\frac{|Q_{ff}B|}{2\pi^2}\frac{k^2}{E_q}\left(1-N-\overline{N}\right),\end{aligned} \tag{7.6}$$

with the Landau-level mode functions:

$$\mathcal{B}_b = \sum_{m=0}^{\infty}\sqrt{k^2-(2m+1)\,|eB|}\,\Theta\left(k^2-(2m+1)\,|eB|\right), \tag{7.7}$$

$$\mathcal{B}_f = \sum_{s=\pm1}\sum_{m=0}^{\infty}\sqrt{k^2-(2m+1-s)\,|Q_{ff}B|}\,\Theta\left(k^2-(2m+1-s)\,|Q_{ff}B|\right). \tag{7.8}$$

For $eB \to 0$ we reproduce the flow equation for the Polyakov-Quark-Meson model without magnetic field [121].

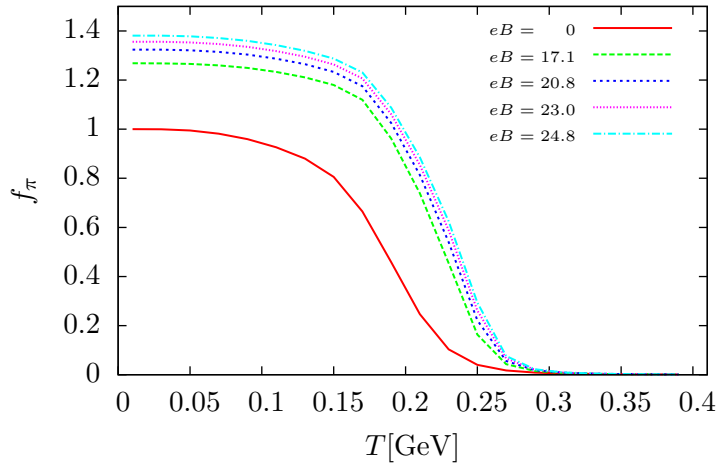

(a)

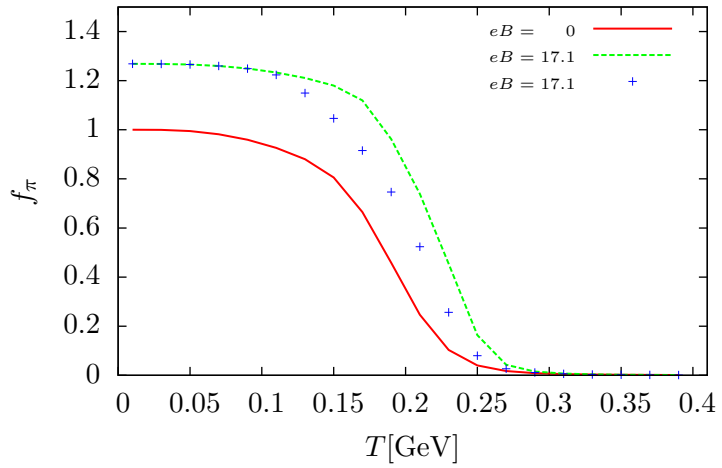

(b)

Figure 7.2.: Normalized pion decay constant: $f_\pi = f_\pi(T)/f_\pi(T=0)$ for (a) $T_0 = const$ (b): comparison of PQM-model with B-field with constant T_0 and $T_0 = T_0(B)$ (points) and PQM-model with $eB = 0$. The values of $T_0(B)$ are extracted from Ref. [122].

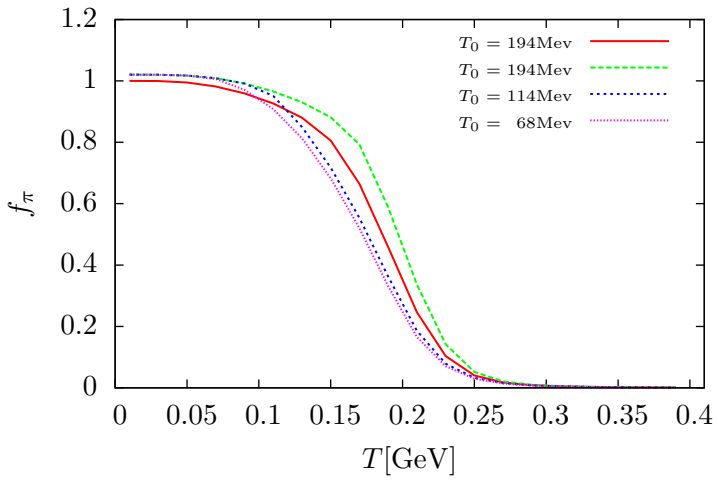

Figure 7.3.: Comparison of PQM model with B-field $eB = 2M_\pi^2$ and variable T_0 and PQM model with $eB = 0$ (red line).

In recent model calculations (like in Ref.[123]) the B-dependent terms were neglected, thus we obtain for the flow equation identical behavior for all three pions. Strictly speaking this is a contradiction. The $O(3)$-symmetry of the three pion is broken, because of the magnetic field and therefore the coupling of the charged pions to the magnetic field and this fact should be visible in the flow equation itself. With the negligence of the B-dependent term the second derivative of the effective action with respect to the fields ($\Gamma^{(2)}$) is diagonal in momentum space and thus can be treated in the familiar way. Nevertheless if we take them into account, $\Gamma^{(2)}$ would be no longer diagonal if we transform $\Gamma(x)$ traditionally in momentum space through expansion in plane waves (Fourier-transformation). We should take instead eigenfunctions which make $\Gamma^{(2)}(p, p')$ diagonal in momentum space. This can be done through expansion in *Ritus-functions*[1] [125, 126, 127, 128]. The charged and uncharged pion should be treated differently in the expected resulting flow equation.

7.2. Chiral catalysis and inverse catalysis effect

The relative increment is defined as follows [122]

$$r = \frac{\rho_{0,k}(T, eB) - \rho_{0,k}(T, eB = 0)}{\rho_{0,k}(T, eB = 0)} \tag{7.9}$$

and describes the influence of the magnetic field to the chiral condensate, i.e. chiral catalysis. Figure 7.1 shows the relative increment as a function of the magnetic field eB for different pion masses at vanishing temperature. If we compare the behavior of $M_\pi = 200$ MeV with that of Ref. [122], we observe that our result has a larger dependence on eB.

In previous model calculations like, e.g. in Ref. [123, 129], T_0 was chosen as a magnetic field-independent constant. These parameters of the effective Polyakov-loop potential are chosen in that way, that they reproduce the deconfinement-transition temperature of pure gauge theory, or of Lattice-QCD with a certain number of flavors. Lattice calculations show that an external magnetic field enhances chiral symmetry breaking, which is called magnetic catalysis. The

[1] In a recent study this was done with Dyson-Schwinger equations, see Ref. [124].

so called valence quarks are responsible for this phenomenon. This behavior was confirmed by various model calculations. Nevertheless, lattice calculations also show, that the chiral transition temperature decreases with increasing magnetic field, which is called inverse magnetic catalysis. For this behavior the Polyakov-loop and the sea quarks are responsible [130, 131, 132]. This behavior could not be observed by model calculations (like, e.g. [123]). If we solve the PQM-model with a $T_0 = T_0(B)$ dependence, we take the finite-B effect of the Polyakov-loop into account, and it is reasonable to assume, that this has a significant influence on the chiral condensate.

From Ref. [122] we take the lattice ($N_f = 2$) value of the critical temperature T_c as a function of the external magnetic field. As a first step we use this number for T_0 in the Polyakov-loop potential. With this function $T_0 = T_0(B)$, we solve this Polyakov-Quark-Meson model and obtain the normalized pion decay constant $f_\pi = f_\pi(T)/f_\pi(T = 0)$ respective chiral condensate $f_\pi = \sqrt{2\rho_{0,k}}$. We observe that for the values of the magnetic field[2] the effect of inverse magnetic catalysis is very small, this effect is compensated by the magnetic catalysis effect, see Figure 7.2. But this is no longer the case if we take smaller values of eB into account, Figure 7.3[3]. In summary we can conclude that at a given magnetic field, a variation of T_0 reveals a small inverse catalysis effect, presupposing that the magnetic field is not too large.

If we repeat the calculations for smaller and larger pion masses the finite magnetic field effects do not change significantly, still the inverse catalysis is at best very small. However, at zero temperature and $eB \neq 0$, the parameters can be adjusted in that way, so that we retain the results (like chiral condensate) in the infrared for $eB = 0$. With this, we have removed the chiral catalysis effect at zero temperature. Consequently, we expect that the inverse catalysis effect is then more visible. But the results (Figure 7.4) show that this effect is still small. Of course, the temperature-dependent part of the flow equations also contribute to the chiral catalysis effect. Indeed, we could adjust our parameters in that way so that we obtain the same relative increment as in the case of lattice simulations, but we have already shown that the inverse catalysis effect is still small if we set the relative increment to zero.

[2] Values of eB are given in units of M_π^2.

[3] Of course the values of $T_0 = T_0(B)$ here used and in Figure 7.4 are arbitrary, we could have used other instead of. Here is shown how the pion decay constant changes under variation of T_0 at a given magnetic field.

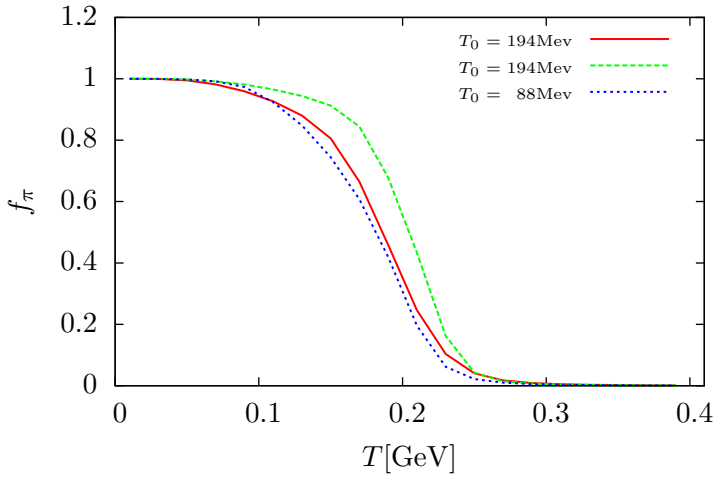

(a)

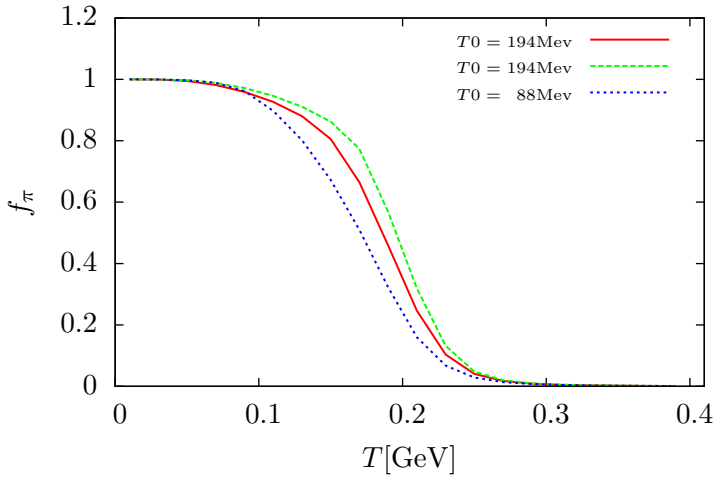

(b)

Figure 7.4.: Comparison of PQM-model with B-field (a) $eB = 20M_\pi^2$ (b) $eB = 2M_\pi^2$, variable T_0 and PQM-model with $eB = 0$ (red line), pion mass $M_\pi = 138$ MeV and adjusted parameters.

8. Conclusion and outlook

In this work we have studied the two-flavor Polyakov-Quark-Meson model with $N_c = 3$. This model is a low-energy effective model of QCD, which contains fermionic, mesonic as well as gluonic degrees of freedom, which in turn allow for a chiral phase as well as a deconfinement phase transition. We used the non-perturbative Functional Renormalization Group and solved in this framework the corresponding flow equations through the so called local potential approximation. Furthermore, we have neglected any momentum dependence of the fields and set the wavefunction renormalizations to one. In infinite volume we have solved the gap-equations on all scales, to account for the back-reaction of the scale dependence of the chiral condensate on the Polyakov-loop-variable. Therefore, we have a scale dependent Polyakov-loop-variable Φ, but still no explicit flow equation for Φ. We compared these results with this case, where the gap-equations were solved only in the infrared regime. Our calculations indicate that the scale dependence of Φ has a small influence on the chiral condensate in the region of the chiral crossover. A significant difference as observed in the case of thermodynamic variables: In the region before the chiral crossover, the pressure remains almost constant, which leads to the consequence that the trace anomaly shows unphysical behavior; it almost vanishes there. If we calculate the pure thermal flow for the pressure, the part of the corresponding flow equation which depends explicitly on the temperature, i.e. without the zero point term, we observe no such phenomenon. Furthermore, the zero point term reduces the quality of convergence of the pressure with increasing truncation order N. We expect that the unphysical behavior of the trace anomaly could be cured if we include a scale dependent wavefunction renormalization, or also possible if we use another regulator for the momentum integration. To obtain a flow equation of the wavefunction renormalization for, e.g. the bosons $Z_{k,\phi}$ we have to expand the bosonic fields instead of a constant field around a field with a small momentum dependence.

For our calculations we assumed for simplicity that the temporal gauge field A_4 is a constant background field. In the general case it depends on all four coordinates $x = (\vec{x}, x_4)$. After Euclidian time integration there would remain a gauge field which depends on the spatial coordinates. It would be reasonable to extend our calculations with a non-constant field, e.g. a gauge field which is restricted to a sphere of finite radius. Outside the sphere the magnitude of $A_4(x)$ should decrease exponentially. Inside the sphere the magnitude might increase but remains constant if $L \to 0$ fm. This should have significant influence to finite volume calculations, especially in the small volume regime.

Finite volume calculations are partly motivated by heavy-ion collisions, which are finite systems and to understand more about the mechanism of Lattice-QCD and its results, what is by definition performed in a finite volume. We have calculated the Polyakov-Quark-Meson model in a finite volume. We allow for periodic or antiperiodic boundary conditions. If we take periodic boundary conditions for bosons as well as for fermions, we have observed unphysical behavior for small volume sizes of the thermodynamic variables, like the pressure, but also in the case of $\chi^{(2)}$. Especially, if we take a non-zero chemical potential into account we observe for small volume sizes a non-monotonous behavior for the Polyakov-loop-variables. Furthermore, we could observe that the local potential approximation for periodic boundary conditions, in those regions where we obtain this behavior, does not converge. Thus, for periodic boundary conditions we cannot give reliable results for the phase diagram. Apart from this the chiral

crossover temperature decreases with increasing chemical potential, as expected. In the case of antiperiodic boundary conditions we obtain no unphysical results for the thermodynamic variables. Also, for a finite chemical potential we find no non-monotonous behavior for the Polyakov-loop-variables. Nevertheless, the phase diagram depends on the chosen boundary conditions. To compare finite-volume studies with heavy-ion experiments one has to choose boundary conditions which are approximately realized in experiments.

Furthermore, we included in our model in infinite volume a non-vanishing magnetic field. Magnetic fields of extreme magnitude are observed in astrophysical objects like magnetars, as well as in heavy-ion collisions. Also, Lattice-QCD with a non-zero magnetic field has no fermion sign problem, thus model calculations with finite magnetic field can be directly compared with results from Lattice-QCD. In our model the gluonic degrees of freedom are implemented through a covariant derivative in the Lagrangian and an effective potential, whose free parameters are adjusted in that way that we can reproduce known lattice results. Especially T_0 depends, e.g. on the number of flavors. Former studies used mostly a constant T_0 and obtain only a magnetic catalysis effect, in contrast to Lattice-QCD, where also an inverse catalysis effect was observed. Therefore, we vary T_0 with the magnetic field to study the possibility of an inverse magnetic catalysis. We obtain that the inverse catalysis effect is present even for small magnetic fields although it is very small and almost negligible. We notice that former studies did not include the breaking of $O(3)$-symmetry of the pions, which was a consequence of the negligence of the B-dependent terms in the effective action. The breaking of $O(3)$-symmetry is due to the magnetic field. This symmetry breaking should be visible in the flow equations itself. If we do not neglect the B-dependent terms, one has to expand the effective action in so called Ritus-functions, instead of in the traditional plane waves to rewrite the effective action in momentum space, which should be done in future studies.

A. Conventions

A.1. Units

Physical constants are set to unity

$$\hbar = c = k_B = 1. \tag{A.1}$$

and we choose the remaining unit to be

$$[\text{Energy}] = \frac{1}{[\text{Time}]} = \frac{1}{[\text{Length}]}, \tag{A.2}$$

in particular

$$1\text{fm} \equiv 0.19733\ \text{GeV}^{-1}. \tag{A.3}$$

A.2. Euclidian space-time and Dirac-matrices

In Minkowski space-time the metric is defined as follows

$$\eta_{\mu\nu} = \begin{pmatrix} 1 & 0 & 0 & 0 \\ 0 & -1 & 0 & 0 \\ 0 & 0 & -1 & 0 \\ 0 & 0 & 0 & -1 \end{pmatrix}. \tag{A.4}$$

To introduce Euclidian space-time, the time component is Wick-rotated, which means that imaginary time is introduced

$$x^4 = ix^0. \tag{A.5}$$

For the derivative with respect to time, the gauge field and the time-like γ-matrix we obtain $\partial_0 \to -i\partial_4$, $A^0 \to -iA^4$ and $\gamma_4 \to i\gamma^0$.

The Dirac representation of the gamma-matrices in $d = 4$ dimensions reads as follows

$$\gamma^i = \begin{pmatrix} 0 & -\tau^i \\ \tau^i & 0 \end{pmatrix}, \gamma^0 = \begin{pmatrix} \mathbb{1}_{2\times 2} & 0 \\ 0 & -\mathbb{1}_{2\times 2} \end{pmatrix}. \tag{A.6}$$

The τ's are the so called Pauli-matrices

$$\tau^1 = \begin{pmatrix} 0 & 1 \\ 1 & 0 \end{pmatrix}, \tau^2 = \begin{pmatrix} 0 & -i \\ i & 0 \end{pmatrix}, \tau^3 = \begin{pmatrix} 1 & 0 \\ 0 & -1 \end{pmatrix}. \tag{A.7}$$

The γ_5 matrix reads

$$\begin{aligned} \gamma_5 &= i\gamma_0\gamma_1\gamma_2\gamma_3 = \gamma_4\gamma_1\gamma_2\gamma_3 \\ &= \begin{pmatrix} 0 & \mathbb{1}_{2\times 2} \\ \mathbb{1}_{2\times 2} & 0 \end{pmatrix}. \end{aligned} \tag{A.8}$$

B. Calculation details of the flow equation

B.1. The bosonic part of the flow equation

To solve the Wetterich equation it is convenient to rewrite the effective action in momentum space. With

$$\phi(x) = \int \frac{\mathrm{d}^d q}{(2\pi)^d} \phi(q) e^{iqx}, \tag{B.1}$$

we obtain

$$\Gamma_k[\phi^a(p)] = \int \frac{\mathrm{d}^d p}{(2\pi)^d} \left\{ \frac{1}{2} p^2 \phi^a(p) \phi^a(-p) + U_k(\rho) \right\}. \tag{B.2}$$

We expand the momentum dependent field around a constant background field

$$\phi^a(p) = \phi \delta_{a1} + \chi^a(p). \tag{B.3}$$

For the second functional derivative $\Gamma_k^{(2)} = \frac{\delta^2 \Gamma_k}{\delta\chi(p)\delta\chi(-p)}$ and the abbreviation $\rho = \frac{1}{2}\phi^2$ we obtain

$$\begin{aligned} \left(\Gamma_k^{(2)}\right)_{11}(p,p') &= \left(p^2 + U_k'(\rho) + 2\rho U_k''(\rho)\right) \delta(p-p'), \\ \left(\Gamma_k^{(2)}\right)_{aa,a\neq 1}(p,p') &= \left(p^2 + U_k'(\rho)\right) \delta(p-p'). \end{aligned} \tag{B.4}$$

Here p^2 denotes the four-vector momentum in Euclidian space-time $p^2 = \vec{p}^{\,2} + p_4^2$. The Wetterich equation then reads

$$\partial_t \Gamma_k = \frac{1}{2} \mathfrak{Tr} \left(\frac{\partial_t R_{k,B}}{R_{k,B} + \Gamma^{(2)}_{k,ab}} \right) = \frac{1}{2} \beta V \int \frac{\mathrm{d}^d p}{(2\pi)^d} \int \frac{\mathrm{d}^d p'}{(2\pi)^d} \sum_{aa}^{N} \left(\frac{\partial_t R_{k,B}}{R_{k,B} + \Gamma^{(2)}_{k,aa}} \right). \tag{B.5}$$

The diagonal matrix Γ_k^2 can be easily inverted, with the Litim regulator, the momentum integration can be performed analytically and with $\Gamma_k = \beta V U_k$ we obtain for the (bosonic) flow equation of the effective action U_k

$$\begin{aligned} \partial_t U_k &= \frac{1}{2} \int \frac{\mathrm{d}^4 p}{(2\pi)^4} \partial_t R_{k,B} \left(\frac{N-1}{p^2 + R_{k,B} + U_k'} + \frac{1}{p^2 + R_{k,B} + U_k' + 2\rho U_k''} \right) \\ &= \frac{T}{2} \sum_{n=-\infty}^{\infty} \int \frac{\mathrm{d}^3 p}{(2\pi)^3} 2k^2 \left(\frac{N-1}{\omega_n^2 + k^2 + U_k'} + \frac{1}{\omega_n^2 + k^2 + U_k' + 2\rho U_k''} \right) \Theta(k^2 - \vec{p}^{\,2}) \\ &= \frac{k^5}{12\pi^2} \left((N-1) \frac{\coth(\frac{\sqrt{k^2+U_k'}}{2T})}{\sqrt{k^2+U_k'}} + \frac{\coth \frac{\sqrt{k^2+U_k'+2\rho U_k''}}{2T}}{\sqrt{k^2+U_k'+2\rho U_k''}} \right) \\ &= \frac{k^5}{12\pi^2} \left\{ (N-1) \frac{1}{\sqrt{k^2+M_\pi^2}} \left(1 + 2n_B(M_\pi)\right) + \frac{1}{\sqrt{k^2+M_\sigma^2}} \left(1 + 2n_B(M_\sigma)\right) \right\}. \end{aligned} \tag{B.6}$$

The hyperbolic function can be rewritten in terms of the Bose-Einstein distribution function

$$n_B(M_i) = \frac{1}{e^{\frac{\sqrt{k^2+M_i^2}}{T}} - 1}, \quad i \in \{\pi, \sigma\}, \tag{B.7}$$

where M_i denotes the pion and sigma mass.

B.2. The fermionic part of the flow equation

In order to rewrite the fermionic part of the effective action in momentum space, we have to transform the fermionic fields

$$\begin{aligned} \psi(x) &= \int \frac{\mathrm{d}^d q}{(2\pi)^d} \psi(q) e^{iqx}, \\ \overline{\psi}(x) &= \int \frac{\mathrm{d}^d q}{(2\pi)^d} \overline{\psi}(q) e^{-iqx}. \end{aligned} \tag{B.8}$$

In the Nambu-Gorkov basis for the denominator of the fermionic part of the flow equation in momentum space we obtain

$$\Gamma_F^{(2)}(p,p') + R_{k,F}(p,p') = \begin{pmatrix} 0 & 1 \\ 1 & 0 \end{pmatrix} (\not{P} + R_{k,F}(p) + gM(p-p'))\delta(p-p'), \tag{B.9}$$

with the mass term and the covariant momentum

$$M_{\alpha,\beta}(p) = (\sigma + i\gamma_5 \vec{\tau} \cdot \vec{\pi})(p) \mathbb{1}_{\alpha,\beta}^{\text{flavor}}, \tag{B.10}$$

$$\not{P} = \not{p} + \gamma_4 \left(p_4 + A^4 + i\mu\right). \tag{B.11}$$

Inserting this in the Wetterich equation, we obtain the flow for the effective action

$$
\begin{aligned}
\partial_t\Gamma_k &= -\frac{1}{2}\mathfrak{S}\mathfrak{T}\mathfrak{r}\left(\partial_t R_{k,F}\cdot[\Gamma_F^{(2)}(p,p')+R_{k,F}(p,p')]^{-1}\right)\\
&= -\frac{1}{2}\mathfrak{S}\mathfrak{T}\mathfrak{r}\left\{\begin{pmatrix}0 & \partial_t R_{k,F}\\ \partial_t R_{k,F} & 0\end{pmatrix}\cdot\begin{pmatrix}0 & \frac{1}{\not{p}+gM+R_{k,F}}\\ \frac{1}{\not{p}+gM+R_{k,F}} & 0\end{pmatrix}\right\}\delta(p-p')\mathbb{1}^{\text{flavor}}_{\alpha,\beta}\\
&= -\frac{1}{2}\mathfrak{S}\mathfrak{T}\mathfrak{r}\begin{pmatrix}\frac{\partial_t R_k}{\not{p}+gM+R_{k,F}} & 0\\ 0 & \frac{\partial_t R_{k,F}}{\not{p}+gM+R_{k,F}}\end{pmatrix}\delta(p-p')\mathbb{1}^{\text{flavor}}_{\alpha,\beta}\\
&= -\mathfrak{S}\mathfrak{T}\mathfrak{r}\left(\frac{\partial_t R_{k,F}}{\not{p}+gM+R_{k,F}}\right)\delta(p-p')\mathbb{1}^{\text{flavor}}_{\alpha,\beta}\\
&= -\mathfrak{S}\mathfrak{T}\mathfrak{r}\left(N_f\frac{\partial_t\not{p}r_k}{gM+\gamma^4(p_4A^4+i\mu)+\not{p}(1+r_k)}\right)\delta(p-p')\Theta(k^2-\vec{p}^{\,2})\\
&= -\mathfrak{T}\mathfrak{r}\left(4N_f\mathrm{tr_c}\frac{\vec{p}^{\,2}(1+r_k)\partial_t r_k}{(p_4+A^4+i\mu)^2+\vec{p}^{\,2}(1+r_k)^2+g^2M^2}\right)\delta(p-p')\Theta(k^2-\vec{p}^{\,2})\\
&= -\beta V\int\frac{\mathrm{d}^4p}{(2\pi)^4}\int\frac{\mathrm{d}^4p'}{(2\pi)^4}\left(4N_f\mathrm{tr_c}\frac{\vec{p}^{\,2}(1+r_k)\partial_t r_k}{(p_4+A^4+i\mu)^2+\vec{p}^{\,2}(1+r_k)^2+2g^2\rho}\right)\delta(p-p')\Theta(k^2-\vec{p}^{\,2})\\
&= -\beta V\int\frac{\mathrm{d}^3p}{(2\pi)^3}\sum_{n=-\infty}^{\infty}\left(4N_f\mathrm{tr_c}\frac{\vec{p}^{\,2}(1+r_k)\partial_t r_k}{((2n+1)\pi T+A^4+i\mu)^2+\vec{p}^{\,2}(1+r_k)^2+M_q^2}\right)\Theta(k^2-\vec{p}^{\,2})\\
&= -\beta V\frac{N_f k^5}{12\pi^2 E_q}\mathrm{tr_c}\left(\tanh\left(\frac{E_q-\mu+iA^4}{2T}\right)+\tanh\left(\frac{E_q+\mu-iA^4}{2T}\right)\right) \qquad \text{(B.12)}
\end{aligned}
$$

At the end we perform the color trace. With $A^4=\frac{\lambda^\mu}{2}A^4_\mu$, the definition of Φ and Φ^*, $\Gamma_k=\beta V U_k$, and the definition of the hyperbolical tangents, we arrive at

$$
\partial_t U_k=\frac{k^5}{12\pi^2}\left(-\frac{2N_fN_c}{E_q}\right)\left(F(T,\mu,\Phi,\Phi^*)+F(T,-\mu,\Phi^*,\Phi)\right), \qquad \text{(B.13)}
$$

where

$$
F(T,\mu,\Phi,\Phi^*)=\frac{-1-\Phi^*e^{\beta(E_q-\mu)}+\Phi e^{2\beta(E_q-\mu)}+e^{3\beta(E_q-\mu)}}{1+3\Phi^*e^{\beta(E_q-\mu)}+3\Phi e^{2\beta(E_q-\mu)}+e^{3\beta(E_q-\mu)}}. \qquad \text{(B.14)}
$$

This term can be rewritten easily into the above expression $N(T,\mu,\Phi,\Phi^*)$, see Eq. 4.23. If we set Φ and Φ^* to one, we reobtain the Fermi-Dirac distribution function.

Literature

[1] C. McBride, E. G. Noya, J. L. Aragones, M. M. Conde, C. Vega. "The phase diagram of water from quantum simulations". Phys. Chem. Chem. Phys. 14 10140-10146, 2012, arXiv:1205.5181 [cond-mat.stat-mech].

[2] R. Ramirez, N. Neuerburg, C. P. Herrero. "The phase diagram of ice: a quasi-harmonic study based on a flexible water model". J. Chem. Phys. 139 084503, 2013, arXiv:1310.1006v1 [physics.chem-ph].

[3] S. Ninet, F. Datchi. "High pressure - high temperature phase diagram of ammonia". J. Chem. Phys. 128 154508, 2008, arXiv:0801.0913v1 [cond-mat.mtri-sci].

[4] Y. Miake K. Yagi, T. Hatsuda. *Quark-Gluon Plasma.* Cambridge University Press, 2008.

[5] R. C. Duncan, C. Thompson. "Formation of very strongly magnetized neutron stars: Implications for gamma-ray bursts". Astrophys. J. 392: L9-L13, 1992.

[6] D. J. Schwarz. "The first second of the Universe". Annalen Phys. 12: 220-270, 2003, arXiv:astro-ph/0303574.

[7] A. Bzdak, V. Skokov. "Event-by-event fluctuations of magnetic and electric fields in heavy in collisions". Phys. Lett. B 710: 171-174, 2012, arXiv:1111.1949v2 [hep-ph].

[8] V. D. Toneev, V. Voronyuk, E. L. Bratkovskaya, V. P. Konchakovski, S. A. Voloshin. "Theoretical analysis of a possible oberservation of the chiral magnetic effect in Au+Au collisions within the RHIC energy scan program". Phys. Rev. C 83 054911, 2011, arXiv:1112.2595 [hep-ph].

[9] D. E. Kharzeev, L. D. McLerran, H. J. Warringa. "The effects of topological charge change in heavy ion collisions: Event by event $\mathcal{P}$ and $\mathcal{CP}$ violation ". Nucl. Phys. A 803: 227-253, 2008, arXiv:0711.0950v1 [hep-ph].

[10] ALICE Collaboration. "Net-Charge Fluctuations in Pb-Pb Collisions at $\sqrt{s_{NN}} = 2.76$ TeV". Phys. Rev. Lett. 110 152301, 2013, arXiv:1207.6068v2 [nucl-ex].

[11] STAR Collaboration. "Beam-energy and system-size dependence of dynamical net charge fluctuations". Phys. Rev. C 79 024906, 2009, arXiv:0807.3269v1 [nucl-ex].

[12] ATLAS Collaboration. "Observation of a Centrality-Dependend Dijet Asymmetry in Lead-Lead Collisions at $\sqrt{s_{NN}} = 2.76$ TeV with the ATLAS Detector at LHC". Phys. Rev. Lett. 105 252303, 2010), arXiv:1011.6182v2 [hep-ex] .

[13] S. De, D. K. Srivastava. "System size dependence of nuclear modification and azimuthal anisotropy of jet quenching". arXiv:1107.5659v3 [nucl-th].

[14] P. Braun-Munzinger, J. Stachel. "The quest for the quark-gluon plasma". Nature 448 302-309, 2007.

[15] P. Braun-Munzinger, J. Wambach. "The Phase Diagram of Strongly-Interacting Matter". Rev. Mod. Phys. Vol 81 1031-1050, 2009, arXiv:0801.4256 [hep-ph].

[16] D. Anchishkin, V. Khryapa, V. Ruuskanen. "Thermal Dilepton Radiation from Finite Fireball". arXiv:hep-ph/0210346.

[17] K. Fukushima, T. Hatsuda. "The phase diagram of dense QCD". Rep. Prog. Phys. 74 014001, 2011, arXiv:1005.4814v2 [hep-ph].

[18] J. Gasser, H. Leutwyler. "Spontaneously broken symmetries: effective lagrangians at finite volume". Nucl. Phys. B307 763-778, 1998.

[19] G. Colangelo. "Finite volume effects in chiral perturbation theory". Nuclear Physics B - Proceedings Supplement Vol 140, arXiv:hep-lat/0409111.

[20] F. Bernardoni, P.H. Damgaard, H. Fukaya, P. Hernandez. "Finite Volume Scaling of Pseudo Nambu-Goldstone Bosons in QCD". JHEP 0810: 008, 2008, arXiv:0808.1986v3 [hep-lat].

[21] P. H. Damgaard, H. Fukaya. "The Chiral Condensate in a Finite Volume". JHEP 0901:052. 2009, arXiv:0812.2797v2 [hep-lat].

[22] P. F. Bedaque, H. W. Grießhammer, G. Rupak. "A nucleon in a tiny box". Phys. Rev. D71 054015, 2005, arXiv:hep-lat/0407009v3.

[23] G. Colangelo, S. Dürr. "The pion mass in finite volume". Eur. Phys. J C33: 543-553, 2004, arXiv:hep-lat/0311023v1.

[24] C. S. Fischer, M. R. Pennington. "Finite volume effects in a quenched lattice-QCD quark propagator". Phys. Rev. D73 034029, 2006, arXiv:hep-ph/0512233v2.

[25] J. Luecker, C. S. Fischer, R. Williams. "Volume behavior of quark condensate, pion mass and decay constant from Dyson-Schwinger equations". Phys. Rev. D81:094005, 2010, arXiv:0912.3686v2 [hep-ph].

[26] J. Braun, B. Klein. "Scaling functions for the O(4) model in d=3 dimensions". Phys. Rev. D77:096008, 2008, arXiv:0712.3574v1 [hep-th].

[27] J. Braun, B. Klein. "Finite-Size Scaling behavior in the O(4)-model". Eur. Phys. J C63: 443-460, 2009, arXiv:0810.0857v2 [hep-ph].

[28] J. Braun, B. Klein, P. P. "On the scaling behavior of the chiral phase transition in QCD in finite and infinite volume". Eur. Phys. J. C71:1576, 2011, arXiv:1008.2155v1 [hep-ph].

[29] L. F. Palhares, E. S. Fraga, T. Kodama. "Finite-size effects and the search for the critical endpoint in heavy ion collisions". PoS CPOD2009:011,2009, arXiv:0910.4363v1 [hep-ph].

[30] J. Braun, B. Klein, B. J. Schaefer. "On the Phase Structure of QCD in a FInite Volume". Phys. Lett. B713 216-223, 2012, arXiv:1110.0849v2 [hep-ph].

[31] R. A. Tripolt, J. Braun, B. Klein, B. J. Schaefer. "The Effect of Fluctuations on the QCD Critical Point in a Finite Volume". arXiv:1308.0164v1 [hep-ph].

[32] O. Kiriyama, T. Kodama, T. Koide. "Finite-size effects on the QCD phase diagram". arXiv:hep-ph/0602086v1.

[33] A. Bhattacharyya, P. Deb, S. K. Ghosh, R. Ray, S. Sur. "Thermodynamics Properties of Strongly Interacting Matter in a Finite Volume using the Polyakov-Nambu-Jona-Lasinio model". Phys. Rev. D87, 054009, 2013 arXiv:1212.5893v2 [hep-ph].

[34] T. K. Herbst, J. M. Pawlowski, B. J. Schaefer. "The phase structure of the Polyakov-quark-meson model beyond mean field". Phys. Lett. B696: 58-67, 2011, arXiv:1008.0081 [hep-ph].

[35] G. Papp, B.J. Schaefer, H.J. Pirner, J. Wambach. "On the Convergence of the Expansion of Renormalization Group Flow Equation". Phys. Rev. D61 096002, 2000, arXiv:hep-ph/9909246v3.

[36] F. Wilczek. "QCD in extreme conditions". arXiv:hep-ph/0003183v1.

[37] A. Pich. "Aspect of Quantum Chromodynamics". arXiv:hep-ph/0001118v1.

[38] J. Steinberger. "On the Use of Subtraction Fields and the Lifetimes of Some Types of Meson Decay". Phys. Rev. 76 1180, 1949.

[39] F. E. Close. *An Introduction to Quarks and Partons.* Academic Press, 1979.

[40] CMS collaboration. "Measurement of the ration of the inclusive 3-jet cross section to the inclusive 2-jet cross section in pp collisions at $\sqrt{s} = 7$ TeV and first determination of the strong coupling constant in the TeV range". arXiv:1304.7498v1 [hep-ex].

[41] S. Bethke. "Experimental Tests of Asymptotic Freedom". Prog. Part. Nucl. Phys. 58: 351-386, 2007, arXiv:hep-ex/0606035v2.

[42] L3 collaboration. "A test of QCD based on 4-jet events from Z^0 decays". Phys. Lett B 248: 227, 1990.

[43] J. Kapusta. *Finite-Temperature Field Theory.* Cambridge University Press, 1989.

[44] M. Le Bellac. *Thermal Field Theory.* Cambridge University Press, 1996.

[45] M. P. Lombardo. "Finite Temperature Field Theory and Phase Transitions". arXiv:hep-ph/0103141v2.

[46] A. Smilga. *Lectures on Quantum Chromodynamics.* World Scientific, 2001.

[47] G. Ecker. "Quantum Chromodynamics". arXiv:hep-ph/0604165v1.

[48] J. Goldstone, A. Salam, S. Weinberg. "Broken Symmetries". Phys. Rev. 127 965, 1962.

[49] K. Rajagopal. "The Chiral Phase Transition in QCD: Critical Phenomena and Long Wavelength Pion Oscillations". arXiv:hep-ph/9504310.

[50] A. Butti, A. Pelissetto, E. Vicari. "On the nature of the finite-temperature transition in QCD". JHEP 0308:029, 2003, arXiv:hep-ph/0307036.

[51] K. Holland, U. J. Wiese. "The Center Symmetry and its spontaneous Breakdown at high Temperatures". arXiv:hep-ph/0011193v1.

[52] V. Azcoiti, A. Galante, V. Laliena. "Theta-vacuum: Phase Transitions and/or Symmetry Breaking at $\theta = \pi$". Prog. Theor. Phys. 109 843-851, 2003, arXiv:hep-th/0305065.

[53] R.D. Peccei, H. Quinn. "CP Conservation in the Presence of Pseudoparicle". Phys. Rev. Lett. 38 1440, 1977.

[54] F. Wilczek. "QCD and Asymptotic Freedom: Perspectives and Prospects". arXiv:hep.ph/9211290v1.

[55] A. Pich. "Review of α_s determinations". arXiv:1303.2262v1 [hep-ph].

[56] C. D. Roberts. "Strong QCD and Dyson-Schwinger Equations". arXiv:1203.5341v1 [nucl-th].

[57] C. B. Lang C. Gattringer. *Quantum Chromodynamics on the Lattice - An Introductory Presentation.* Springer, 2010.

[58] O. Philipsen. "Lattice QCD at finite temperature and density". Eur. Phys. J. ST 152: 29-60, 2007, arXiv:0708.1293v2 [hep-lat].

[59] P. de Forcrand. "Simulating QCD at finite temperature". PoS (LAT2009) 010, 2009, arXiv:1005.0539v2 [hep-lat].

[60] J. B. Kogut, M. A. Stephanov, D. Toublan, J. J. M. Verbaarschot, A. Zhitnitsky. "QCD-like Theories at finite Baryon Density". Nucl. Phys. B 582: 477-513, 2000, arXiv:hep-ph/0001171v2.

[61] L. v. Smekal. "Universal Aspects of QCD-like Theories". Nucl. Phys. B (Proc. Suppl.) 228 179-220, 2012 arXiv:1205.4205v1 [hep-ph].

[62] A. Maas, B. H. Wellegehausen. "G2 gauge theories". PoS (Lattice 2012) 080, arXiv:1210.7950v1.

[63] A. Maas, L. v. Smekal, B. Wellegehausen, A. Wipf. "The phase diagram of a gauge theory with fermionic baryons". Phys. Rev. D 86 111901(R), 2012, arXiv:1203.5653v2 [hep-lat].

[64] M. Pepe, U. J. Wiese. "Exceptional Deconfinement in G(2) Gauge Theory". Nucl. Phys. B768:21-37, 2007, arXiv:hep-lat/0610076v1.

[65] M. Stephanov. "QCD phase diagram: an overview". PoS LAT2006:024, 2006, arXiv:hep-lat/0701002v1.

[66] M. Stephanov. "QCD phase diagram and the critical point". Int. J. Mod. Phys. A 20: 4387-4392, 2005, arXiv:hep-ph/0402115v1.

[67] S. Hands. "The Phase Diagram of QCD". Contemp. Phys. 42: 209-225, 2001, arXiv:physics/0105022v1.

[68] G. Endrödi, Z. Fodor, S. D. Katz, K. K. Szabo. "The QCD phase diagram at nonzero quark density". JHEP 1104: 001, 2011, arXiv:1102.1356v1 [hep-lat].

[69] M. G. Alford, A. Schmitt. "Color superconductivity in dense quark matter". Rev. Mod. Phys. 80: 1455-1515, 2008, arXiv:0709.4635v2 [hep-ph].

[70] M. G. Alford. "Quark matter in neutron stars". Nucl. Phys. A 830: 385c-392c, 2009, arXiv:0907.0200v2 [nucl-th].

[71] M. A. Stephanov J. B. Kogut. *The Phases of Quantum Chromodynamics - From Confinement to Extreme Environments.* Cambridge University Press, 2004.

[72] J. P. Blaizot, A. Ipp. "Perturbation theory and non-perturbative renormalization flow in scalar field theory at finite temperature". Nucl. Phys. A 784: 376-406, 2007, arXiv:hep-ph/0610004v2.

[73] K. Lichtenegger, D. Zwanziger. "Contribution to the QCD Pressure beyond Perturbation Theory". PoS Confinement 8: 125, 2008, arXiv:0812.3325v1 [hep-ph].

[74] K. Kajantie, M. Laine, K. Rummukainen, Y. Schröder. "Pressure of hot QCD up to $g^6 \ln(1/g)$". Phys. Rev. D 67 105008, 2003.

[75] M. Quiros. "Finite Temperature Field Theory and Phase Transitions". arXiv:hep-ph/9901312v1.

[76] R. Bouchendira, P. Clade, S. Guellati-Khelifa, F. Nez, F. Biraben. "New Determination of the Fine Structure Constant and Test of the Quantum Electrodynamics". Phys. Rev. Lett. 106 080801, 2011.

[77] A. V. Manohar. "Effective Field Theories". arXiv:hep-ph/9606222v1.

[78] A. Pich. "Effective Field Theory". arXiv:hep-ph/9806303v1.

[79] C. P. Burgess. "Introduction to Effective Field Theory". Ann. Rev. Nucl. Part. Sci. 57: 329-362, 2007, arXiv:hep-th/0701053v2.

[80] H. Leutwyler. "On the Foundations of Chiral Perturbation Theory". Annals Phys. 235: 165-203, 1994, arXiv:hep-ph/9311274.

[81] B. Kubis. "An introduction to chiral perturbation theory". arXiv:hep-ph/0703274v1.

[82] M. R. Schindler, S. Scherer. "Chiral effective field theories of the strong interaction". Eur. Phys. J.ST. 198: 95-116, 2011, arXiv:1104.3134v1 [hep-ph].

[83] L. P. Kadanoff. "Scaling laws for Ising models near T(c)". Physics 2: 263-272, 1966.

[84] T. Yu Cao. *Conceptual Foundations of Quantum Field Theory.* Cambridge University Press, 1999.

[85] J. Cardy. *Scaling and Renormalization in Statistical Physics.* Cambridge University Press, 1996.

[86] K. G. Wilson, J. Kogut. "The renormalization group and the ϵ expansion". Phys. Rept. 12: 75-200, 1974.

[87] C. Wetterich. "Exact evolution equation for the effective potential". Phys. Lett. B 301: 90-94, 1993.

[88] H. Gies. "Introduction to the functional RG and applications to gauge theories". arXiv:hep-ph/0611146.

[89] B. Delamotte. "An introduction to the nonperturbative renormalization group". arXiv:cond-mat/0702365v1.

[90] J. Berges. "QCD in Extreme Conditions and the Wilsonian 'Exact Renormalization Group'". arXiv:hep-ph/9902419v1.

[91] J. Berges, N. Tetradis, C. Wetterich. "Non-Perturbative Renormalization Flow in Quantum Field Theory and Statistical Physics". Phys. Rept. 363: 223-386, 2002, arXiv:hep-ph/0005122v1.

[92] D. F. Litim. "Optimisation of the exact renormalisation group". Phys. Lett. B 486: 92-99, 2000, arXiv:hep-th/0005245v1.

[93] M. Peskin, D. Schröder. *An Introduction to Quantum Field Theory.* Westview Press, 1995.

[94] A. Zee. *Quantum Field Theory in a Nutshell.* Princeton University Press, 2010.

[95] V. A. Miransky. *Dynamical Symmetry Breaking in Quantum Field Theories.* World Scientific, 1993.

[96] J. Berges, D. Mesterhazy. "Introduction to the nonequilibrium functional renormalization group". arXiv:1204.1489v1 [hep-ph].

[97] J. Greensite. *An Introduction to the Confinement Problem.* Springer, 2011.

[98] V. Koch. "Aspects of Chiral Symmetry". Int. J. Mod. Phys. E6: 203-250, 1997, arXiv:nucl-th/9706075v2.

[99] C. Ratti, M. A. Thaler, W. Weise. "Phases of QCD: lattice thermodynamics and a field theoretical model". Phys. Rev. D 73 014019, 2006, arXiv:hep-ph/0506234.

[100] B. J. Schaefer, J. M. Pawlowski, J. Wambach. "The phase structure of the Polyakov-Quark-Meson Model". Phys. Rev. D 76 074023, 2007, arXiv:0704.3234v2 [hep-ph].

[101] K. Fukushima. "Phase diagrams in the three-flavor Nambu-Jona-Lasinio model with the Polyakov loop". Phys. Rev. D 77, 2008, arXiv:0803.3318v3.

[102] S. K. Gosh, T. K. Mukherjee. "PNJL model with a Vandermonde term". Phys. Rev. D 77 094024, 2008, arXiv:0710.2790v2 [hep-ph].

[103] K. Fukushima. "QCD matter in extreme environments". arXiv:1108.2939v1 [hep-ph].

[104] J.P. Blaizot, R. Mendez-Galain, N. Wschebor. "Non perturbative renormalisation group and momentum dependence of n-point functions (I)". Phys. Rev. E74:051116, 2006, arXiv:hep-th/0512317.

[105] N. Tetradis, C. Wetterich. "Critical Exponents from the Effective Average Action". Nucl. Phys. B422 1994, 541-592, arXiv:hep-ph/9308214.

[106] T. K. Herbst. "Polyakov Loop Dynamics with the Renormalization Group". Diploma Thesis, 2009 University Graz.

[107] V. Skokov, B. Friman, E. Nakano, K. Redlich, B. J. Schaefer. "Vacuum fluctuations and the thermodynamics of chiral models". Phys. Rev. D 82 034029, 2010, arXiv:1005.3166v1 [hep-ph].

[108] U. S. Gupta, V. K. Tiwari. "Revisiting the Phase Structure of the Polyakov-quark-meson Model in the presence of Vacuum Fermion Fluctuation". Phys. Rev. D 85 014010, 2012, arXiv:1107.1312v1 [hep-ph].

[109] P. Petreczky for HotQCD Collaboration. "On trace anomaly in $2+1$ flavor QCD". PoS (Lattice 2012) 069, arXiv:1211.1678 [hep-lat].

[110] J. Braun. "Functional Renormalization Group Methods in Quantum Chromodynamics". Dissertation, 2006, University Tübingen.

[111] N. Strodthoff, L.v. Smekal. "Polyakov-Quark-Meson-Diquark Model for two-color QCD". arXiv:1306.2897 [hep-ph].

[112] R. A. Tripolt. "The QCD Phase Diagram for Finite Volumes". Diploma Thesis, 2011 University Graz.

[113] F. Karsch. "Determination of Freeze-out Conditions from Lattice QCD Calculations". arXiv:1202.4173v1 [hep-lat].

[114] V. Koch. "Hadronic Fluctuations and Correlations". arXiv:0810.2520v1 [nucl-th].

[115] S. Mrowczynski. "Overview of event-by-event fluctuations". Acta Phys. Polon. B 40: 1053-1074, 2009, arXiv:0902.0825v1 [nucl-th].

[116] F. Karsch, K. Redlich. "Probing freeze-out conditions in heavy ion collision with moments of charge fluctuations". Phys. Lett. B 695: 136-142, 2011, arXiv:1007.2581v1 [hep-ph].

[117] X. Luo for the STAR Collaboration. "Beam Energy Dependence of Higher Moments of Net-proton Multiplicity Distributions in Heavy-ion Collisions at RHIC". arXiv:1306.3106v1 [hep-ex].

[118] A. Bazavov, H. T. Ding, P. Hegde, O. Kaczmarek, F. Karsch, E. Laermann, S. Mukherjee, P. Petreczky, C. Schmidt, D. Smith, W. Soeldner and M.Wagner. "Freeze-out Conditions in Heavy Ion Collisions from QCD Thermodynamics". Phys. Rev. Lett. 109 192302, 2012, arXiv:1208:1220v1 [hep-lat].

[119] F. Karsch, B.J.-Schaefer, M. Wagner, J. Wambach. "Towards finite density QCD with Taylor expansions". Phys. Lett. B698: 256-264, 2011, arXiv:1009.5211 [hep-ph].

[120] C. Sasaki, B. Friman, K. Redlich. "Susceptibilities and the Phase Structure of an Effective Chiral Model with Polyakov-Loops". Int. J. Mod. Phys. E16:2319-2324, 2007, arXiv:hep-ph/0702206.

[121] J. O. Andersen, A. Tranberg. "The chiral transition in a magnetic background: Finite density effects and the functional renormalization group". 10.1007/JHEP08 002, 2012, arXiv:1204.3360v3 [hep-ph].

[122] M. D'Elia. "Lattice QCD Simulations in External Background Fields". arXiv:1209.0374v2 [hep-lat].

[123] V. Skokov. "Phase diagram in an external magnetic field beyond a mean field approximation". Phys. Rev. D 85 034026, 2012, arXiv:1112.5137 [hep-ph].

[124] N. Müller. "Landau Gauge Quark Propagator with External Magnetic Fields". Master Thesis, 2013 University Giessen.

[125] E.J. Ferrer, V. de la Incera. "Dynamically generated anomalous magnetic moment in massless QED". Nucl. Phys, B 824 217-238, 2010, arXiv:0905.1733 [hep-ph].

[126] C.N. Leung, S.Y. Wang. "Gauge independent approach to chiral symmetry breaking in a strong magnetic field". Nucl. Phys. B 747 266-293, 2006, arXiv:hep-ph/0510066.

[127] D. Jana. "Charged Scalar Field in an external magnetic Field: Renormalisation and Universal Diamagnetism". Nucl. Phys. B 473 659-684, 1996, arXiv:cond-mat/9607053.

[128] G. Murguia, A. Raya, A. Sanchez, E. Reyes. "The Electron Propagator in External Electromagnetic Fields in Lower Dimensions". Am. J. Phys. 78 700, 2010, arXiv:0910.1881 [hep-th].

[129] K. Fukushima, M. Ruggieri, R. Gatto. "Chiral magnetic effect in the PNJL model". arXiv:1003.0047v2 [hep-ph].

[130] G. S. Bali, F. Bruckmann, G. Endrődi, Z. Fodor, S. D. Katz, S. Krieg, A. Schäfer, K. K. Szabo. "The QCD phase diagram for external magnetic fields". JHEP 02 044, 2012, arXiv:1111.4956v2 [hep-lat].

[131] G. S. Bali, F. Bruckmann, G. Endrődi, Z. Fodor, S. D. Katz, S. Krieg, A. Schäfer, K. K. Szabo. "The finite temperature QCD transition in external magnetic fields". arXiv:1111.5155v1 [hep-lat].

[132] G. S. Bali, F. Bruckmann, G. Endrődi, T. G. Kovacs. "Inverse magnetic catalysis and the Polyakov Loop". arXiv:1303.3972v2 [hep-lat].

Acknowledgment

First of all, I would like to thank my supervisor Lorenz v. Smekal for giving me the opportunity to be a part of his group and to work on this interesting topic. Furthermore, I want to thank everyone who helped me to perform this work and to complete it. Especially my colleagues who helped me to reduce my difficulties in programming. Futhermore, I want to thank those who proofread my work. I also want to thank HGS-HIRe for this structured PhD-program and in particular for the famous soft-skill courses and the interesting lecture weeks. I also want to thank the Helmholtz-Association and the Technical University Darmstadt for financial support. Notably, I want to thank my friends who helped me to survive this time and not giving up hope for a successful end to this all.

Curriculum vitae

- name: Piotr Piasecki
- date of birth: 18.02.1984
- birthplace: Warsaw
- nationality: german

Education

- 01.01.90 – 13.07.94: Elementary School in Groß Laasch
- 08/1994 – 19.07.00: Gymnasium Johann Wolfgang von Goethe in Neustadt-Glewe
- 31.08.00 – 27.06.03: Goethe-Gymnasium in Ludwigslust, specialized courses: mathematics and chemistry, graduation: Abitur, 2.2
- 01.10.04 – 06.07.10: Study of physics at the Friedrich-Schiller University (FSU) in Jena with subsidiary subjects chemistry and philosophy, graduation: diploma, 1.4
- 05/2009 – 05/2010: Diploma thesis at Theoretisch-Physikalisches Institut at FSU Jena, topic: Phasenübergänge und kritische Dynamik in endlichen Volumina, 1.0
- since 1.10.10 graduate studies in physics at TU Darmstadt

Erklärung

Hiermit erkläre ich, dass ich die vorliegende Arbeit selbstständig verfasst und keine anderen Quellen benutzt habe als die angegebenen und dass ich noch keinen weiteren Promotionsversuch unternommen habe.

Darmstadt, den 30.06.2014

Piotr Piasecki